Deposition and growth of novel silicon oxide and ammonium salt coatings

Spanos, Christos

DEPOSITION AND GROWTH OF NOVEL SILICON OXIDE AND AMMONIUM SALT COATINGS

Christos Spanos

Ph.D. Thesis

Department of Chemistry

University of Durham

April 2001

DEPOSITION AND GROWTH OF NOVEL SILICON OXIDE AND AMMONIUM SALT COATINGS

Christos Spanos

Ph.D. Thesis

Department of Chemistry

University of Durham

April 2001

In memory of my father

and

to my wife Yola

STATEMENT OF COPYRIGHT

DECLARATION

The work described in this thesis was carried out in the Department of Chemistry at the University of Durham between January 1996 and September 1999. It is the original work of the author except where otherwise acknowledged, and has not been previously submitted for a degree in this or any other university.

Polymer blends and aminosilane/acrylate/itaconic acid coatings were provided by Dow Corning.

Oxygen permeability measurements of the aminosilane / acrylate / itaconic acid coated polypropylene films were performed by Dow Corning.

Atomic Force Microscopy work was carried out by S. Ebbens (University of Durham).

Nuclear Magnetic Resonance experiments were performed by Dr D. C. Apperley and Dr A. M. Kenwright (University of Durham).

LIST OF PUBLICATIONS

Work in this thesis will be submitted for publication as follows:

C. G. Spanos, S. J. Ebbens, J. P. S. Badyal, A. J. Goodwin, P. J. Merlin *Surface Segregation and Plasma Oxidation of Polydimethylsiloxane Doped Polyolefins*, submitted to Macromolecules.

C. G. Spanos, S. J. Ebbens, J. P. S. Badyal, A. J. Goodwin, P. J. Merlin, D. Futter, M. Owen *Surface Segregation and Plasma Oxidation of Polyethylene-Polydimethylsiloxane Copolymer Doped Polyolefins,* in preparation.

C. G. Spanos, J. P. S. Badyal, *Single Step Solventless Growth of Polymeric Salt Networks*, in preparation.

ACKNOWLEDGEMENTS

I would like to thank my supervisor, Professor Jas Pal Badyal for his assistance and encouragement throughout my Ph.D., and A. J. Goodwin, and Dr P. J. Merlin, my industrial sponsors at Dow Corning.

Thanks to George and Kelvin in the electrical workshop, Gordon, Ray, and Malcolm the glassblowers, Jim and Neil in the mechanical workshop for their technical assistance and Joe and Jimmy in the stores for all last minute orders.

Thanks to all the members of Lab 98 past and present; especially Elinor, Stephen (the editors of this thesis), Luke (the other Dow Corning Dance performer), and Jonathan (for helping me with the industrial reports).

Special thanks to George Semertzakis and Leonidas Tzonis for providing me with substantial support (food and cigarettes) and Mary Kilitziraki for all the nice coffee breaks.

ABSTRACT

Modification of solid surfaces provides a cost effective route for producing novel properties, such as adhesion, permeability, wettability, etc. The aim of this work was to modify polyolefin surfaces with silicon dioxide and ammonium salt overlayers.

Silicon dioxide layers were formed by oxygen plasma treatment of polydimethylsiloxane (PDMS) rich polyolefin surfaces. PDMS enrichment at the surface was achieved by preparing polymer blends containing PDMS homopolymer or copolymer and polyolefin. The surface segregation behaviour of these blends was studied using X-ray photoelectron spectroscopy (XPS), atomic force microscopy (AFM) and contact angle measurements.

Next, e-beam treatment of solvent-cast 3-(-2-aminoethylamino) propyltrimethoxy-silane (Z-6020 / pentaerythritol tetracrylate (PETA) / itaconic acid (ITA) mixtures onto polypropylene films was investigated. An enhancement in gas barrier was measured. This was attributed to the formation of ammonium salt, cross-linking, and siloxane networks. The findings of this work lead to the development of a novel solventless method for depositing ionically-interacting polymeric networks. This new approach comprised plasma co-polymerisation/deposition of monomers containing carboxylic, amine, and anhydride groups.

The final part of this thesis describes the formation of highly fluorinated surfaces using CF_4 plasma treatment of the polydimethylsiloxane / polyethylene (PDMS/PE), polydimethylsiloxane / polypropylene (PDMS/PP) blends, and pure PDMS films. The importance of plasma parameters such as the input power, duration, and of pulse duty cycle on the extent of fluorination was investigated.

CONTENTS

CHAPTER 1

INTRODUCTION

1.1 SURFACE MODIFICATION OF POLYMERS

Surface chemistry (and morphology) determines the way in which polymeric materials interact with their environment. The modern world is replete with examples of materials that rely on tailored surface properties resulting from careful control of the chemical functionalities present in their outermost regions. Water repellent garments, non-stick surfaces, anti-fog lenses, adhesives and many more all rely on surface modification.

Physical modifications of polymer surfaces include plasma treatment (with gases[1,2] or vapour of monomer precursors[3]), electron-beam curing, wet chemical treatment, surface grafting, UV irradiation, and flame treatment.[4] Another strategy exploits the fact that in some polymer systems mixing in a low concentration of a polymer or small molecular additive can enrich the surface with a desired functionality (bulk modification).

1.1.1 Bulk modification

Four types of two-component polymer mixtures are commonly identified: homopolymer-homopolymer blends, copolymers where blocks of different types of monomer are linked together by chemical bonds,[5] copolymer-homopolymer mixtures and homopolymer-additive systems.

1.1.1.1 Homopolymer-homopolymer blends

Blending two or more polymers has been widely practised as a route to new polymeric materials with different bulk and surface properties to the starting homopolymers. In some polymer mixtures preferential surface segregation of one polymer may occur, resulting in enrichment at the surface of that component. This preferential segregation is typically driven by differences in surface energy between the respective blend constituents: where the lower surface energy component preferentially segregates towards the surface, thereby minimising the net free energy at the air-solid interface.[6] This reduction in the interfacial energy should compensate for the entropy decrease and/or in the enthalpy increase (in the case of exothermically miscible blends) associated with the de-mixing of the components.

In addition to these thermodynamic considerations, kinetics also play an important role to the surface segregation by determining the degree and the rate of attainment of equilibrium. Annealing of polymeric materials above their

glass transition temperature, T_g, allows equilibrium to be more closely approached. At elevated temperatures, polymer chains are able to relax, migrate and then reorganise into a more thermodynamically favourable state.[7]

The interplay between thermodynamic and kinetic factors of a polymeric mixture will govern the extent of surface enrichment with the low surface energy homopolymer. In order to assess the contribution of the above mentioned factors to the surface composition, the characteristics of the polymeric constituents in the mixture such as miscibility, size, degree of branching, and crystallinity will have to be considered.

The degree of bulk mixing affects the degree of surface segregation, the lower the former the higher the latter

The migration at the surface of low molecular weight polymer chains is more favourable than for high molecular weight ones. The conformational entropy of the polymer chain increases with the molecular weight. As the chain moves towards to the surface, it experiences compression along the direction perpendicular to the film surface which results in lowering of its conformational entropy.[8] Therefore, the enrichment of the surface with the low molecular weight chain is favoured due to the lesser reduction in conformational entropy. Furthermore, decrease in the molecular weight of the lower surface energy polymer reduces its surface tension even more and that leads to an increase in its surface free energy driven segregation.[9] Finally, shorter polymer chains can diffuse more readily towards the surface than their longer counterparts.

The effects of the crystallinity on the surface segregation can be examined from both thermodynamic and kinetic points of view. If the favourable enthalpic interactions between the blend constituents in the melt are strong, the low surface energy component might remain within the crystallisable phase of the other polymeric component upon cooling and no surface enrichment in this case will be obtained. If the favourable enthalpic interactions are very strong, surface segregation might not take place even upon annealing. When unfavourable enthalpic interactions occur between the components of the blend the low surface polymer will be "rejected" from the crystallisable phase, and surface enrichment can proceed upon heating.[10] In addition, crystallites can act as cross-links in the polymer matrix thus reducing diffusional freedom toward the surface of the low surface energy polymer.

Finally the blending procedures, especially when they are performed at room temperature (i.e. solvent-cast), can affect the surface composition.[11]

1.1.1.2 Copolymers

Again the lower surface energy constituent exhibits a preferential affinity for the free surface. The bulk composition of the copolymer system, the length of the individual blocks, the architecture and the processing conditions affect the extent of surface segregation.

In general, high levels of surface enrichment can be obtained by increasing the bulk loading and/or molecular weight (length) of the low energy segment.[12,13,14] Using diblock and triblock rather than multi/random or alternating copolymers favours surface segregation in the following order: diblock > triblock > random > alternating.[15,16,17]

Annealing can promote surface segregation by allowing equilibrium to be more closely approached. Furthermore, it can minimise the solvent effect[18] upon the copolymer's surface composition.[12]

1.1.1.3 Copolymer-homopolymer

Blending two homopolymers can sometimes lead to only temporary surface modifications. This can be more evident in the case of extremely imiscible polymers where the low surface energy polymer exhibits a pronounced migration towards the surface which can lead to its release from the polymer mixture.

Blending a copolymer with a homopolymer, where the surface active block is linked to a polymeric segment miscible with the host polymer, can provide a means for controlling this undesired exudation. Usually, this employs the design of a copolymer with the miscible block having the same chemical identity as the host homopolymer. It has been shown in the past that addition of even small amounts of copolymer into homopolymer can induce surface segregation comparable to that observed for the pure copolymer alone.[19] In general, the surface enrichment is more prevalent when diblock rather than tri/multi/star copolymers are used and the molecular weight of the miscible block is much lower to that of the homopolymer.[19]

In addition, processing conditions of the blends such as solvents used, heating, etc. play also an important role in segregation phenomena.[20]

1.1.1.4 Homopolymer-additive

Low molecular weight additives with low surface energy can also be used for modifying polymer surfaces.[21,22] As for the polymer mixtures, the difference in surface energy between the additive and polymer drives surface segregation. The chemical and physical structure of the host polymer, the additive's size and shape are among the factors affecting surface enrichment.[23]

1.1.2 Physical modifications

1.1.2.1 Plasmas

The use of plasmas for modifying polymer surfaces over recent years has become of great scientific and industrial interest because of the technique's numerous advantages over more conventional processes in terms of speed, cost, minimal environmental impact, etc.

Plasma is a partially ionised gas that contains charged and neutral particles, and the whole of the plasma is neutral. The plasma remains electrically neutral when its physical dimensions are significantly greater than the Debye length λ_D, Equation1, which defines the distance over which a charge imbalance can occur.

$$\lambda_D = (\varepsilon_o k T_e / n_e e^2)^{½} \quad (1)$$

Where ε_o is the permittivity of free space, k is the Boltzman constant, T_e is the electron temperature, n_e is the electron density and e is the charge on the electron.

There are two main types of plasma: equilibrium (thermal plasmas) and non-equilibrium (cold plasmas). In an equilibrium plasma the electron and gas temperatures are approximately equal.[24] Examples of this type are plasma arcs and plasma jets. These types of plasma generally require high temperatures to produce them (around 30000 K) and as such are impractical for polymer modification. In a non-equilibrium plasma the electron temperature, (~10000 K), far exceeds that of the gas (~300 K), and hence this type of plasma is preferred for treatment of heat sensitive substrates.

Cold plasmas can be produced under low (as in the work presented in this thesis) or high pressure conditions. Examples of the latter are corona discharge,[25] atmospheric pressure glow discharge (APGD),[26] and dielectric barrier discharge.[27] Cold plasmas are usually generated from a gas inside an

electric field. A direct current (DC) or alternating current (AC) electrical power supply provides the electric field. The applied field causes the acceleration of a small amount of naturally occurring free electrons present in the gas. As the kinetic energy of the electron increases, elastic and inelastic collisions take place with the atoms and molecules of the gas. If the electron has sufficient kinetic energy it can cause ionisation of the atoms or molecules through inelastic collisions. The new electrons produced in the ionisation process are in turn accelerated by the electric field and produce further ionisation. A cascade process thus takes place.

Plasmas are a reactive media consisting of electrons, radicals, ions, metastables, molecules and photons. Reactions initiated by them can be classified as homogeneous (occurring within the bulk discharge) or heterogeneous (between the plasma and reactor wall/sample)[28]. Homogeneous reactions can further subdivided into reactions between electrons and heavy species and reactions between heavy species. Heterogeneous reactions occur between a solid surface and plasma species (atoms, monomer molecules, radicals, or a polymer formed in the gas discharge phase).

1.1.2.2 Plasma modification

The main effects of monatomic or inorganic gas plasmas on organic polymers can be classified into two categories:[29] (a) direct reaction of activated gas with the polymer surface, (e.g. oxidation[30,31] halogenation, etc), and (b) generation of free chemical radicals at the polymer surface and subsequent reaction of these radicals with either particles contained in the plasma, or with other media which is brought into contact at a later stage (i.e. grafting).

Plasma treatments can lead to the formation of useful functional groups at polymer surfaces. As an example, in the case of polysiloxane films, chemically inert gases such as Ar or N_2 in microwave generated plasmas produce Si-H functionalities,[32] whereas ammonia plasma treatment of polydimethylsiloxane (PDMS) yields amide groups.[33] Oxygen plasma treatment of polysiloxanes can produce silica-like surfaces with increased surface energy (i.e. improved hydrophilicity), whereas in contrast fluoro-containing glow discharges give rise to formation of fluorinated groups and a more hydrophobic surface.

1.1.2.3 Plasma polymerisation

The term "plasma polymerisation" refers to the formation of polymeric material under the influence of plasma.[34] Plasma polymers differ greatly from ordinary polymers being highly cross-linked, pinhole free and usually not showing a repetition unit. Two possible mechanisms of polymerisation can be considered. Plasma induced polymerisation and plasma state polymerisation.[35] The first is the conventional free radical polymerisation of molecules containing an active bond (e.g. C=C) but because plasma polymerisation occurs at low pressures it has been demonstrated it's very unlikely to give a large contribution to the process. Plasma state polymerisation instead depends on the presence of species energetic enough to break any kind of bond, thus producing free radicals, which react to give the products. This mechanism makes it possible to obtain polymers from unconventional monomers such as alkanes and benzene. The mechanism of plasma polymerisation, rather than a chain growth polymerisation ($M_n^{\cdot}+M \rightarrow M_{n+1}^{\cdot}$) is a step-growth reaction, Figure 1.

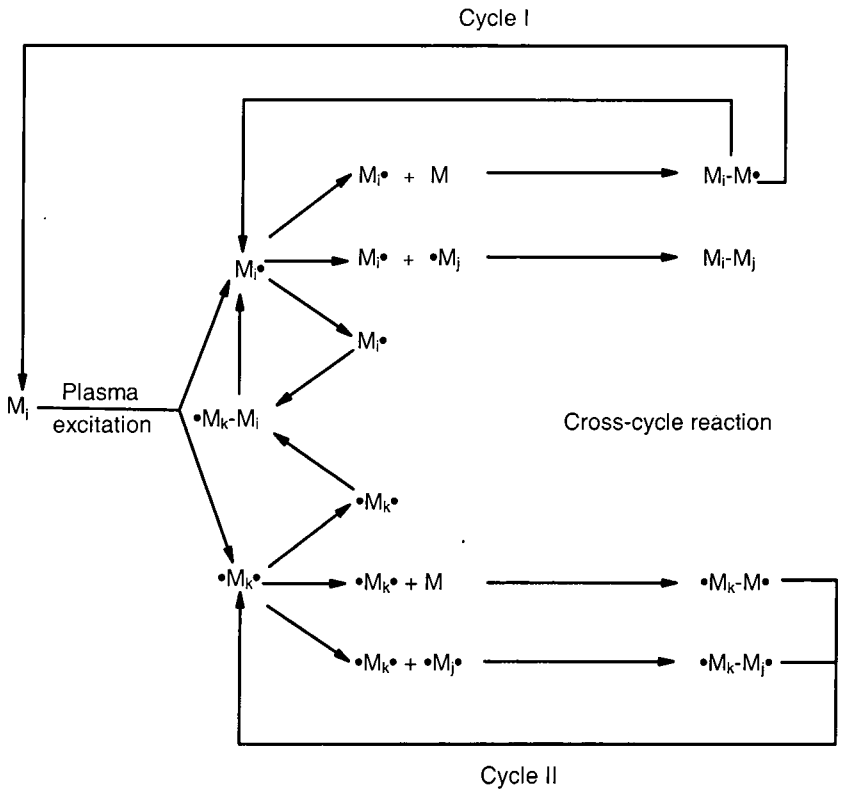

Figure 1: Schematic representation of step-growth mechanism during plasma polymerisation.[34]

Even if ionisation is essential in creating and sustaining plasma, it does not play a predominant role in initiating plasma polymerisation. The scission of bonds (fragmentation) requites less energy and occurs with greater frequency than ionisation and the concentration of free radicals is usually five to six orders of magnitude higher than ions.

1.1.2.4 Pulsed plasmas

As has been mentioned in the previous section, plasma polymers can differ significantly from their monomer precursor. Pulsing the RF discharge provides a means for depositing plasma polymers with good structural retention.[36,37] In pulsing experiments a frequency generator triggers a power supply and an oscilloscope monitors the pulse width and amplitude. A fundamental parameter of pulsed RF discharges is the duty cycle, which is defined as $t_{on}/(t_{on}+t_{off})$, and correlates with the average power output as shown in Equation 2.

$$\langle P \rangle = P_p \left(\frac{t_{on}}{t_{on} + t_{off}} \right) \tag{2}$$

It is apparent from Equation 2, that by varying the peak power (P_p), the on-time (t_{on}) and the off-time (t_{off}), low average power values can be achieved. Lower powers result in less monomer fragmentation, and decreased damage of the growing film due to reduced ion bombardment and VUV irradiation. In addition, radical-initiated polymerisation reactions may occur during the off-period.[3]

1.2 CHARACTERISATION TECHNIQUES

1.2.1 X-ray Photoelectron Spectroscopy (XPS)

XPS uses soft x-rays to photoeject[38] core level electrons from atoms in the uppermost region of the sample (1-8 nm).[39] These photoelectrons pass through an electron analyser prior to detection, resulting in a spectrum of electron intensity as a function of kinetic energy (KE). According to energy conservation the binding energy (BE) of the electrons is given by Equation 3:

$$KE = h\nu - BE - \phi \tag{3}$$

where $h\nu$ is the energy of the incident photons and ϕ is the spectrometer work function.

Ultra-high vacuum is necessary to ensure that the photoelectrons reach the electron analyser without colliding with background gas molecules.[40] Suitable x-ray sources must have line widths sufficiently narrow so as not to limit energy resolution, and a characteristic energy high enough to eject a wide range of core level electrons. Mg Kα ($h\nu$ = 1253.6 eV; line width = 0.7 eV) and Al Kα ($h\nu$ = 1486.6 eV; line width = 0.85 eV) satisfy these conditions.

Each elements' core level electrons have a characteristic binding energy (although H and He cannot be photoionised by usual X-ray sources), and so XPS spectra provide elemental analysis. If suitable reference compounds are available, then the intensity of XPS signals can be quantified to give surface elemental abundances. Binding energies show small variations according to the atoms' chemical environment. For example, the attachment of groups that withdraw electron density from the atom (e.g. fluorination), will cause an increase in core level electron binding energies as a result of their decreased nuclear screening. Greater electron withdrawal results in a greater increase in binding energy.[41]

The surface sensitivity of XPS is a result of the inelastic mean free path length, λ, of the photoelectrons. λ is a statistical quantity reflecting the average distance an emitted electron can travel within the solid before being involved in an inelastic collision. Once such collisions occur, the electron will no longer appear in the XPS peak. Inelastic path lengths depend on the energy of the electron, and so vary for different elements, Figure 2. However, most elements contained in polymers emit photoelectrons with energies in the range of 100 eV - 1000 eV. Such electrons can only escape from within a few monolayers of the sample surface, Figure 2.

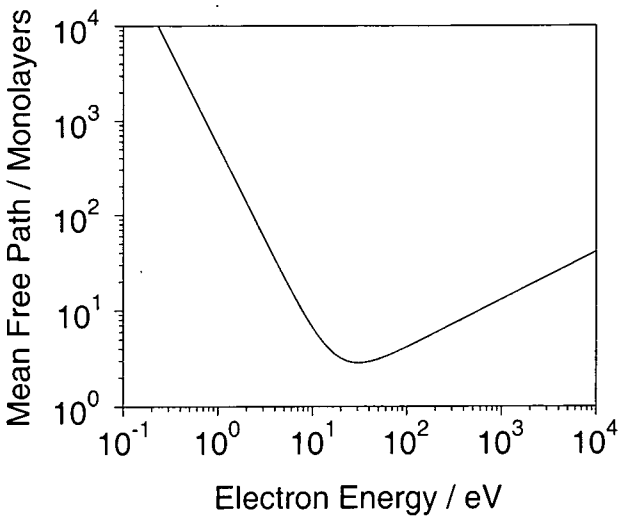

Figure 2: The dependence of inelastic mean free path length, λ on the emitted electron energy for elements.

When electrons are detected normal to the sample surface, 95 % of electrons at a given energy emerge from within 3λ of the sample surface (the escape depth). However by changing the angle at which electrons are detected (the angle of emission relative to the normal to surface, θ) the escape depth is scaled to $3\lambda\cos\theta$, Figure 3.[40]

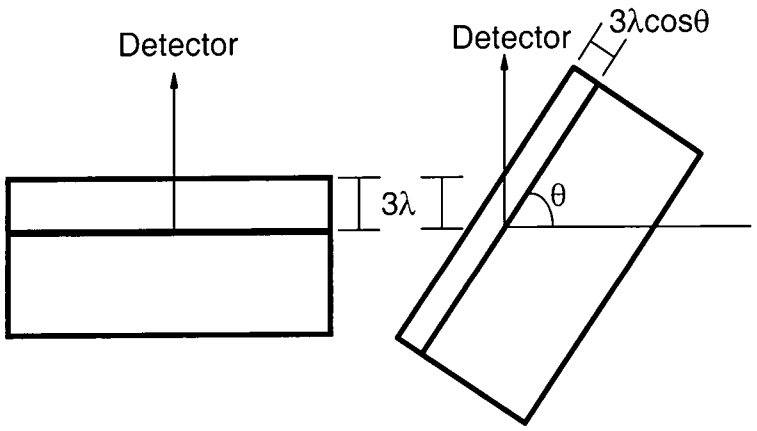

Figure 3: Angle resolved XPS.

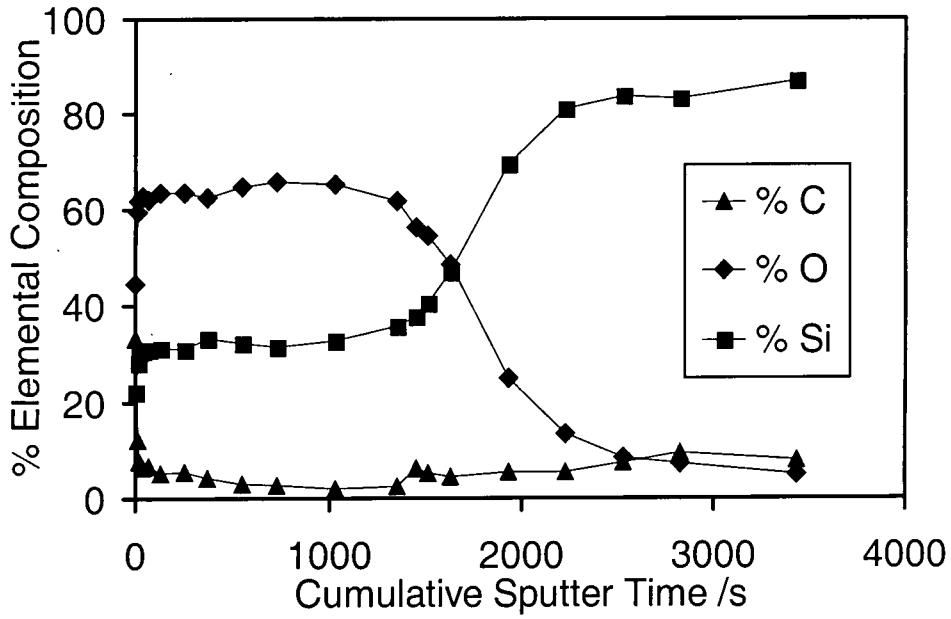

Figure 4: Depth profile of 20 nm silicon dioxide film onto silicon substrate.

Deeper sampling depths (>8 nm) can be achieved by ion sputtering the surface, and then analysing the bottom of the sputtered crater using XPS. By repeating this procedure at regular time intervals, depth compositional profiles deep into sample surface can be generated, Figure 4. In order to convert the sputter time into a depth a reference sample with known thickness is required. For the depth profiles acquired in Chapter 3, a 20 nm thick (determined using ellipsometry) silicon dioxide film deposited onto silicon substrate was used as depth calibration standard, Figure 4.

1.2.2 Atomic Force Microscopy

Atomic force microscope (AFM) is an exciting technique available for a host of applications ranging from relatively simple visualisation of morphology to more advanced examination of surface structure and properties on the nanometer scale. The microscope can be operated in three modes: contact, Tapping Mode, and non-contact mode.

In contact AFM mode, also known as repulsive mode, an AFM tip makes soft "physical contact" with the sample. The tip is attached to the end of a cantilever with a low spring constant. As the scanner gently traces the tip across the sample (or the sample under the tip), the contact force causes the

cantilever to bend in order to accommodate changes in topography. The deflection of the tip is monitored using a laser beam-bounce method. Thus, the AFM is able to monitor the atomic force interactions between the tip and the surface and the resulting image is a topographical map of the sample. Advantages of this mode include fast scanning speeds at very high resolutions whereas its main drawbacks are associated with possible damage to both sample and tip due to combined lateral and high adhesive forces between the probe and the surface which in turn may create artefacts in the image data.[42]

In Tapping Mode AFM a sharp tip is made to oscillate at or near to its resonance frequency so that it makes intermittent contact with the sample surface.[43] This reduces the lateral forces associated with contact mode AFM, and so allows the examination of soft samples, such as polymers. Height images are recorded by using a feedback circuit to maintain constant oscillation amplitude. In addition, phase shift images can be simultaneously recorded to allow the mapping of heterogeneous surfaces.[44]

In the non-contact mode the probe is oscillating in a small distance above the sample. Attractive van der Waals' forces acting between the tip and the sample are detected by measuring the changes in the oscillation amplitude, and topographic images are constructed by scanning the tip above the surface. This mode provides substantially lower resolution than either contact or Tapping Mode due to weaker strength of the attractive van der Waals' forces compared to contact ones.

1.2.3 Infrared Spectroscopy

The basis of infrared spectroscopy is the vibrational excitation of molecules by the absorption of infrared radiation (wavelength 1-100 μm). This occurs at characteristic photon energies, enabling structural analysis. For a vibrational transition to be infrared active there must be a change in the dipole moment.[45]

IR spectroscopy is normally performed in transmission mode, i.e. radiation is passed through the sample. This is bulk technique, inappropriate for detecting surface change. A more surface sensitive method is attenuated total reflectance fourier transform infra-red spectroscopy (ATR-FTIR). Here the sample is held in intimate contact with an IR transparent crystal (e.g. KRS-5 or diamond) into which infrared radiation is directed. The difference in refractive indices between the optically dense crystal and the sample result in internal

reflection at their interface. However, the beam is not completely reflected at this junction: some propagates a short way into the sample, where it can excite vibrations and be absorbed.[46] The penetration of these phenomena is dependent upon the incident wavelength but is typically about 0.1 - 10 μm, providing information complementary to that of XPS.

1.2.4 Video Contact Angle (VCA) Measurements

Contact angle analysis is an extremely surface sensitive technique (top 5-10 Å).[47] The VCA apparatus employs the sessile drop technique, where a droplet of known volume of purified liquid is dispensed on the solid surface by means of a motorised syringe. A CCD camera focused on the droplet resting on the substrate allows the capture of a static image. The operator places markers around the droplet image and the computer software is then used to calculate the contact angle, Figure 5. This type of measurement is called static and was used in the work presented in the following chapters as a simple and fast way for estimating the degree of hydrophobicity/hydrophilicity of the studied surfaces (higher angles indicating greater hydrophobicity).

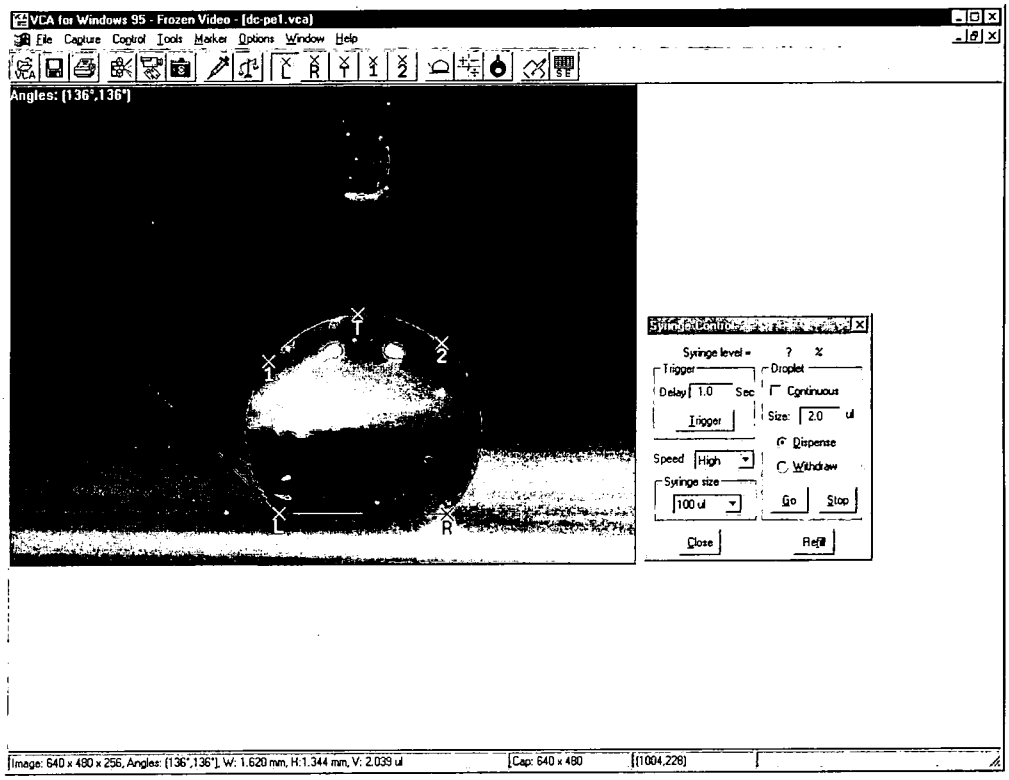

Figure 5: Snapshot of the VCA software interface.

1.3 REFERENCES

1 Hopkins, J.; Badyal, J. P. S. *Langmuir* **1996**, *12*, 3666.

2 Hopkins, J.; Boyd, R. D.; Badyal, J. P. S. *J. Phys. Chem.* **1996**, *100*, 6755.

3 Ryan, M. E.; Hynes, A. M.; Badyal, J. P. S. *Chem. Mater.* **1996**, *8*, 37.

4 Garbassi, F.; Morra, M.; Occhiello, E. *Polymer Surfaces: From Physics to Technology*; Wiley: New York, 1994.

5 Schmitt, R. L.; Gardella, J. A.; Magill, J. H.; Salvat, I. L.; Chin, R. L *Macromolecules* **1985**, *18*, 2675.

6 Donald, A. M. *Nature* **1989**, *338*, 20.

7 Kassis, C. M.; Steehler, J. K.; Bates, D. E.; Guan, Z.; Romack, T. J.; DeSimone, J. M; Linton, R. W. *Macromolecules* **1996**, *29*, 3247.

8 Shuto, K., Oishi, Y., Kajiyama, T., Han, C. C. Macromolecules **1993**, 26, 6589

9 Bhatia, Q. S., Pan, D. H., Koberstein, J. T. Macromolecules, **1988**, 21, 2166

10 Sakellariou, P. Polymer **1993**, 34(16), 3408.

11 Volkov, I. O.; Gorelova, M. M.; Pertsin, A. J.; Filimonova, L. V.; Torres, M. A. P. R.; Oliveira, C. M. F. J. Appl. Polym. Sci. **1998**, *68*, 517.

12 Chen, X.; Lee, H. F.; Gardella, J. A., Jr. *Macromolecules*, **1993**, *26*, 4601.

13 Zhao, J.; Rojstaczer, S. R.; Chen, J.; Xu, M.; Gardella, J. A., Jr. *Macromolecules*, **1999**, *32*, 455.

14 Chen, X.; Gardella, J. A., Jr.; Kumler, P. L. *Macromolecules*, **1993**, *26*, 3778.

15 Chen, X.; Gardella, J. A., Jr.; Kumler, P. L. *Macromolecules*, **1992**, *25*, 6621.

16 Chen, X.; Gardella, J. A., Jr.; Kumler, P. L. *Macromolecules*, **1992**, *25*, 6631.

17 Hariharan, A.; Harris, J. G. *J. Phys. Chem.* **1995**, *99*, 2788.

18 Benrashid, R.; Nelson, G. L.; Linn, J. H., Hanley, K. H.; Wade, W. R. *J. Appl. Polym. Sci.* **1993**, *49*, 523.

19 Chen, X.; Gardella, J. A., Jr. *Macromolecules* **1994**, *27*, 3363.

20 Chen, J.; Gardella, J. A., Jr.; *Macromolecules* **1994**, *31*, 9328.

21 Sargent, R. R.; Alexander, J. R. US 5560992, 1996.

22 Champagne, F.; Li, J. -F.; Schreiber, H. P.; Dipola-Baranyi, G. *J. Appl. Polym. Sci.* **1994**, *54*, 743.

23 Földes, E. *Angew. Makromol. Chem.* **1998**, *261*, 65.

24 Bell, A, T. In *Techniques and Applications of Plasma Chemistry*; Hollahan, J. R., Bell, A. T. Eds.; Wiley: New York, 1974.

25 Hillborg, H.; Gedde, U. W. *Polymer* **1998**, *39*, 1991.

26 Kanazawa, S.; Kogoma, M.; Moriwaki, T.; Okazaki, S. *J. Phys. D: Appl. Phys.* **1988**, *21*, 838.

27 Greenwood, O. D.; Boyd, R. D.; Hopkins, J.; Badyal, J. P. S. *J. Adhesion Sci. Technol.* **1995**, *9*, 311.

28 Grill, A. In *Cold Plasma in Materials Fabrication – From Fundamentals to Applications*; IEEE PRESS: New York, 1994.

29 Maksimov, A. I.; Krotova, G. D.; Kitaev, V. P.; Denisov, A. N. *Electron. Obrab. Mater.* **1988,** *5*, 52

30 Namatsu, H. *J. Electrochem. Soc.* **1989**, *136*, 2676.

31 Morra, M.; Occhielo, E.; Marola, R.; Garbassi, F.; Humphrey, P.; Johnson, *J. Colloid Interf. Sci.* **1990**, *137*, 11.

32 Gaboury, S. R.; Urban, M. W. *Polym. Commun.* **1991**, *32*, 390.

33 Gaboury, S. R.; Urban, M. W. *J. Appl. Polym. Sci.***1992**, 44, 401.

34 Yasuda, H. In *Plasma Polymerization;* Academic Press: New York, 1985.

35 Yasuda, H. Glow Discharge Polymerisation In *Thin Film Processes*; Vossen, J. L., Kern, W. Eds; Academic Press: New York, 1978.

36 Han, L.N.; Timmons, R.B. *J. Polym. Sci.: Part A* **1998,** *36,* 3121.

37 Han, L.N.; Timmons, R.B.; Bagdal, D.; Pielichowsky, J. *Chem Mater.* **1998,** *10,* 1422

38 Sherwood, P. M. A. In *Spectroscopy*, Straughan, B. P., Walker, S., Eds.; Chapman and Hall: London, 1976.

39 Ratner, B. D.; Castner, D. G. Electron Spectroscopy for Chemical Analysis In *Surface Analysis – The Principal Techniques*; Vickerman, J. C., Ed.; Wiley: Chichester, 1997.

40 *Practical Surface Analysis*, 2nd ed.; Briggs, D., Seah, M. P., Eds.; Wiley: New York, 1990; Vol. 1.

41 Beamson, G.; Briggs, D. In *High Resolution XPS of Organic Polymers: The Scienta ESCA300 Database*; Wiley: New York, 1992.

42 Digital Instruments Application Notes. http://www.di.com/appnotes/TapMode/tapmodeMain.html (accessed January 2001).

43 Zhong, Q.; Innis, D.; Kjoller, K. K.; Elings, V. B. *Surf. Sci. Lett.* **1993**, *290*, L688.

44 Bar, G.; Thomann, Y.; Brandsch, R.; Cantow, H. J.; Whangbo, M. -H *Langmuir* **1997**, *13*, 3807.

45 Banwell, C. N. In *Fundamentals of Molecular Spectroscopy*; McGraw-Hill: Maidenhead, U.K., 1966

46 Hoflund, G.B.; Rivière, J. C. Less Commonly Used Techniques for Analysis of Surfaces and Interfaces In *Handbook of Surface and Interface Analysis*; Rivière, J. C., Myhra, S., Eds.; Marcel Dekker: New York, 1998.

47 Langmuir, I. *Phys. Rev.* **1929**, *33*, 954.

CHAPTER 2

SURFACE SEGREGATION AND PLASMA OXIDATION OF POLYSILOXANE DOPED POLYOLEFINS

2.1 INTRODUCTION

The physicochemical nature of polymer surfaces is important for many everyday applications,[1] for example adhesion, wettability, friction, dye uptake, gloss, biocompatibility, permeability, etc. One way of devising desirable surface and bulk properties is to mix two or more polymers in order to make a blended material which displays very different surface properties compared to the bulk. The overall driving force for such behaviour often stems from a difference in surface energy between the respective blend constituents: where the lower surface energy component preferentially segregates towards the surface, thereby minimising the net free energy at the air-solid interface.[2]

Polysiloxane / polyolefin blends are a case in point, where the polysiloxane component can migrate towards the surface as consequence of its lower surface energy.[3] Such polysiloxane enrichment can be beneficial for lowering friction, acting as an anti-blocking agent,[4,5] fire proofing,[6] and improving release behaviour.[7] In this article, the surface segregation behaviour of polydimethylsiloxane / polyethylene and polydimethylsiloxane / polypropylene melt blown films is compared in order to determine how the nature of the polyolefin host influences surface composition. Plasma oxidation of these blends has also been explored with the aim of generating a well-adhered SiO_x surface layer, thereby providing an alternative and more direct route for making SiO_x coated substrates compared to conventional approaches (e.g. PECVD,[8] electron beam evaporation,[9] etc.).

2.2 EXPERIMENTAL

Linear polydimethylsiloxane (PDMS) containing a $-SiMe_2CH{=}CH_2$ endblock (Dow Corning, M_w = 500,000 and T_g = 146 K) was mixed with linear low density polyethylene / low density polyethylene (LLDPE / LDPE) or polypropylene (PP) during film extrusion via the bubble-film process, Table 1.

Solvent washing studies were carried out using mixtures of cyclohexane (BDH, 99.5 % purity) / propan-2-ol (BDH, 99.7 % purity) for 30 s. In the case of annealing experiments, a vacuum oven (LTE, Qualivac) was employed. Oxygen plasma treatment of the polymer blend surfaces comprised 60 s exposures at powers ranging from 2-20 W in a cylindrical glass reactor (4.5 cm diameter, 505 cm^3 volume) enclosed in a Faraday cage. This was fitted with a gas inlet, a thermocouple pressure gauge, and a two-stage mechanical rotary

pump attached to a liquid air cold trap, (base pressure of 2×10^{-2} mbar and a leak rate better than 1.2×10^{-3} cm^3 min^{-1}). A copper coil (5 mm diameter, 10 turns, spanning 8-16 cm from the gas inlet) wound externally around the reactor walls was coupled to a 13.56 MHz RF power supply via an LC matching circuit. Prior to each experiment, the chamber was cleaned with a 40 W air plasma at 0.2 mbar pressure for 10 min. Next, a piece of the polymer substrate was placed into the centre of the reactor and purged with oxygen (BOC, 99.6 % purity) at 0.8 mbar pressure for 10 min, followed by plasma ignition at 0.2 mbar pressure and 1 cm^3 min^{-1} flow rate. Upon termination of plasma treatment, oxygen gas was allowed to continue to flow over the substrate for a further 5 min prior to bringing the reactor up to atmosphere.

Table 1: Physical properties of polymer constituents.

Polymer	$M_n \times 10^3$	$M_w \times 10^3$	M_w / M_n	T_g / K	T_m / K
LDPE / LLDPE	29	104	3.6	148	390.5
PP	49	204	4.2	265	437.5

M_n = Number average molar mass

M_w = Weight average molar mass

M_w / M_n = Heterogeneity index

T_g = Glass transition temperature

T_m = Melting point

A Kratos ES300 electron spectrometer equipped with a Mg Kα X-ray source (1253.6 eV), and a concentric hemispherical analyser (CHA) was used for XPS analysis. Photo-emitted electrons were collected at a take-off angle of 30° from the substrate normal, with electron detection in the fixed retarding ratio (FRR, 22:1) mode. XPS spectra were accumulated on an interfaced PC computer and fitted using a Marquardt minimisation algorithm assuming that all the peaks are Gaussian with equal full-width-at-half-maximum (FWHM).[10] Instrument sensitivity factors using reference chemical standards were taken as C(1s) : O(1s) : Si (2p) equals 1.00 : 0.57 : 0.72.

AFM micrographs were acquired with a Digital Instruments Nanoscope III. Damage to the tip or sample was minimised by using Tapping Mode AFM.[11] These studies used a stiff silicon cantilever oscillating at close to its resonance frequency. In addition to height images, phase images reflecting the mechanical

properties of the surface were obtained by choosing a setpoint : free amplitude ratio of 0.5 (setpoint = 50 nm ; free amplitude = 100 nm).[12] All images were acquired in air at room temperature and are presented as unfiltered data. Large area scans were taken on the 100 μm scale in order to check that the reported images were representative of the whole surface. Cross-sectional microtoming of the polymer blend films prior to AFM analysis was carried out at 243 K using a cryogenic microtoming apparatus (Leica RM 2165).

Sessile drop contact angle measurements were carried out at 20 °C using a video capture apparatus (A.S.T. Products VCA2500XE). The chosen probe liquid was high purity water (B.S. 3978 Grade 1).

2.3 RESULTS

The amount of polysiloxane removal from the polymer blend surfaces achieved by washing was found to be dependent upon solvent composition, Figure 1. More silicon-containing material was lost from the surface with increasing non-polar (cyclohexane) content. This trend provided a means for controlling the composition of the surface region for both the polyethylene and polypropylene doped substrates. Washing in a 50 / 50 cyclohexane / propan-2-ol solvent mixture for 30 s resulted in virtually all the polysiloxane species being lost from the top 3-5 nm of the substrate (i.e. the Si(2p) XPS sampling depth).[13] These conditions were taken as being optimum. Subsequent annealing in a vacuum oven for 30 min gave rise to some polysiloxane material diffusing from the bulk into the near-surface region, Figure 2. This behaviour was temperature dependent, and found to reach a maximum at around 100 °C for polyethylene, and 80 °C for polypropylene. In the latter case, the amount of PDMS detected by XPS dropped off at higher annealing temperatures. Greater surface segregation was observed for the polyethylene host matrix, and this was found to correlate to the overall bulk loading of PDMS in the blend, Figure 3. The absence of any binding energy shift in the Si(2p) spectra confirmed that PDMS species were not undergoing oxidation during annealing, Figure 4.

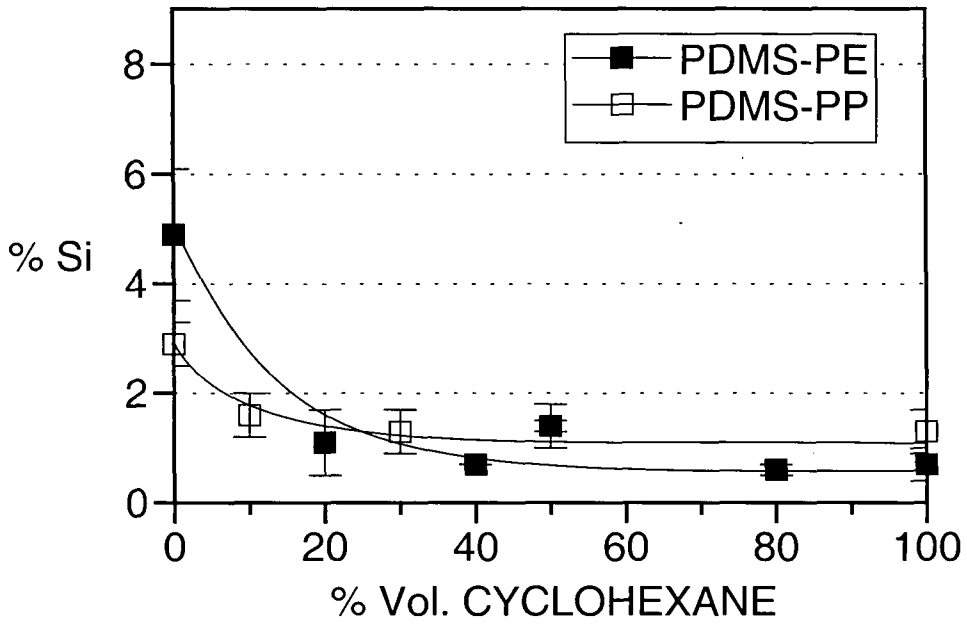

Figure 1: Variation in silicon concentration at the surface of 2.5% PDMS doped polyethylene films following washing in cyclohexane / propan-2-ol solvent mixtures.

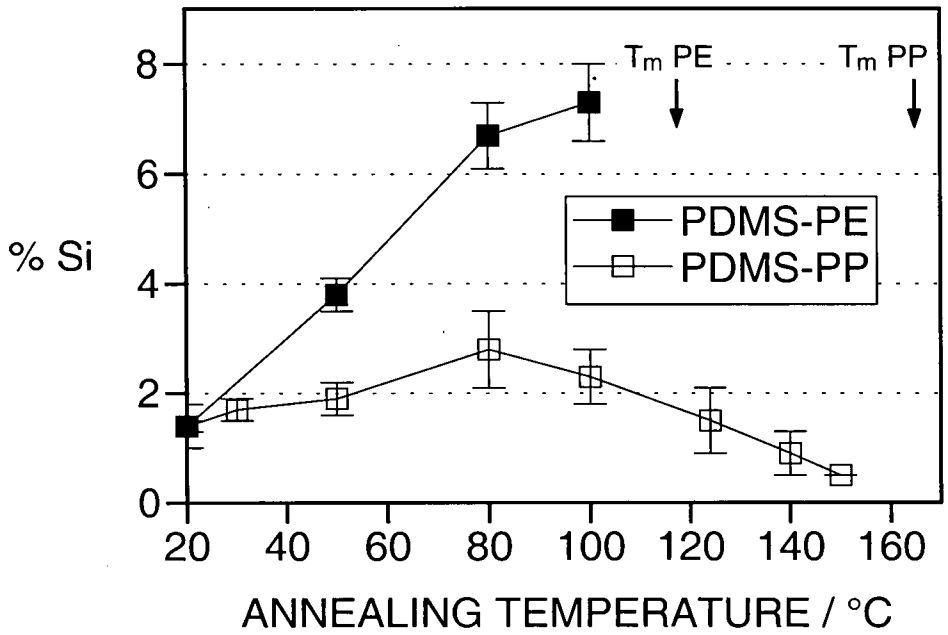

Figure 2: Silicon concentration at the surface of 2.5% PDMS doped polyethylene and polypropylene films following washing in a 50 / 50 cyclohexane / propan-2-ol solvent mixture and then annealing at various temperatures.

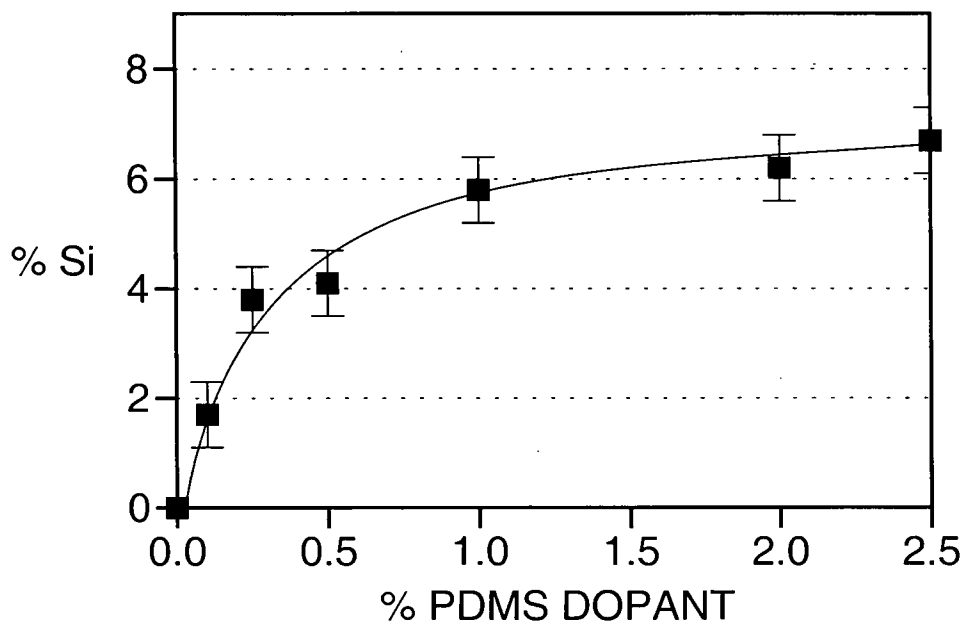

Figure 3: Silicon concentration at the surface of PDMS doped polyethylene films as a function of bulk polysiloxane loading (% wt.), following washing in 50 / 50 cyclohexane / propan-2-ol solvent mixture and then annealing at 80° for 30 min.

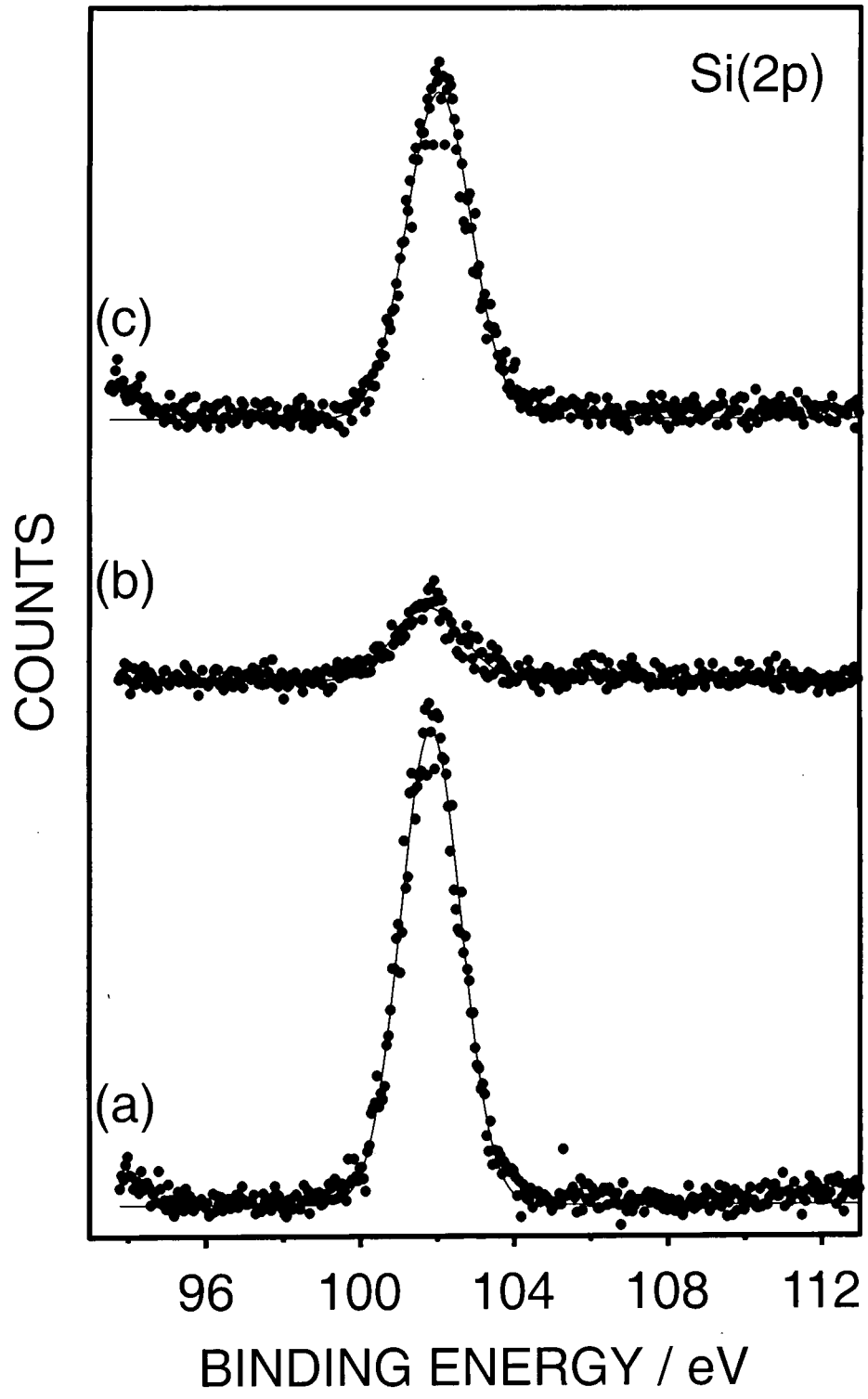

Figure 4: Si(2p) XPS spectra of 2.5% PDMS doped polyethylene film: (a) before washing; (b) washed in 50 / 50 cyclohexane / propan-2-ol solvent mixture for 30 s; and (c) washed in 50 / 50 cyclohexane / propan-2-ol solvent mixture for 30 s and then heated at 80 °C for 30 min.

Consecutive solvent washing followed by annealing cycles eventually led to almost total exhaustion of silicon-containing species from the near surface region (i.e. heating could no longer replenish the surface with polysiloxane moieties after solvent washing), Figure 5.

Oxygen plasma treatment of PDMS doped polyolefin films which had previously undergone one solvent washing / annealing cycle (i.e. contained a well-defined quantity of PDMS at the surface) resulted in surface oxidation, Figure 6. As expected, the relative amount of silicon present at the surface depended upon oxygen incorporation and carbon loss. Interestingly, the surface composition following oxygen plasma treatment was found to be very similar for both the polyethylene and polypropylene hosts, despite the former containing a much larger concentration of polysiloxane at the surface prior to plasma exposure. Plasma oxidation caused a shift in the Si(2p) peak from 102.0 eV (polysiloxane) to 103.4 ± 0.1 eV (SiO_x);[14,15] this was accompanied by the appearance of oxidised C(1s) moieties:[14] $\underline{C}$–CO_2 at 285.7 eV, $\underline{C}$–O– at 286.6 eV, $\underline{C}$=O, O–$\underline{C}$–O at 287.8 eV, –O–$\underline{C}$=O at 289.0 eV, and –O–$\underline{C}$O–O– at 290.0 eV, Figures 7 and 8. Broadening of the O(1s) envelope towards higher binding energies was noted, however accurate deconvolution of O(1s) spectra was impossible due to the close overlap of various different oxygen environments:[14,15,16,17] e.g. polysiloxane at 532.6 eV, Si$\underline{O}_2$ at 532.5 - 533.2 eV, C–$\underline{O}$– at ~532.6 eV, C=$\underline{O}$ at ~532.3 eV, –$\underline{O}$–C=O at ~533.6 eV, –$\underline{O}$–CO–$\underline{O}$– at ~533.9 eV, etc. Control plasma oxidation experiments using undoped polyolefin films did not yield any silicon at the surface, thereby ruled out the possibility of sputtering off the reactor walls.

Washing low power plasma oxidised 2.5% PDMS doped polyolefin surfaces in a 50 / 50 cyclohexane / propan-2-ol solvent mixture for 30 s gave rise to an overall increase in the proportion of silicon-containing species at the surface, Figure 9; this is most likely to be due to the removal of low molecular weight oxidised polyolefin material, as confirmed by the attenuation of the high binding energy shoulder in the C(1s) envelope.[18] Annealing these plasma treated surfaces at 80 °C produced a substantial build-up of PDMS at the surface; some of this polysiloxane material could subsequently be removed by washing in the solvent mixture (this being more prevalent for the polypropylene

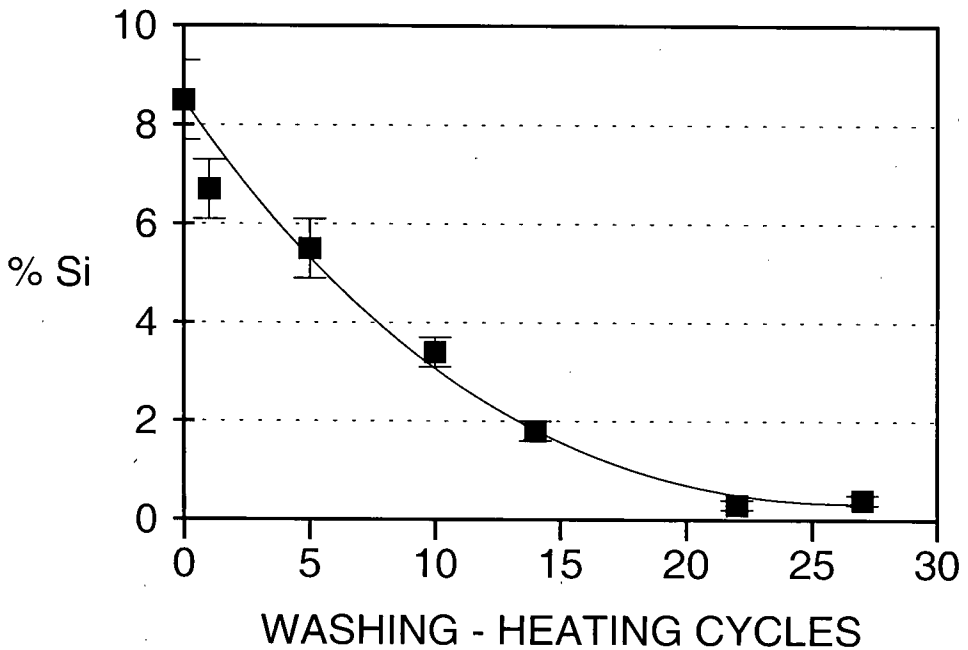

Figure 5: Variation in silicon concentration at the surface of 2.5% PDMS doped polyethylene film as function of the number of washing-heating cycles.

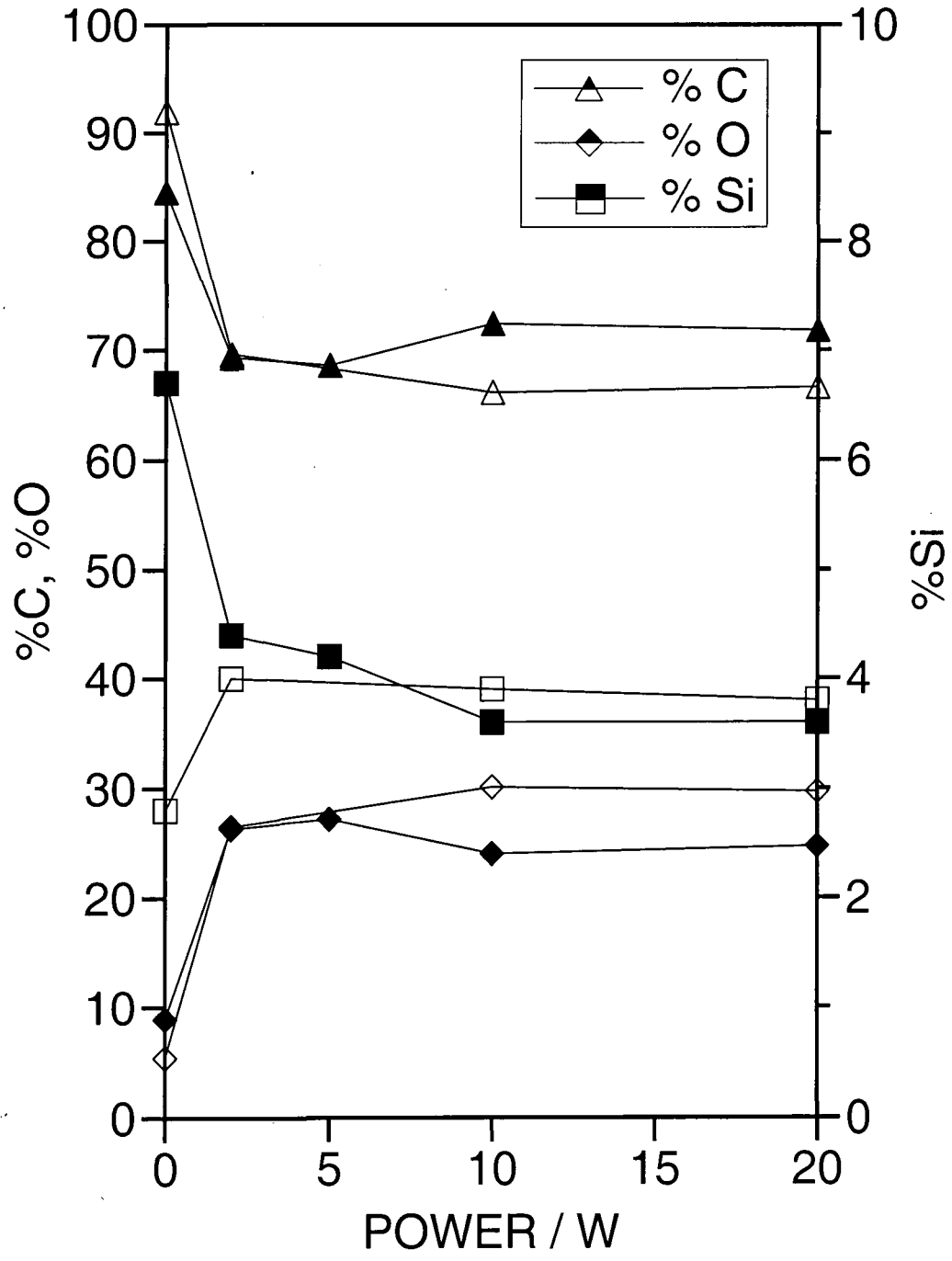

Figure 6: Change in elemental composition at the surface of 2.5% PDMS doped polyethylene (shaded symbols) and polypropylene (unshaded symbols) films as a function of oxygen glow discharge power level.

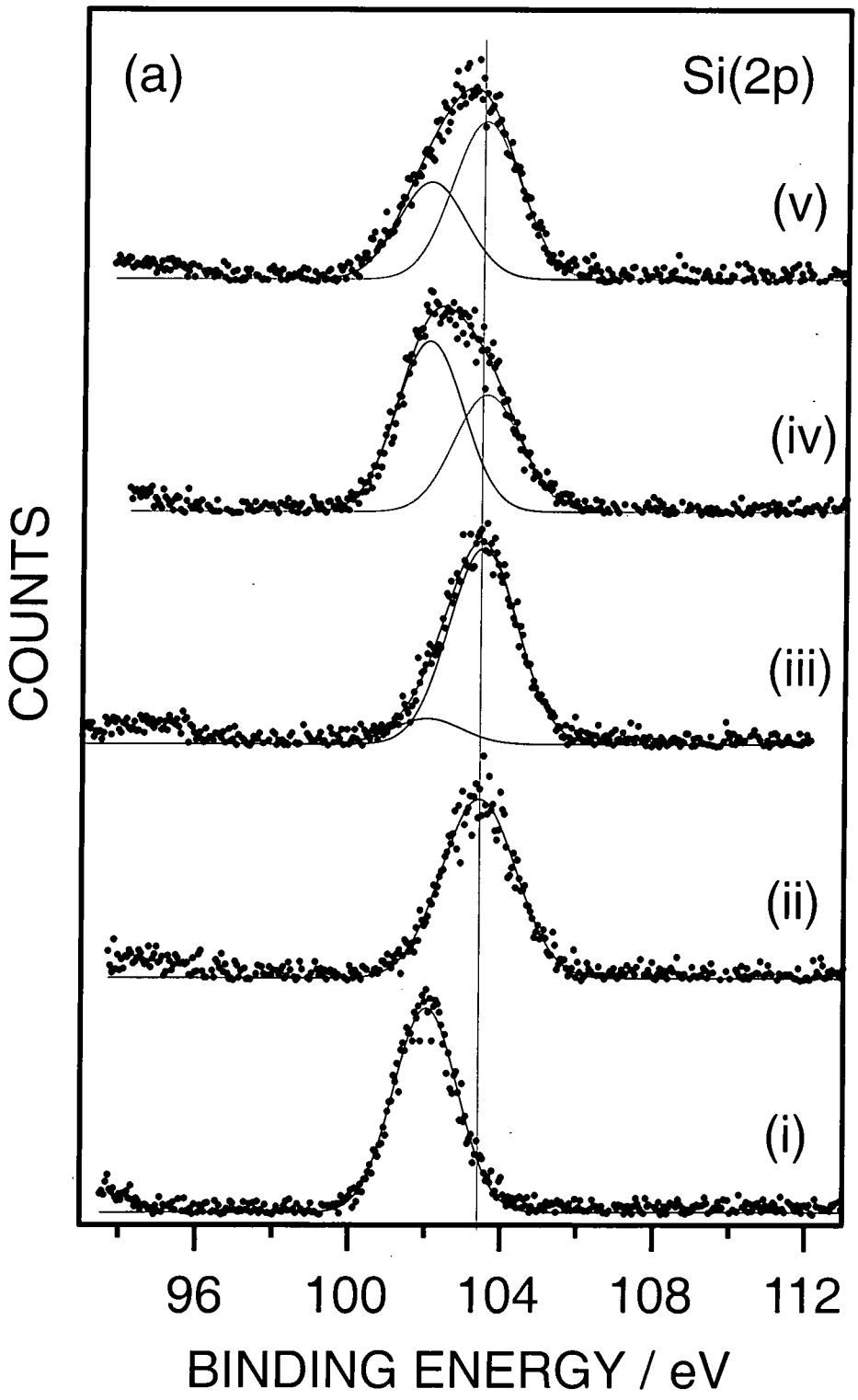

Figure 7a: Si(2p) XPS spectra of PDMS doped polyethylene film: (i) washed in 50 / 50 cyclohexane / propan-2-ol solvent mixture for 30 s and then heated at 80 °C for 30 min; (ii) 2 W O_2 plasma treatment for 60 s; (iii) 2 W O_2 plasma treatment for 60 s followed by washing in 50 / 50 cyclohexane / propan-2-ol solvent mixture for 30 s; (iv) 2 W O_2 plasma treatment for 60 s followed by annealing at 80 °C for 30 min; and (v) 2 W O_2 plasma treatment for 60 s followed by annealing at 80 °C for 30 min and then washing in 50 / 50 cyclohexane / propan-2-ol solvent mixture for 30 s. (All spectra have been normalised).

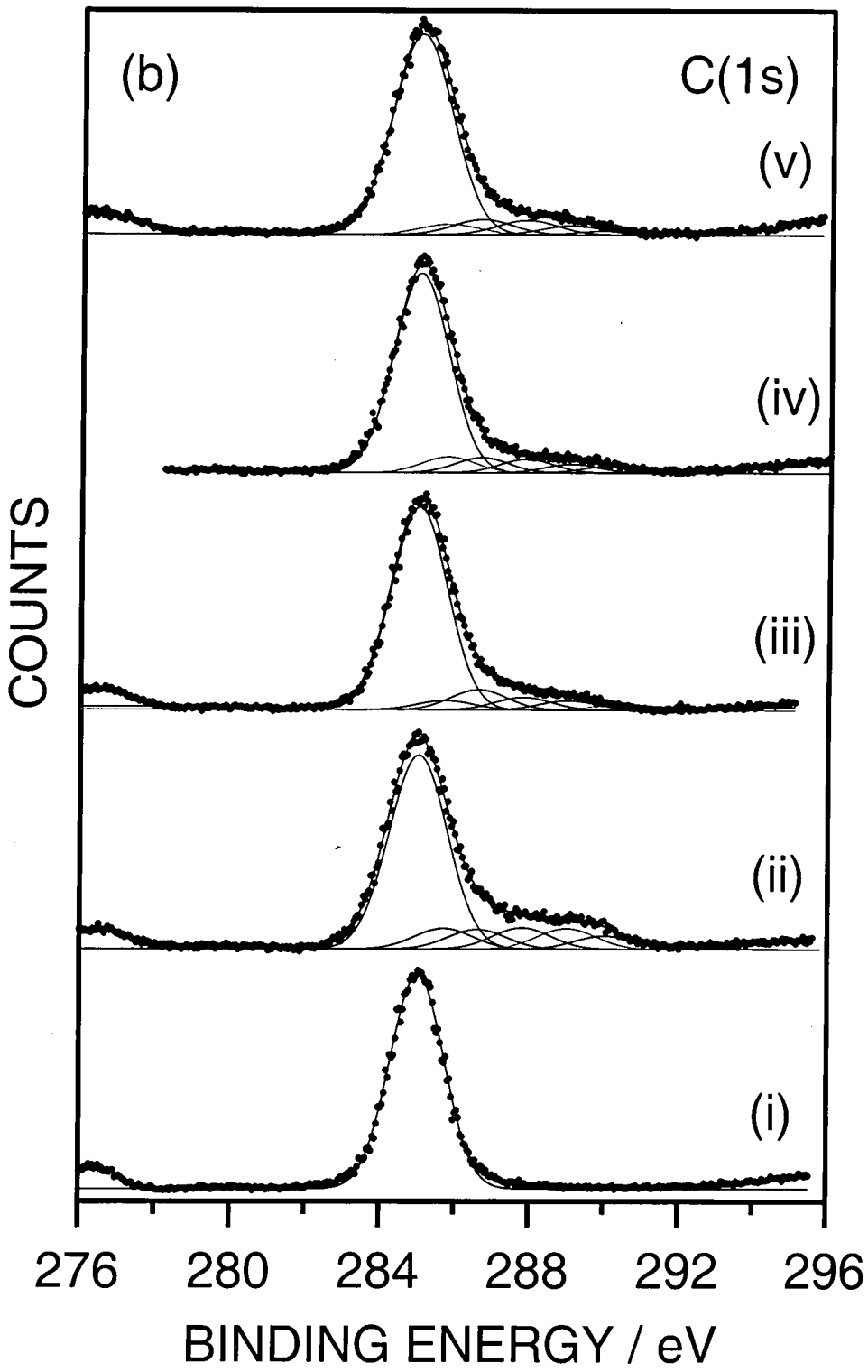

Figure 7b: C(1s) XPS spectra of PDMS doped polyethylene film: (i) washed in 50 / 50 cyclohexane / propan-2-ol solvent mixture for 30 s and then heated at 80 °C for 30 min; (ii) 2 W O_2 plasma treatment for 60 s; (iii) 2 W O_2 plasma treatment for 60 s followed by washing in 50 / 50 cyclohexane / propan-2-ol solvent mixture for 30 s; (iv) 2 W O_2 plasma treatment for 60 s followed by annealing at 80 °C for 30 min; and (v) 2 W O_2 plasma treatment for 60 s followed by annealing at 80 °C for 30 min and then washing in 50 / 50 cyclohexane / propan-2-ol solvent mixture for 30 s. (All spectra have been normalised).

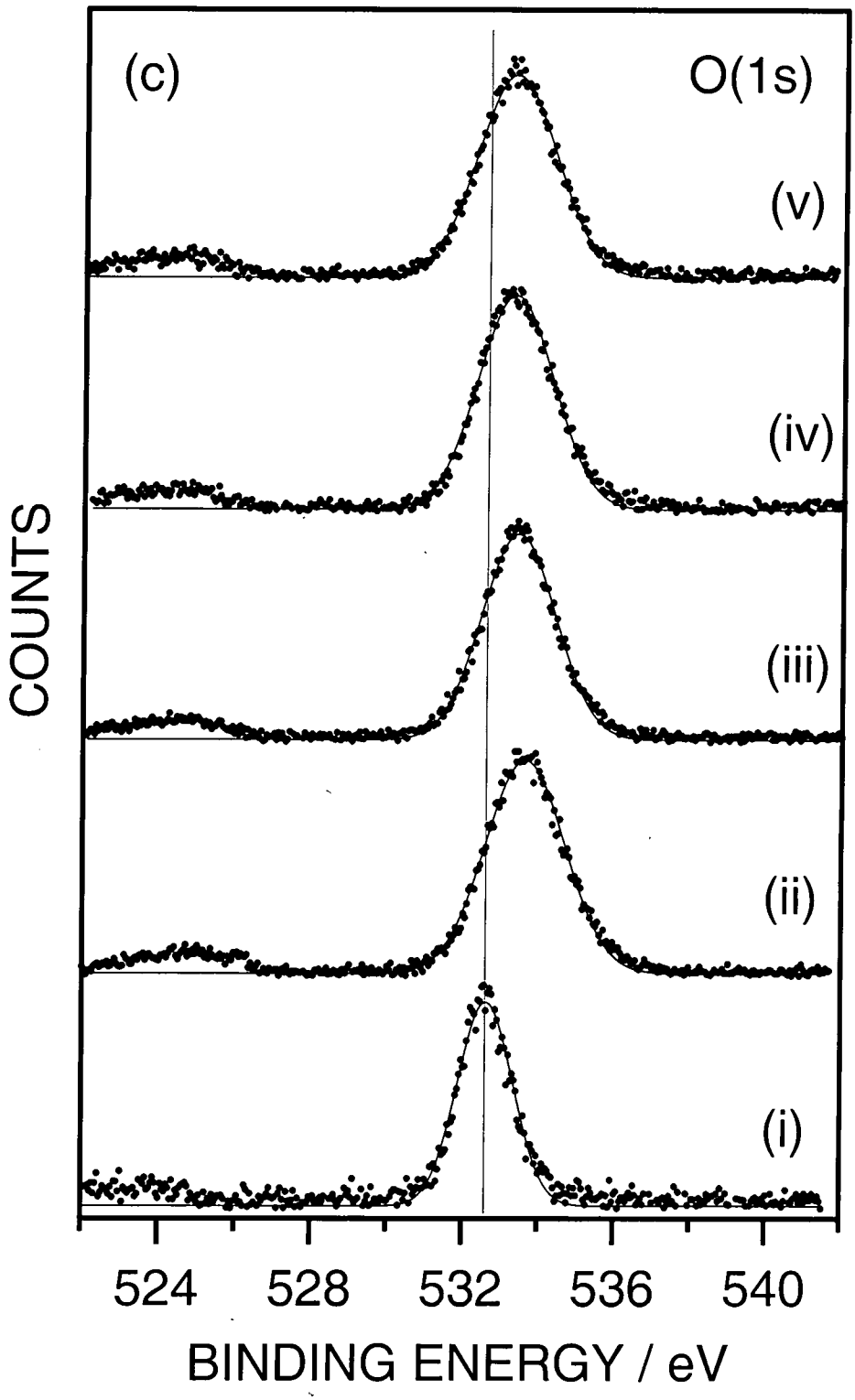

Figure 7c: O(1s) XPS spectra of PDMS doped polyethylene film: (i) washed in 50 / 50 cyclohexane / propan-2-ol solvent mixture for 30 s and then heated at 80 °C for 30 min; (ii) 2 W O_2 plasma treatment for 60 s; (iii) 2 W O_2 plasma treatment for 60 s followed by washing in 50 / 50 cyclohexane / propan-2-ol solvent mixture for 30 s; (iv) 2 W O_2 plasma treatment for 60 s followed by annealing at 80 °C for 30 min; and (v) 2 W O_2 plasma treatment for 60 s followed by annealing at 80 °C for 30 min and then washing in 50 / 50 cyclohexane / propan-2-ol solvent mixture for 30 s. (All spectra have been normalised).

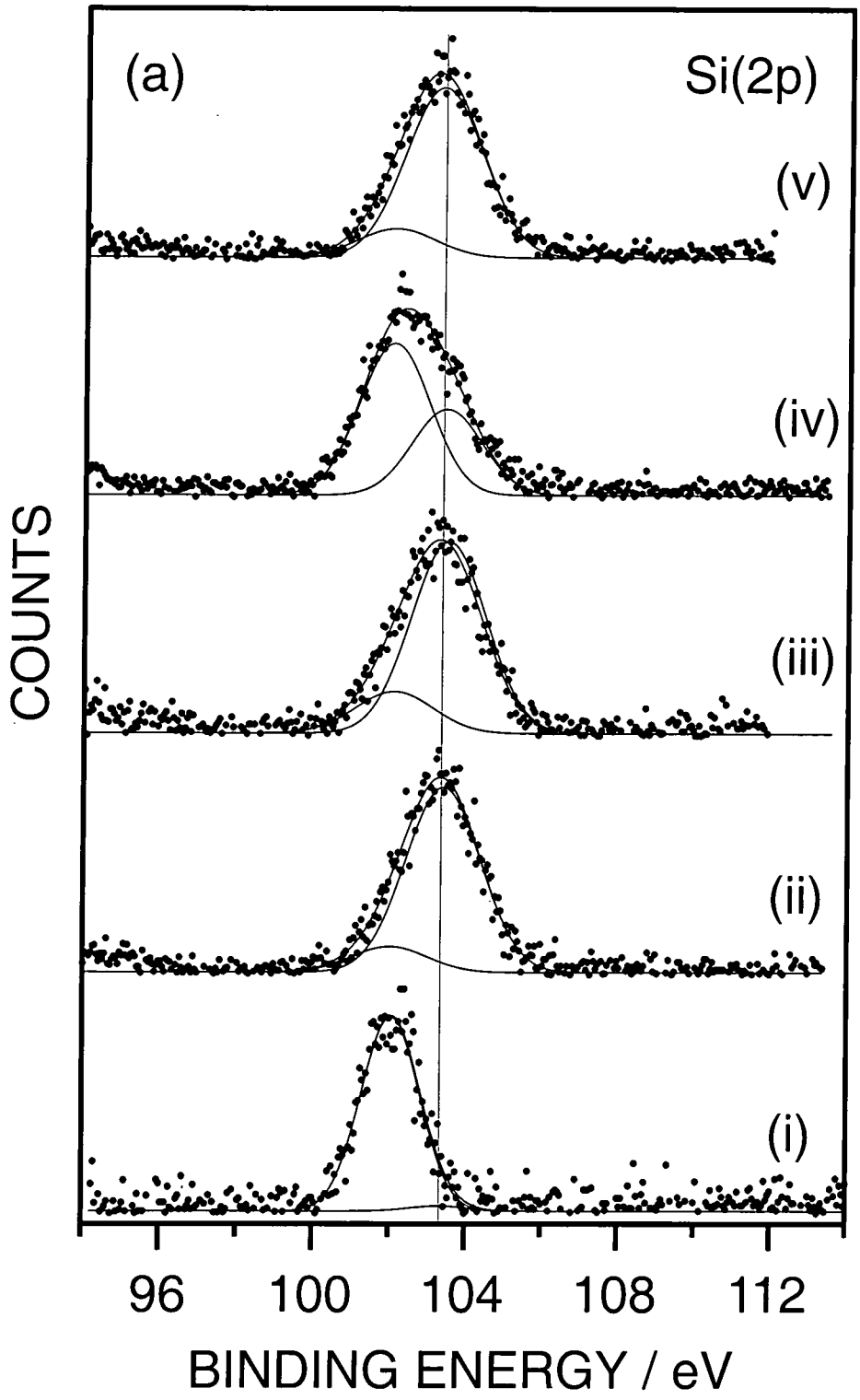

Figure 8a: Si(2p) XPS spectra of PDMS doped polypropylene film: (i) washed in 50 / 50 cyclohexane / propan-2-ol solvent mixture for 30 s and then heated at 80 °C for 30 min; (ii) 2 W O_2 plasma treatment for 60 s; (iii) 2 W O_2 plasma treatment for 60 s followed by washing in 50 / 50 cyclohexane / propan-2-ol solvent mixture for 30 s; (iv) 2 W O_2 plasma treatment for 60 s followed by annealing at 80 °C for 30 min; and (v) 2 W O_2 plasma treatment for 60 s followed by annealing at 80 °C for 30 min and then washing in 50 / 50 cyclohexane / propan-2-ol solvent mixture for 30 s. (All spectra have been normalised).

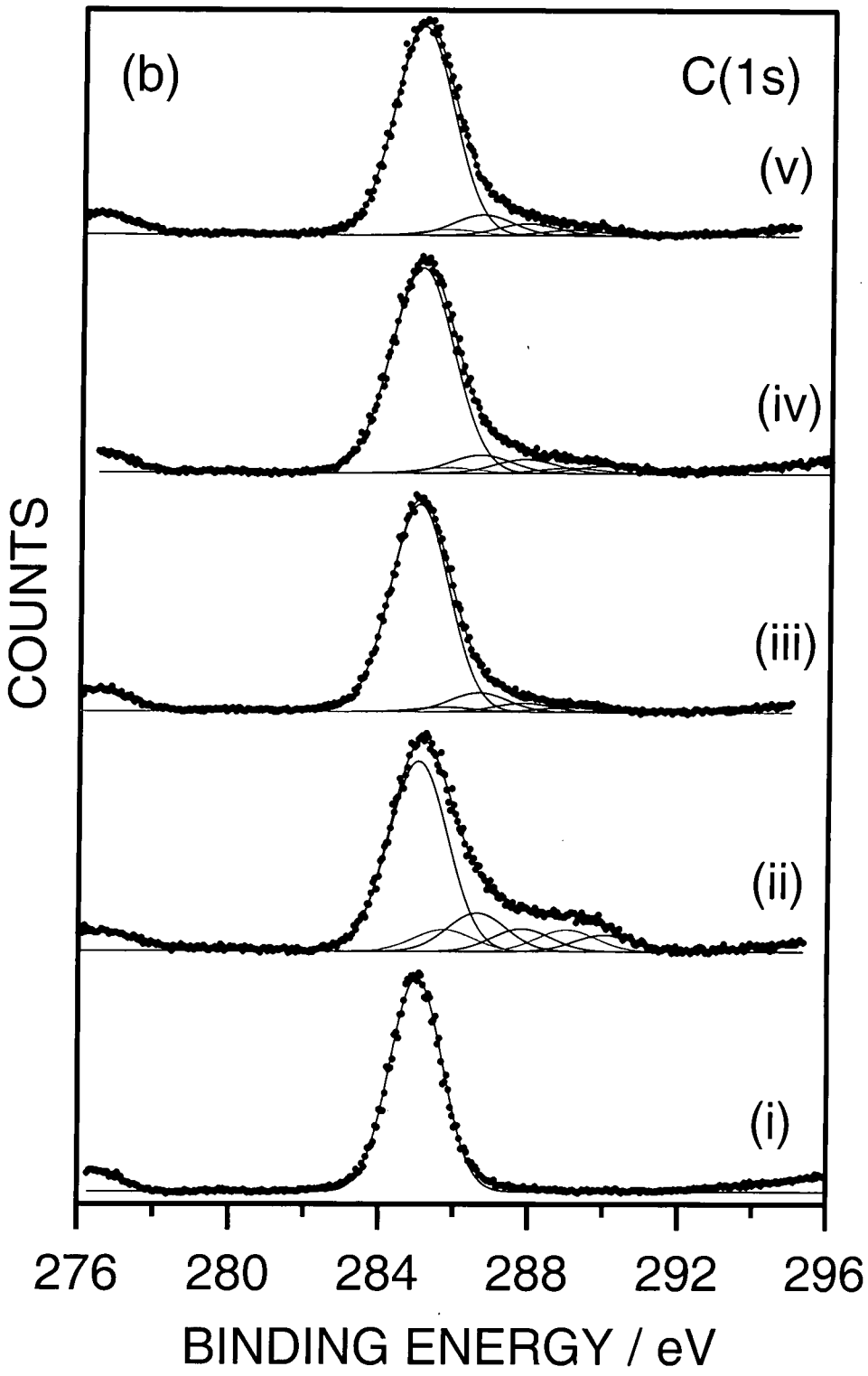

Figure 8b: C(1s) XPS spectra of PDMS doped polypropylene film: (i) washed in 50 / 50 cyclohexane / propan-2-ol solvent mixture for 30 s and then heated at 80 °C for 30 min; (ii) 2 W O_2 plasma treatment for 60 s; (iii) 2 W O_2 plasma treatment for 60 s followed by washing in 50 / 50 cyclohexane / propan-2-ol solvent mixture for 30 s; (iv) 2 W O_2 plasma treatment for 60 s followed by annealing at 80 °C for 30 min; and (v) 2 W O_2 plasma treatment for 60 s followed by annealing at 80 °C for 30 min and then washing in 50 / 50 cyclohexane / propan-2-ol solvent mixture for 30 s. (All spectra have been normalised).

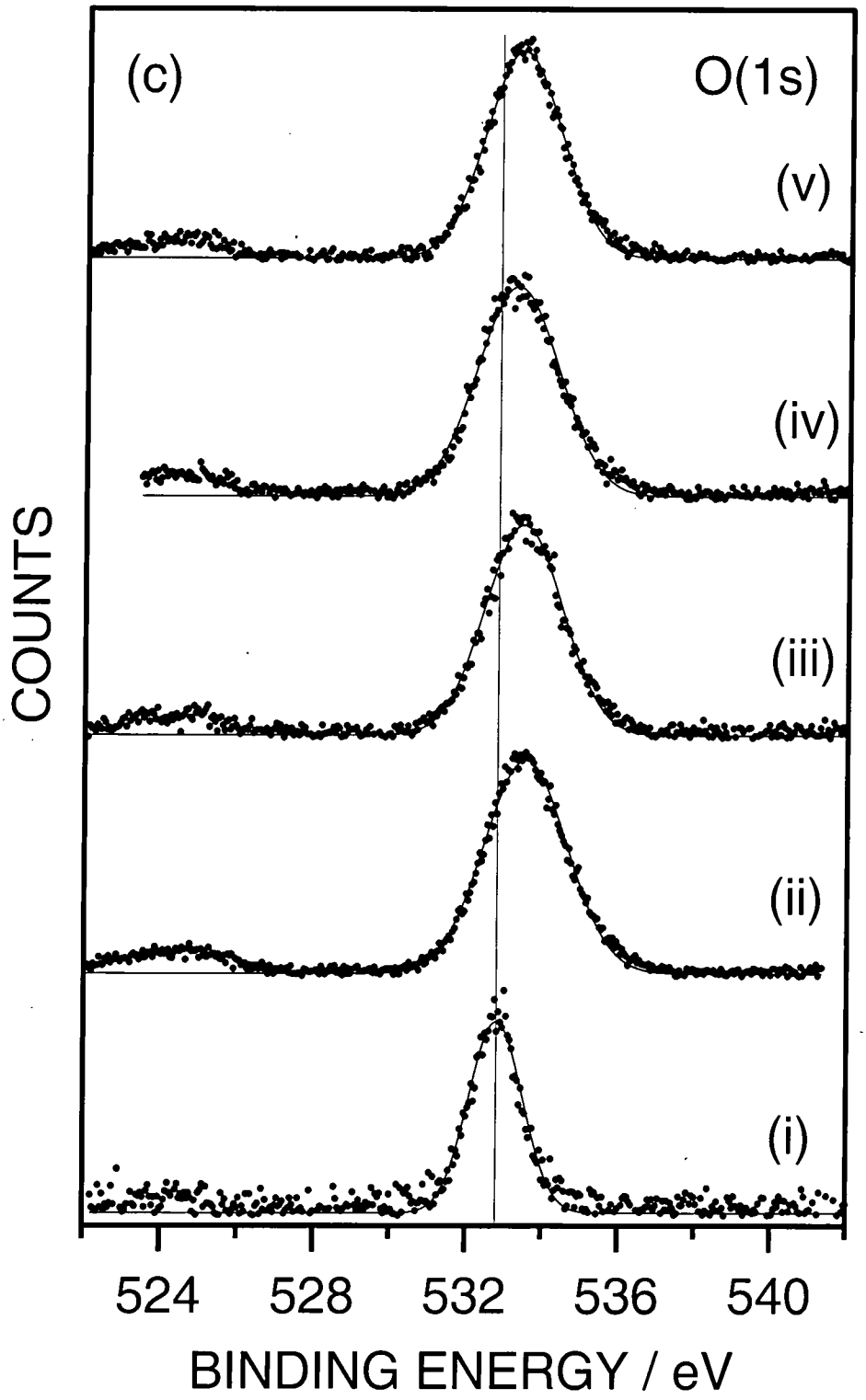

Figure 8c: O(1s) XPS spectra of PDMS doped polypropylene film: (i) washed in 50 / 50 cyclohexane / propan-2-ol solvent mixture for 30 s and then heated at 80 °C for 30 min; (ii) 2 W O_2 plasma treatment for 60 s; (iii) 2 W O_2 plasma treatment for 60 s followed by washing in 50 / 50 cyclohexane / propan-2-ol solvent mixture for 30 s; (iv) 2 W O_2 plasma treatment for 60 s followed by annealing at 80 °C for 30 min; and (v) 2 W O_2 plasma treatment for 60 s followed by annealing at 80 °C for 30 min and then washing in 50 / 50 cyclohexane / propan-2-ol solvent mixture for 30 s. (All spectra have been normalised).

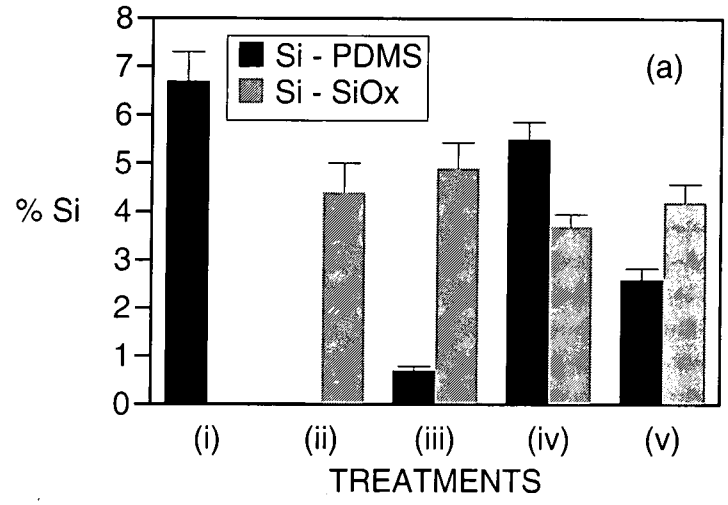

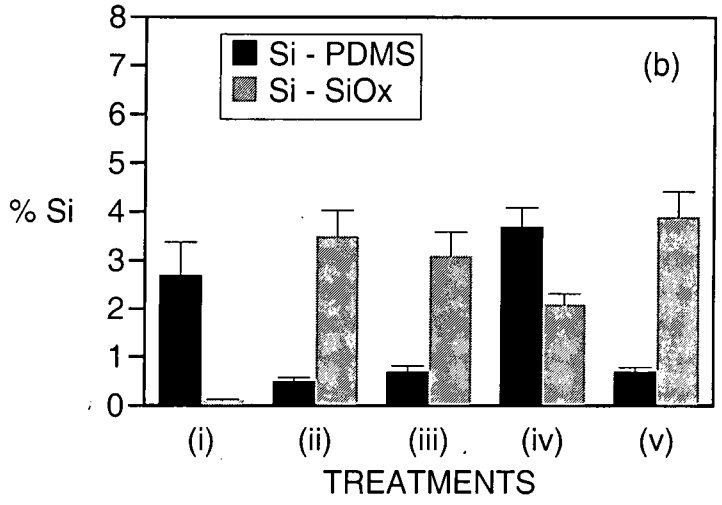

Figure 9: Relative amount of silicon associated with PDMS versus SiO_x at the surface of 2.5% PDMS doped (a) polyethylene; and (b) polypropylene: (i) solvent washed and then heated at 80 °C for 30 min; (ii) 2 W O_2 plasma treatment for 60 s; (iii) 2 W O_2 plasma treatment for 60 s followed by washing in 50 / 50 cyclohexane / propan-2-ol solvent mixture for 30 s; (iv) 2 W O_2 plasma treatment for 60 s followed by annealing at 80 °C for 30 min; and (v) 2 W O_2 plasma treatment for 60 s followed by annealing at 80 °C for 30 min and then washing in 50 / 50 cyclohexane / propan-2-ol solvent mixture for 30 s.

substrate). However, the amount of oxidised silicon species (SiO_x) appeared to be resilient towards solvent washing and annealing, rather it was the mobile polysiloxane constituent which altered the overall elemental silicon concentration detected by XPS at the surface.

Consecutive plasma oxidation followed by annealing cycles were undertaken in order to maximise SiO_x formation at the polymer blend surfaces, Figure 10. This reached limiting values after 4 cycles, with PDMS doped polyethylene yielding approximately twice as much SiO_x compared to its polypropylene counterpart.

Phase imaging atomic force microscopy clearly showed the presence of polysiloxane regions on the surface of the as-prepared films, Figure 11. Solvent washing caused these patches to disappear. Whilst subsequent annealing gave rise to the re-emergence of PDMS at the surface. Plasma oxidation produced silicon oxide domains which were found to be stable towards solvent washing. Repetitive annealing followed by oxygen plasma treatment cycles resulted in the build-up of silicon oxide moieties across the surface of the polysiloxane/polyethylene and polysiloxane/polypropylene blend films. Cross-sectional analysis of the PDMS/polyolefin blend films indicated that phase separation of PDMS domains had occurred within the bulk of the substrate, Figure 12.

Water contact angle measurements showed that the PDMS/polyolefin films which had undergone repetitive annealing / plasma oxidation cycling were more wettable and stable compared to the respective PDMS and polyolefin substrates, Figure 13.

2.4 DISCUSSION

There is a large difference in surface energy between polydimethylsiloxane and polyethylene / polypropylene (γ_{PDMS} = 24.0 mJ m^{-2}, γ_{PE} = 31.0 mJ m^{-2}, γ_{PP} = 34.0 mJ m^{-2}).[19] Therefore, one would expect the lower surface energy constituent, polysiloxane to segregate towards the surface of the PDMS / polyolefin blends under investigation. Indeed PDMS enrichment at the polymer blend surfaces does occur, with it being more prevalent in the case of polysiloxane / polyethylene compared to polysiloxane / polypropylene. However, the extent of surface segregation need not necessarily be proportional to the difference

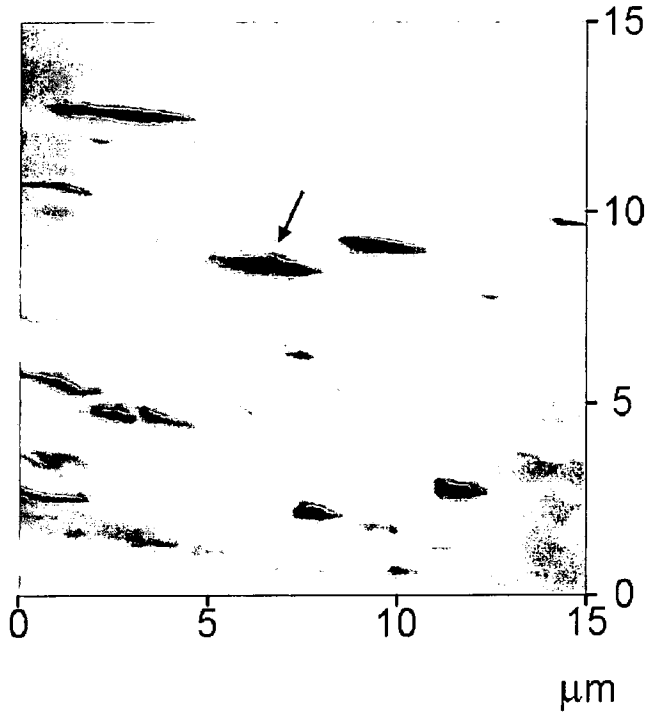

Figure 12: Cross-section AFM image of microtomed 2.5% PDMS doped polyethylene film.

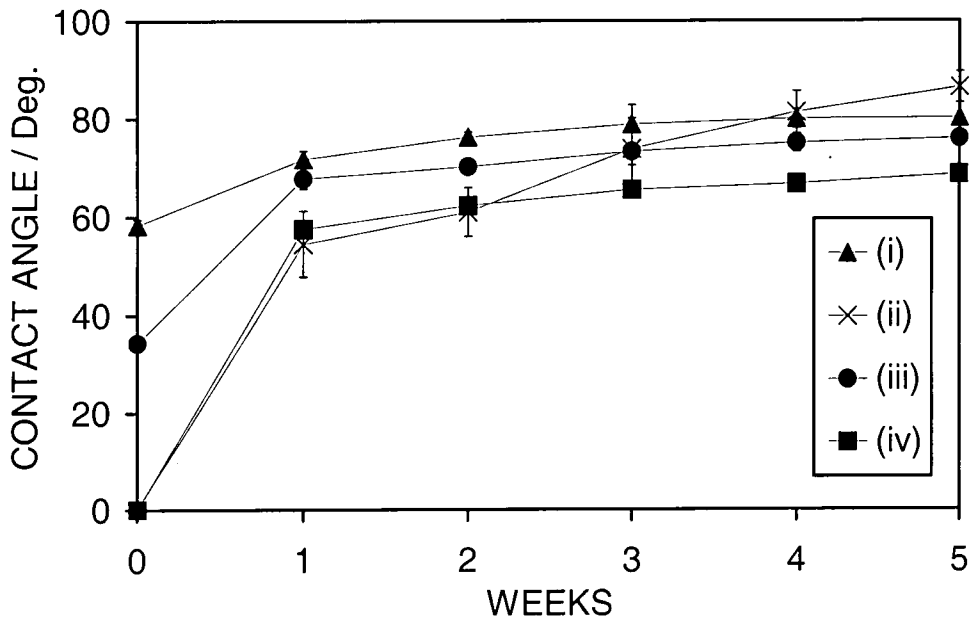

Figure 13: Water contact angle measurements as a function of ageing time: (i) 2W O_2 plasma treatment for 60 s of polyethylene; (ii) 2W O_2 plasma treatment for 60 s of PDMS; (iii) washed and annealed 2.5% PDMS doped polyethylene followed by 2W O_2 plasma treatment for 60 s; and (iv) 2W O_2 plasma treatment for 4 cycles of 2.5% PDMS doped polyethylene.

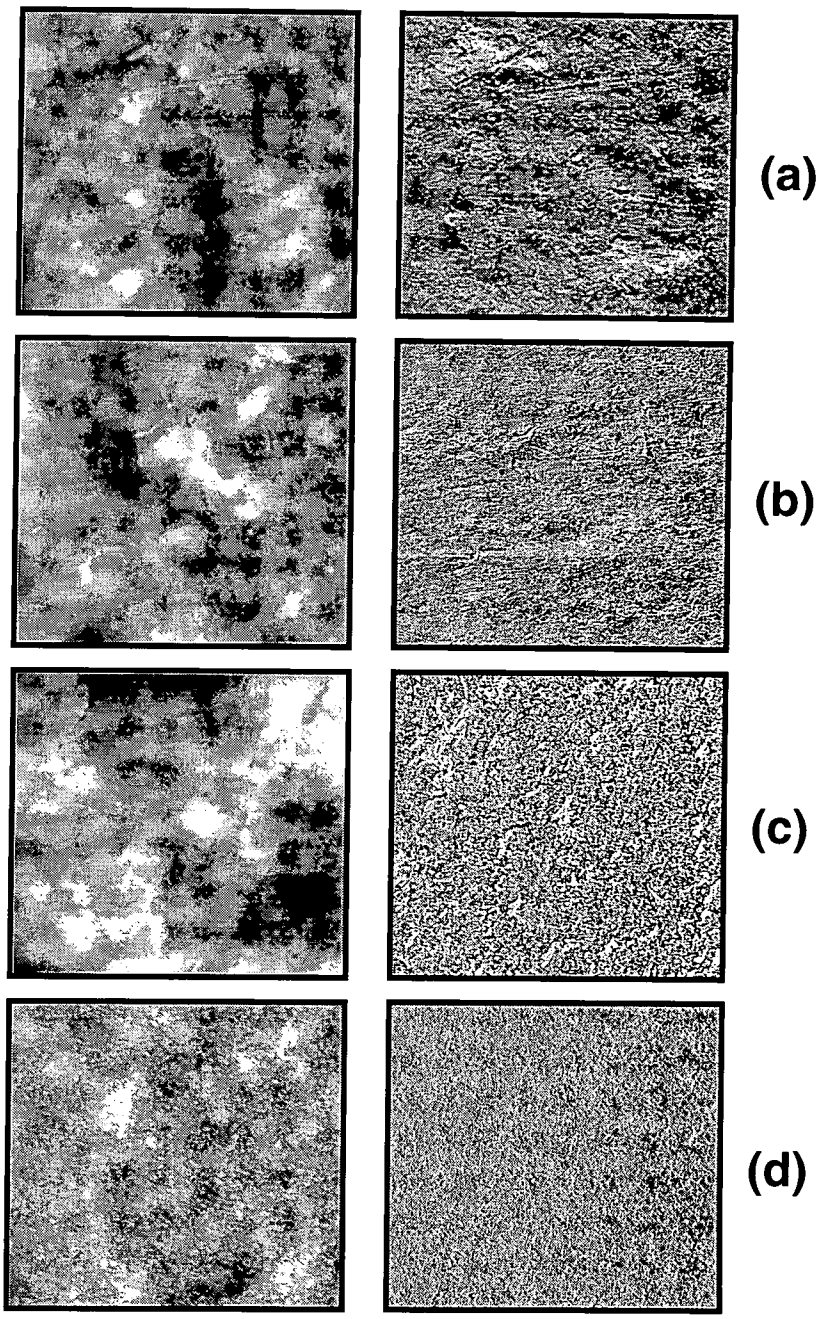

Figure 11: Atomic force phase images of 2.5% PDMS doped polyethylene: (a) before washing; (b) after solvent washing; (c) solvent washing followed by annealing at 80 °C for 30 min; and (d) 2W O_2 plasma treatment for 4 cycles (scan size = 20 μm).

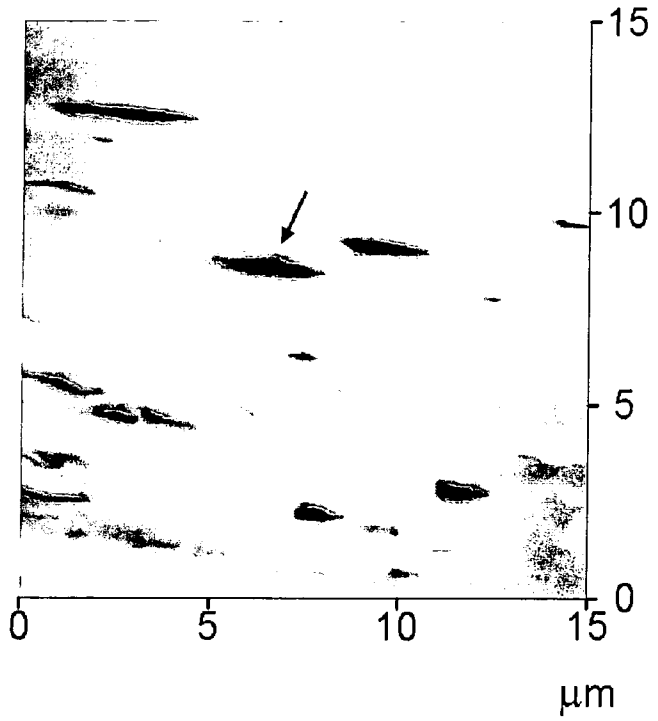

Figure 12: Cross-section AFM image of microtomed 2.5% PDMS doped polyethylene film.

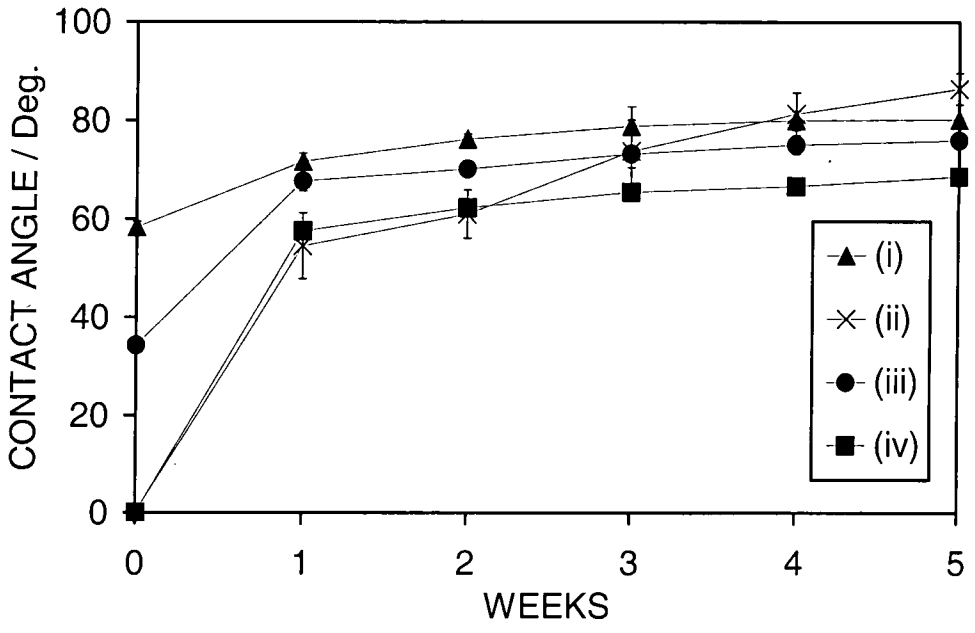

Figure 13: Water contact angle measurements as a function of ageing time: (i) 2W O_2 plasma treatment for 60 s of polyethylene; (ii) 2W O_2 plasma treatment for 60 s of PDMS; (iii) washed and annealed 2.5% PDMS doped polyethylene followed by 2W O_2 plasma treatment for 60 s; and (iv) 2W O_2 plasma treatment for 4 cycles of 2.5% PDMS doped polyethylene.

in surface energy.[20] In order to explain this difference, the bulk thermodynamics must be taken into consideration.

The overall behaviour of polymer blend surfaces is governed by entropic and enthalpic factors. Entropic contributions are dependent upon the molecular weight of the respective homopolymers contained in the blend. Whilst the enthalpic component is influenced by differences in surface energy as well as favourable versus unfavourable interactions between the blend constituents (which can be quantified by the Flory-Huggins interaction parameter - χ).[21] The χ_{12} interaction parameter is a measure of the difference in energy (enthalpy of mixing) between a chain of homopolymer *1* immersed in pure homopolymer *1* compared to when it is present in pure homopolymer *2*. This provides an indication of the likelihood for *1-1* and *2-2* interactions to be replaced by *1-2* interactions during mixing of the two homopolymers.[22] Negative values of χ_{12} predict miscibility, whereas positive values indicate immiscibility; with the magnitude corresponding to the strength of enthalpic interactions between the two homopolymers.[23] For incompatible polymers blends (χ_{12} is positive), and as explained above, the lower surface energy polymeric component migrates to the surface.[24] Silicone polymers are barely miscible in polyolefins and therefore the heat of mixing tends to be endothermic.[3] In this case, the interaction parameter can be approximated by reference to solubility parameters[22] using Equation 1:

$$\chi_{12} = \frac{V_R}{RT}(\delta_1 - \delta_2)^2 \qquad (1)$$

Where χ_{12} is the interaction parameter per segment of polymer, V_R is the reference segment volume that can be approximated by the smallest polymer repeat unit (for practical purposes it is often taken to be 100 $cm^3\ mol^{-1}$), and δ_i is the solubility parameter of polymer *i*. Substituting the values[19] δ_{PDMS} = 7.3 - 7.6 $(cal\ cm^{-3})^{1/2}$, δ_{PE} = 7.7 - 8.8 $(cal\ cm^{-3})^{1/2}$, and δ_{PP} = 9.2 - 9.4 $(cal\ cm^{-3})^{1/2}$ into Equation 1, it is found that $\chi_{12} = 4 \times 10^{-4} - 9 \times 10^{-2}$ for the PDMS / PE blend and $\chi_{12} = 11 - 18 \times 10^{-2}$ for the PDMS / PP blend, and therefore one would expect PDMS to be more incompatible with polypropylene compared to polyethylene, hence causing greater surface enrichment for the PDMS / polypropylene blend.

In fact, the opposite is found in practice, and therefore other factors must be influencing PDMS surface segregation, such as the polymer molecular weight,[25,26,27,28] crystallinity[24] of the films, and the kinetics of polymer chain diffusion towards the surface.[29]

For instance, polyethylene has a lower average molecular weight, glass transition temperature (T_g) and melting point (T_m) compared to polypropylene, Table 1. Annealing at 80 °C will produce greater segmental motion of the polyethylene polymeric chains compared to their polypropylene counterparts. Thus one would anticipate higher diffusion rates of PDMS towards the surface in the polyethylene matrix compared to its polypropylene counterpart at a given temperature. The experimental data appear to be consistent with this explanation up to near the melting point of polyethylene, Figure 2. At higher temperatures, the PDMS / PP system exhibits a drop in surface segregation, which is probably due to thermal desorption of low molecular volatile polysiloxane moieties from the polypropylene surface,[30] or alternatively, competitive migration of low molecular weight polypropylene chains towards the surface as a consequence of favourable kinetic, entropic, and surface energy factors.[3,26,27,28,31]

Non-isothermal plasma modification of such polymer blends is appealing from a technological perspective in terms of speed, cost, and minimal environmental impact. Plasma treatment of bulk polydimethylsiloxane has been widely explored in the past for improving its wettability[32,33] and adhesion.[33,34] However, there are associated drawbacks which include hydrophobic recovery and the formation of microcracks at the surface.[32,35] The current approach comprising heating-plasma treatment cycles produces comparable wetting behaviour to that observed for oxygen plasma treated bulk PDMS, however hydrophobic recovery is much slower (water contact angle of untreated PDMS = 116° ± 2), Figure 13.

2.5 CONCLUSIONS

Controlled surface segregation of PDMS from PDMS/polyolefin blend films can be achieved by solvent washing followed by annealing. Plasma oxidation of these surfaces gives rise to the formation of ultra thin layers of SiO_x.

2.6 REFERENCES

1 Feast, W. J.; Munro, H. S.; Richards, R. W. In *Polymer Surface and Interfaces*; Wiley: New York, 1993; Vol. 2.

2 Donald, A. M. *Nature* **1989**, *338*, 20.

3 Garbassi, F.; Morra, M.; Occhiello, E. In *Polymer Surfaces - From Physics to Technology*; Wiley: Chichester, 1994.

4 Murshall, U.; Speith, A.; Pfeiffer, H. DE 4031784, 1992.

5 Belloni, R.; Keung, J. K.; Keller, L. E. EP 411968, 1991.

6 MacLaury, M. R.; Schroll, A. L. *J. Appl. Polym. Sci.* **1985**, *30*, 461.

7 Gul, V. E.; Bulgakov, V. Y.; Pyatigorskaya, L. V.; Genel, S. V.; Kestel'man, V. N.; Shiler, G. G.; Konchakovskii, G. A. SU 834023, 1982.

8 Iyer, R.; Lile, D.L.; McConica, C.M. *J. Electrochem. Soc.* **1993**, *140*, 1430,

9 Schiller, S.; Neumann, M.; Morgner, H.; Schiller, N. *Society of Vacuum Coaters 36th Annual Technical Proceedings* **1993**, 278.

10 Johanson, G.; Hedman, J.; Berndtsson, A.; Klasson, M.; Nilsson, R. *J. Electron Spectr.* **1973**, *2*, 295.

11 Zhong, Q.; Innis, D.;Kjoller, K. Elings, V.B. *Surf. Sci.* **1993**, *14*, 3045

12 Magonov, S. N.; Elings, V. B.; Whangbo, M. H. *Surf. Sci.* **1997**, *375*, L385.

13 Clark, D. T.; Thomas, H. R. *J. Polym. Sci. Chem. Ed.* **1977**, *15*, 2843.

14 Beamson, G.; Briggs, D. In *High Resolution XPS of Organic Polymers: The Scienta ESCA300 Database*; Wiley: New York, 1992.

15 Moulder, J. F.; Stickle, W. F.; Sobol, P. E.; Bomben, K. D. In *Handbook of X-ray Photoelectron Spectroscopy*; Chastain, J., Ed.; Perkin-Elmer Corporation: Minnesota, 1992.

16 Clark, D. T.; Feast, J,; Dilks, A. *J. Polym. Sci. Chem. Ed.* **1979**, *17*, 957.

17 Pawson, D. J.; Ameen, A. P.; Short, R. D.; Denison, P.; Jones, F. R. *Surf. Interface Anal.* **1992**, *18*, 13.

18 Boyd, R.D.; Kenwright, A.M.; Briggs, D.; Badyal, J.P.S. *Macromolecules* **1997**, *30*, 5429.

19 *Polymer Handbook*; Brandrup, J., Immergut, E. H., Eds.; John Wiley & Sons: New York, 1989.

20 Jones, R. A. L.; Kramer, E. J. *Polymer* **1993**, *34*, 115.

21 Flory, P. J., In *Principles of Polymer Chemistry*; Cornell University Press: Ithaca, 1953.

22 Cowie, J. M. G. In *Polymers: Chemistry & Physics of Modern Materials*, 2nd ed.; Blackie Academic & Professional: London, 1991.

23 Cortazar, M. M.; Calahorra, M. E.; Guzman G. M. *Eur. Polym. J.* **1982**, *18*, 165.

24 Sakellariou, P. *Polymer* **1993**, *34*, 3408.

25 Shuto, K.; Oishi, Y.; Kajiyama, T.; Han, C. C. *Macromolecules* **1993**, *26*, 6589.

26 Bhatia, Q. S.; Pan, D. H.; Koberstein, J. T. *Macromolecules*, **1988**, *21*, 2166.

27 Hariharan, A.; Kumar, S. K.; Russell, T. P. *J. Chem. Phys.* **1993**, *99*, 4041.

28 Brant, P.; Karim, A.; Douglas, J. F.; Bates, F. S. *Macromolecules* **1996**, *29*, 5628.

29 Hwang, S. S.; Ober, C. K.; Perutz, S.; Iyengar, D. R.; Schneggenburger, L. A.; Kramer, E. J. *Polymer* **1995**, *36*, 1321.

30 Jovanovic, J. D.; Govedarica, M. N.; Dvornic, P. R.; Popovic, I. G. *Polymer Degratation and Stability* **1998**, *61*, 87.

31 Dee, G. T.; Sauer, B. B. *Macromolecules* **1993**, *26*, 2771.

32 Owen, M. J.; Smith, P. J. *J. Adhesion Sci. Technol.* **1994**, *8*, 1063.

33 Owen, M. J.; Stasser, J. L. *Polym. Prepr.* **1997**, *38*, 1087.

34 Morra, M.; Occhiello, E.; Garbassi, F.; Humphrey, P.; Johnson, D. *J. Colloid Interface Sci.* **1990**, *137*, 11.

35 Fritz, J. L.; Owen, M. J. *J. Adhes.* **1995**, *54*, 33.

CHAPTER 3

SURFACE SEGREGATION AND PLASMA OXIDATION OF POLYETHYLENE-POLYDIMETHYLSILOXANE COPOLYMER DOPED POLYETHYLENE FILMS

3.1 INTRODUCTION

There are two generic ways for modifying the surface properties of polymeric materials. Firstly, there are external methods, such as gas plasma treatment,[1] plasma coating deposition,[2] surface grafting,[3] and photochemistry.[4] Alternatively, surface segregation from within the material bulk can be utilized, e.g. polymer blend systems.[5] The latter typically entails blending two homopolymers (A) and (B), or mixing a block copolymer (AB) with a homopolymer (A). A strong perturbation of the surface versus bulk composition occurs if the polymer / polymer segment (B) has a lower surface energy compared to the host homopolymer / block (A). The overall driving force in this case is a net lowering of the surface tension for the polymer blend system leading to the surface enrichment of B relative to its bulk concentration. The degree and spatial distribution of polymer segregation at the air-solid interface is governed by a number of factors. These include bulk composition, molecular weight of the constituents (block length and architecture in the case of copolymers), and processing conditions.[6] A major advantage of using copolymers instead of homopolymers is considered to be the fact that potentially better anchoring of the surface segregant (adhesion) to the host bulk polymer can be achieved via the copolymer segment (A).[7,8] Otherwise there exists the danger of the active polymeric constituent undergoing complete phase separation or leaching out from the host homopolymer.

Polydimethylsiloxane (PDMS) is considered to have a low surface tension (γ_{PDMS} = 24.0 mJ m^{-2}).[9] Therefore PDMS is often chosen as a homopolymer or included as a segment in block copolymers for mixing into polymer blend systems.[10] Typically this leads to surface enrichment of the PDMS component. For instance, numerous polydimethylsiloxane copolymer / homopolymer blend mixtures have been studied in the past, examples include PDMS-co-poly(methyl methacrylate) / poly(methyl methacrylate),[11] PDMS–co-polyurethane / phenoxy,[12] PDMS-co-Bisphenol A Polycarbonate / Bisphenol A Polycarbonate,[13] and PDMS-co-polystyrene / polystyrene.[14]

Subsequent oxygen plasma treatment of siloxane-rich polymer surfaces is a potentially attractive route for making ultrathin inorganic silica-like layers. In the case of PDMA-containing polymer blend systems, the primary advantage is that the precursor material is already available at the polymer surface (rather

than having to resort to external line-of-sight deposition techniques). Potential applications of such thin oxide layers include hydrophilicity and adhesion.

In this chapter, the surface segregation behaviour of a polyethylene-co-polydimethylsiloxane-co-polyethylene ABA copolymer blended with polyethylene homopolymer is described. Plasma oxidation of these siloxane enriched surfaces to form silica-like material has also been investigated.

3.2 EXPERIMENTAL

$A_{30}B_{30}A_{30}$ triblock polyethylene-*co*-polydimethylsiloxane-*co*-polyethylene copolymer (Dow Corning, M_n = 420 for the PE blocks, and M_n = 2200 for the PDMS block) was mixed with linear low density polyethylene / low density polyethylene (Dow Corning, LLDPE / LDPE, M_n = 29000) during film extrusion via the bubble-film process to give 2.5% wt% PDMS in the bulk. Solvent washing studies of these polymer blend films were carried out using a 50/50 mixture of cyclohexane (BDH, 99.5 % purity) / propan-2-ol (BDH, 99.7 % purity) for 30 s. Subsequent annealing experiments entailed placing the washed films in a vacuum oven (LTE, Qualivac).

Plasma treatment of the polymer blend surfaces was performed using an inductively coupled cylindrical glass reactor (5 cm diameter, 650 cm^3 volume) enclosed in a Faraday cage, Figure 1. This was fitted with a gas inlet, a thermocouple pressure gauge, a heated substrate stage controlled by a thermostatic circulation bath, and a two-stage mechanical rotary pump attached to a liquid air cold trap, (base pressure of 2×10^{-2} mbar and a leak rate better than 1.2×10^{-3} cm^3 min^{-1}). The temperature of the substrate was monitored with a thermocouple probe. A 13.56 MHz RF power supply was coupled to a copper coil (5 mm diameter, 10 turns, spanning 8-16 cm from the gas inlet) wound externally around the reactor via an LC matching circuit. Prior to each experiment, the chamber was cleaned with a 40 W air plasma at 0.2 mbar pressure for 10 min. Next, a piece of polymer substrate was placed into the centre of the reactor, and oxygen (BOC, 99.6 % purity) introduced at a pressure of 0.2 mbar and 1 cm^3 min^{-1} flow rate for 10 min, followed by plasma ignition. Continuous wave oxygen plasma treatment was carried out for 60 s at 0.2 mbar pressure for powers ranging from 2 - 20 W. In the case of the pulsed plasma exposure, the conditions comprised, t_{on} varying between 50 - 2000 μs, t_{off} varying between 100 - 50000 μs, and peak power set at 20 W (the oxygen gas

pressure and treatment time were kept the same as for continuous wave experiments).

A Kratos ES300 electron spectrometer equipped with a Mg Kα X-ray source (1253.6 eV), and a concentric hemispherical analyser (CHA) was used for XPS analysis of the polymer blend surfaces. Photo-emitted electrons were collected at a take-off angle of 30° from the substrate normal, with electron detection in the fixed retarding ratio (FRR, 22:1) mode. XPS spectra were accumulated on an interfaced PC computer and fitted using a Marquardt minimisation algorithm assuming Gaussian peak-shapes with equal full-width-at-half-maximum (FWHM).[15] Instrument sensitivity factors were calculated using reference chemical standards to be C(1s) : O(1s) : Si (2p) equals 1.00 : 0.57 : 0.72. An argon ion gun source was used for ion sputter depth profiling studies (operating at 3 keV ion energy, 1.5 μA beam current, and 2×10^{-6} mbar pressure). The etch rate was calibrated to be 0.5 nm min^{-1} by using a known thickness of SiO_2 (as measured by ellipsometry) grown onto a silicon wafer.

AFM micrographs were acquired with a Digital Instruments Nanoscope III. Damage to the tip or sample was minimised by using Tapping Mode AFM.[16] As well as topographical height images, phase images reflecting the mechanical properties of the surface were obtained by choosing a setpoint: free amplitude ratio of 0.5 (setpoint = 50 nm; free amplitude = 100 nm).[17] All images were acquired in air at room temperature and are presented as unfiltered data. Large area scans were taken on the 100 μm scale in order to check that the images presented are representative of the whole surface.

Sessile drop contact angle measurements were carried out at 20 °C using a video capture apparatus (A.S.T. Products VCA2500XE). High purity water (B.S. 3978 Grade 1) was employed as the probe liquid to test hydrophilicity/hydrophobicity of the polymer blend surfaces.

3.3 RESULTS

Washing of the polymer blend surface with a 50 / 50 cyclohexane / propan-2-ol solvent mixture for 30 s was sufficient to remove most of the polysiloxane species from the top 3-5 nm of the substrate (i.e. the Si(2p) XPS sampling depth),[18] Table 1. Subsequent annealing at 80 °C for 30 min led to polysiloxane

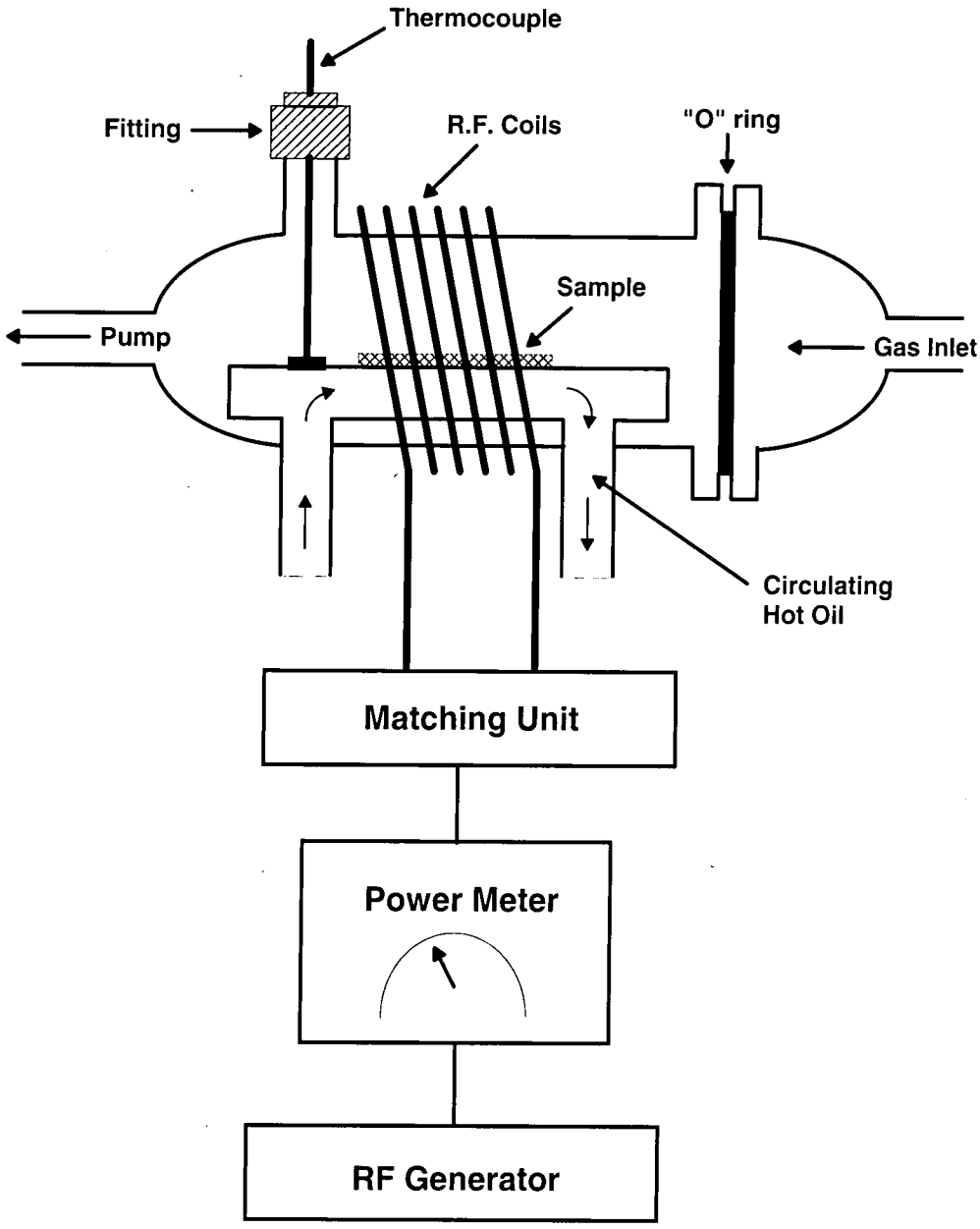

Figure 1: Schematic of heated substrate plasma reactor.

Table 1: XPS analysis summarising changes in elemental composition and SiO_x content at the surface of ABA copolymer doped polyethylene film (2.5 wt % PDMS in the bulk).

Treatment	Elemental %			Si(2p)			% SiO_x		
	%C	%O	%Si	PDMS	$SiO_{3/2}$	$SiO_{4/2}$	%$SiO_{3/2}$	% $SiO_{4/2}$	Total
Theoretical bulk composition	99.0	0.5	0.5	0.5	-	-	-	-	-
as received (1)	71.3	15.5	13.2	13.2	-	-	-	-	-
washed (2)	92.5	4.3	3.2	3.2	-	-	-	-	-
washed and annealed (3)	63.7	18.2	18.1	18.1	-	-	-	-	-
(3) + 2 W O_2 plasma	31.7	49.3	18.9	2.7	9.1	7.2	22.8	21.6	44.4
(2) + 2 W O_2 plasma (h.s)	47.6	31.4	21.1	7.8	6.0	7.3	15.0	21.9	36.9
(3) + 20 W O_2 pulsed plasma t_{on} = 120 μs, t_{off} = 1360 μs	35.5	46.3	18.2	3.7	8.3	6.1	20.8	18.3	39.1
(2) + 20 W O_2 pulsed plasma (h.s) t_{on} = 120 μs, t_{off} = 1360 μs	26.1	52.6	21.4	0.9	8.6	11.9	21.5	35.7	57.2

h.s. : heated substrate

material diffusing from the bulk into the near-surface region. The absence of any binding energy shift in the XPS Si(2p) spectra confirmed that the PDMS component was not undergoing oxidation during annealing, Figure 2. By using this washing/annealing procedure, a reproducible polymer blend surface composition could be produced.

Oxygen plasma treatment of the washed and annealed copolymer doped polyethylene film gave rise to oxygen incorporation at the expense of carbon loss (although not much change in the concentration of silicon at the surface was observed), Table 1. The relative amounts of oxygenated silicon environments were estimated by fitting the Si(2p) envelope:[19] $\underline{Si}O_{PDMS}$ at 102.0 eV, $\underline{Si}O_{3/2}$ at 103.0 eV, and $\underline{Si}O_2$ at 104.0 eV, Figure 2 and Table 1. The greatest amount of SiO_x formation corresponded to oxygen plasma treatment at 80 °C using pulsed conditions, Table 1. The optimum duty cycle t_{on} and t_{off} settings for the pulsed discharge were obtained using computer aided simplex optimisation (Multisimplex™). It was found that t_{off} has a greater influence on SiO_x formation at the polymer blend surface compared to t_{on}, Figure 3.

Ar^+ ion depth profiling of the pulsed plasma treated ABA copolymer doped polyethylene samples confirmed the existence of a thin, highly oxidised layer at the surface (1.3 nm) followed by a drop in oxidation below the surface, Figure 4. This was consistent with there being surface enrichment of PDMS segments during annealing, Table 1.

Heating of the plasma oxidised polymer blend surface beyond electrical discharge extinction produced a progressive build up of PDMS material at the surface. This was evident from the shift in the Si(2p) peak towards lower binding energies: 104.0 eV ($\underline{Si}O_2$) to 102.0 eV ($\underline{Si}O_{PDMS}$), Figure 5. A drop in intensity of the oxidised C(1s) shoulder was also noted:[20] $\underline{C}–CO_2$ at 285.7 eV, $\underline{C}$–O– at 286.6 eV, $\underline{C}$=O, O–$\underline{C}$–O at 287.8 eV, –O–$\underline{C}$=O at 289.0 eV, and –O–$\underline{C}$O–O– at 290.0 eV, to leave behind a hydrocarbon-rich environment centred at 285.0 eV, Figure 5 and Table 2.

Polyethylene lamellar features could be clearly seen in the height image[21] following solvent washing of the polymer blend surface, Figure 6. The corresponding phase image confirmed the absence of PDMS at the surface. Subsequent annealing clearly showed the build-up of separate PDMS-rich regions on the polyethylene surface in the AFM phase image, whereas no

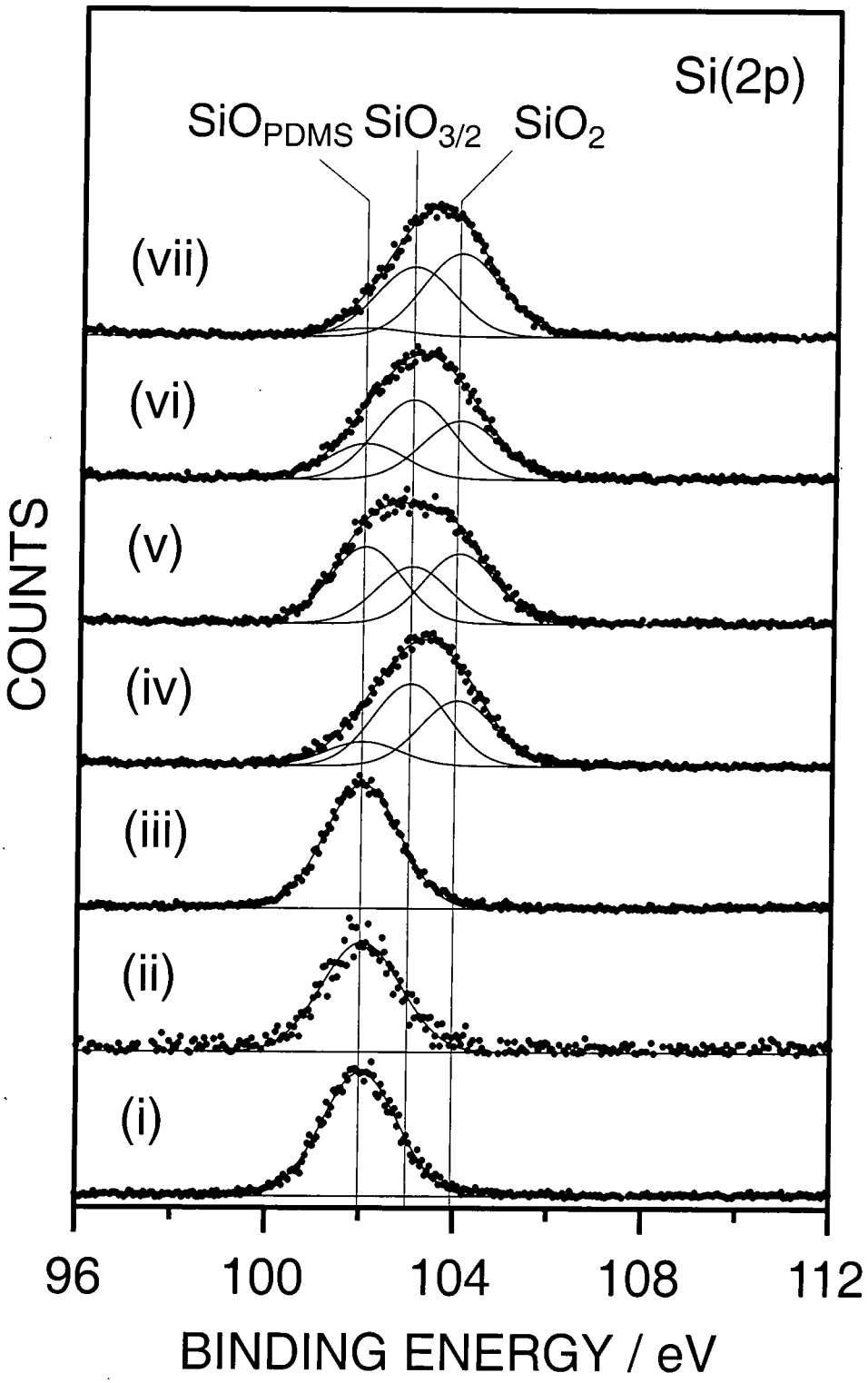

Figure 2: Si(2p) XPS spectra of 2.5% $A_{30}B_{30}A_{30}$ copolymer doped polyethylene blend: (i) as received; (ii) washed; (iii) washed and annealed; (iv) 2 W O_2 plasma treatment of (iii) for 60 s at room temperature; (v) 2 W O_2 plasma treatment of (ii) for 60 s - heated substrate; (vi) O_2 pulsed plasma (P_p = 20 W, t_{on} = 120 μs, t_{off} = 1360 μs) of (iii) for 60 s at room temperature; (vii) O_2 pulsed plasma (P_p = 20 W, t_{on} = 120 μs, t_{off} = 1360 μs) of (ii) for 60 s - heated substrate. (Note that all Si(2p) peak areas have been normalised to 100%).

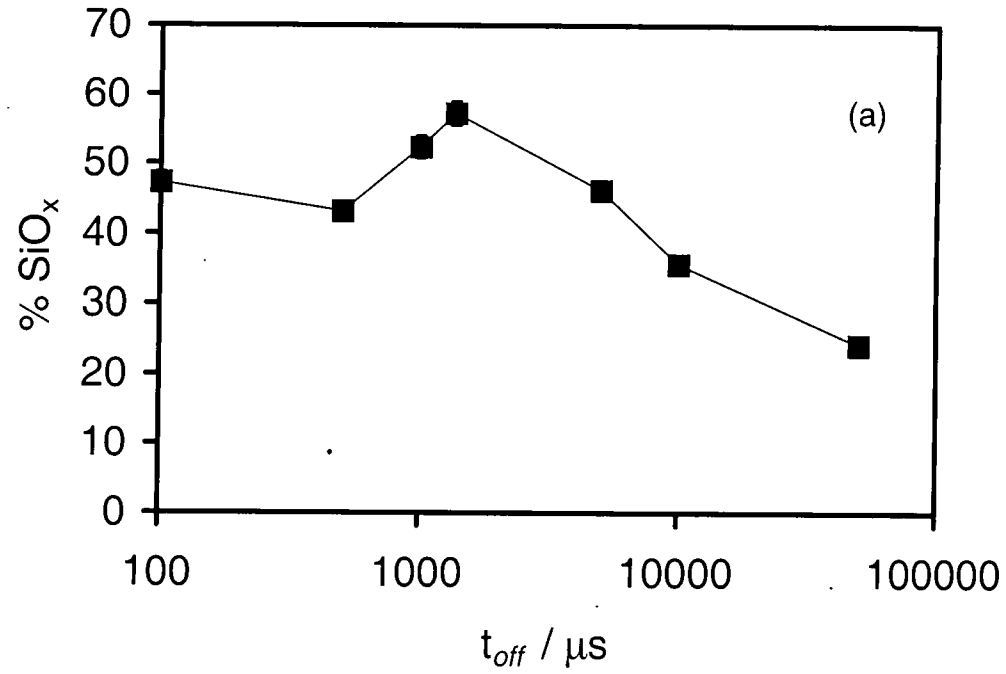

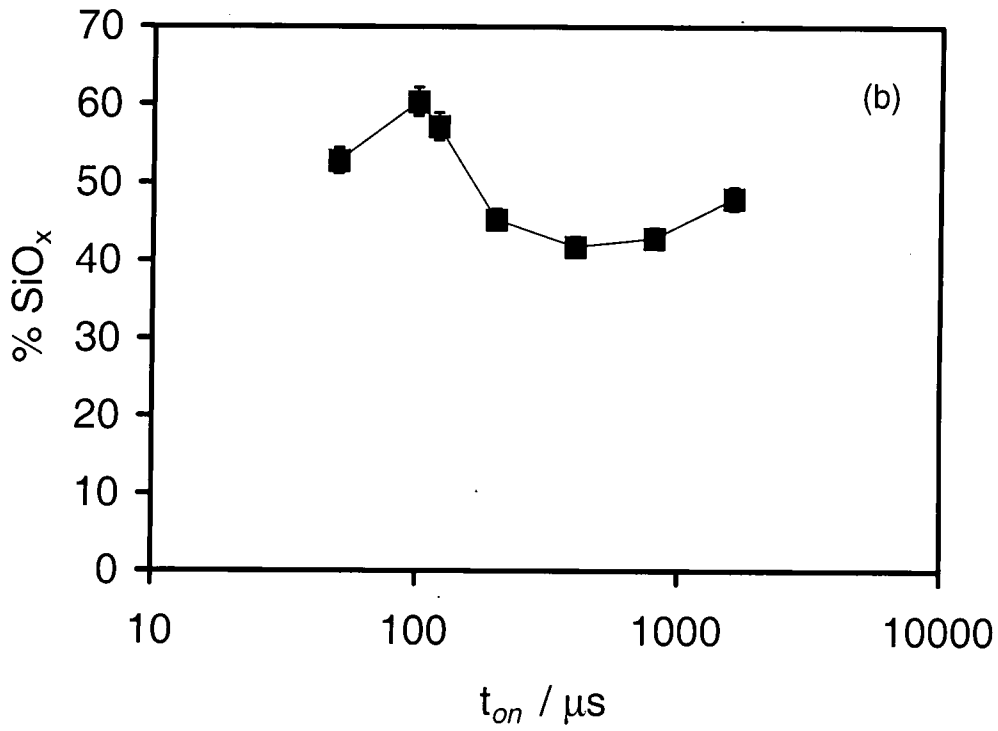

Figure 3: Proportion of silicon present as SiO_x at the surface as a function of (a) t_{off} (P_p = 20 W, t_{on} = 120 μs, substrate heated to 80 °C, total duration = 60 s); and (b) t_{on} (P_p = 20 W, t_{off} = 1360 μs, substrate heated to 80 °C, total duration = 60 s).

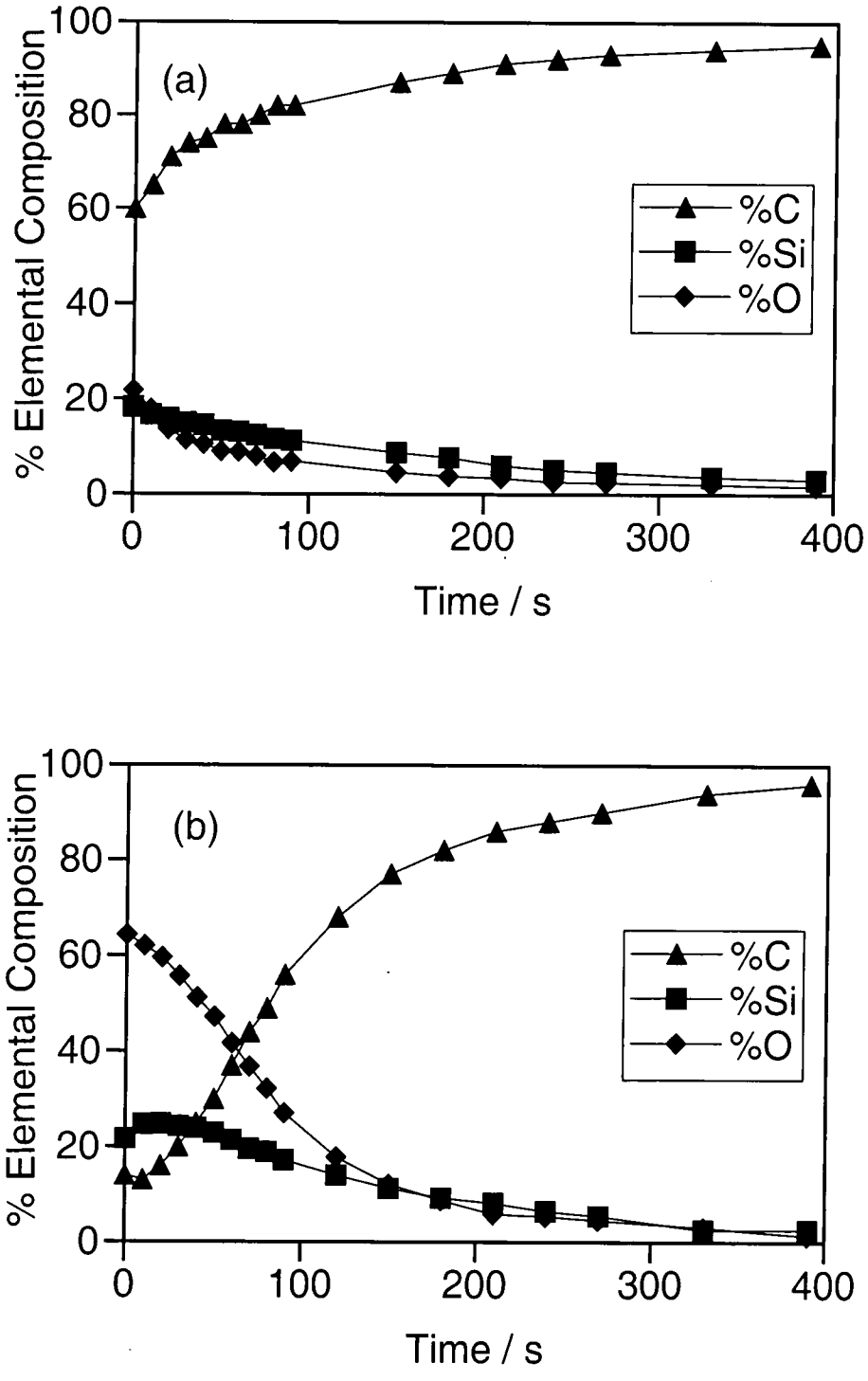

Figure 4: Depth profile of: (a) washed and annealed $A_{30}B_{30}A_{30}$ copolymer doped polyethylene blend; and (b) oxygen plasma treated $A_{30}B_{30}A_{30}$ copolymer / PE blend (P_p = 20 W, t_{on} = 120 μs, t_{off} 1360 μs, 60 s, substrate heated to 80 °C).

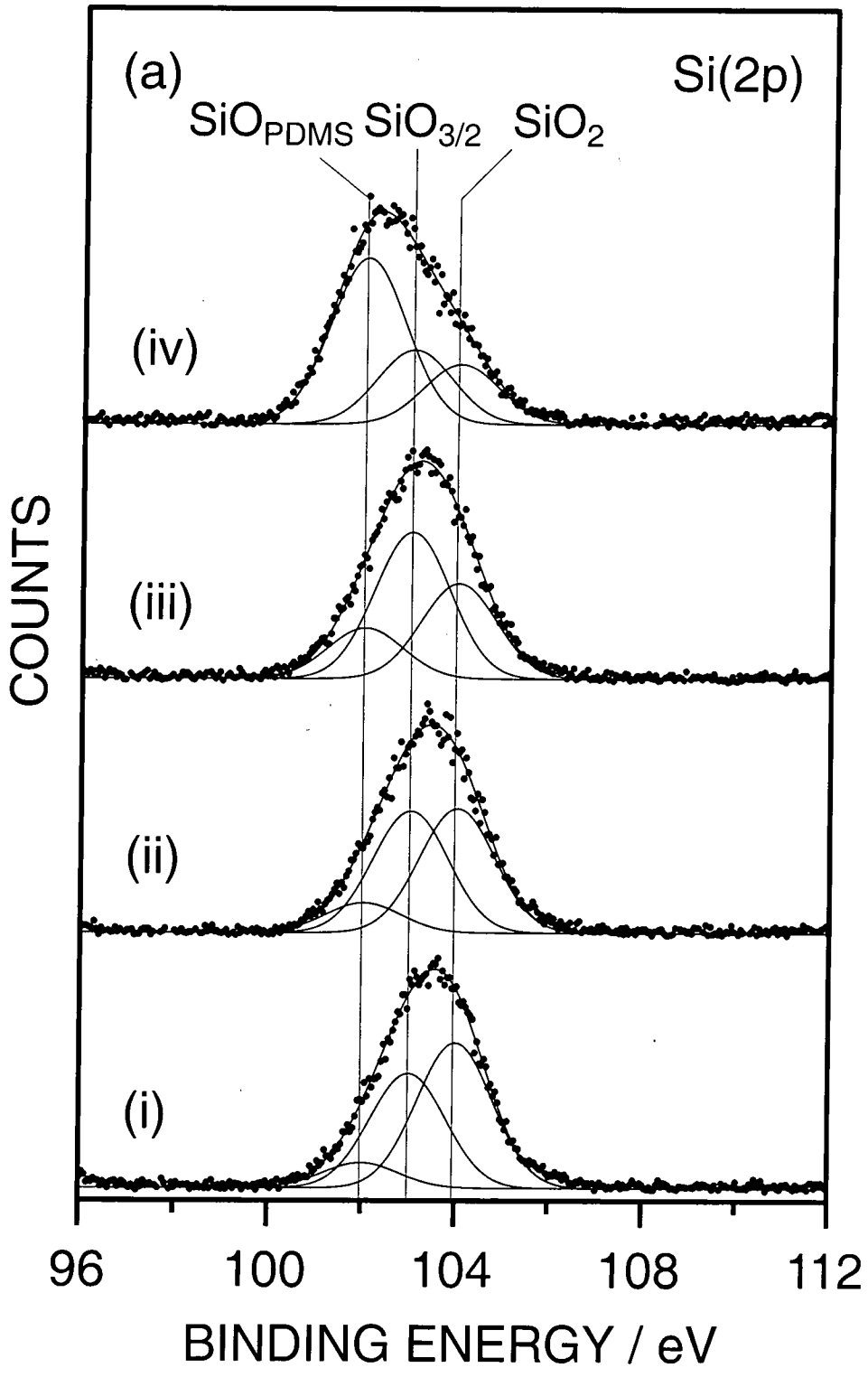

Figure 5a: Si(2p) XPS spectra of 2.5% $A_{30}B_{30}A_{30}$ copolymer doped polyethylene blend: (i) O_2 pulsed plasma treatment (P_p = 20 W, t_{on} = 120 μs, t_{off} = 1360 μs, substrate heated to 80 °C); (ii) annealing of (i) at 80 °C for 10 min: (iii) annealing of (i) at 80 °C for 30 min; and (iv) annealing of (i) at 80 °C for 41 hours. (Note that the XPS peak areas have been normalised to 100%).

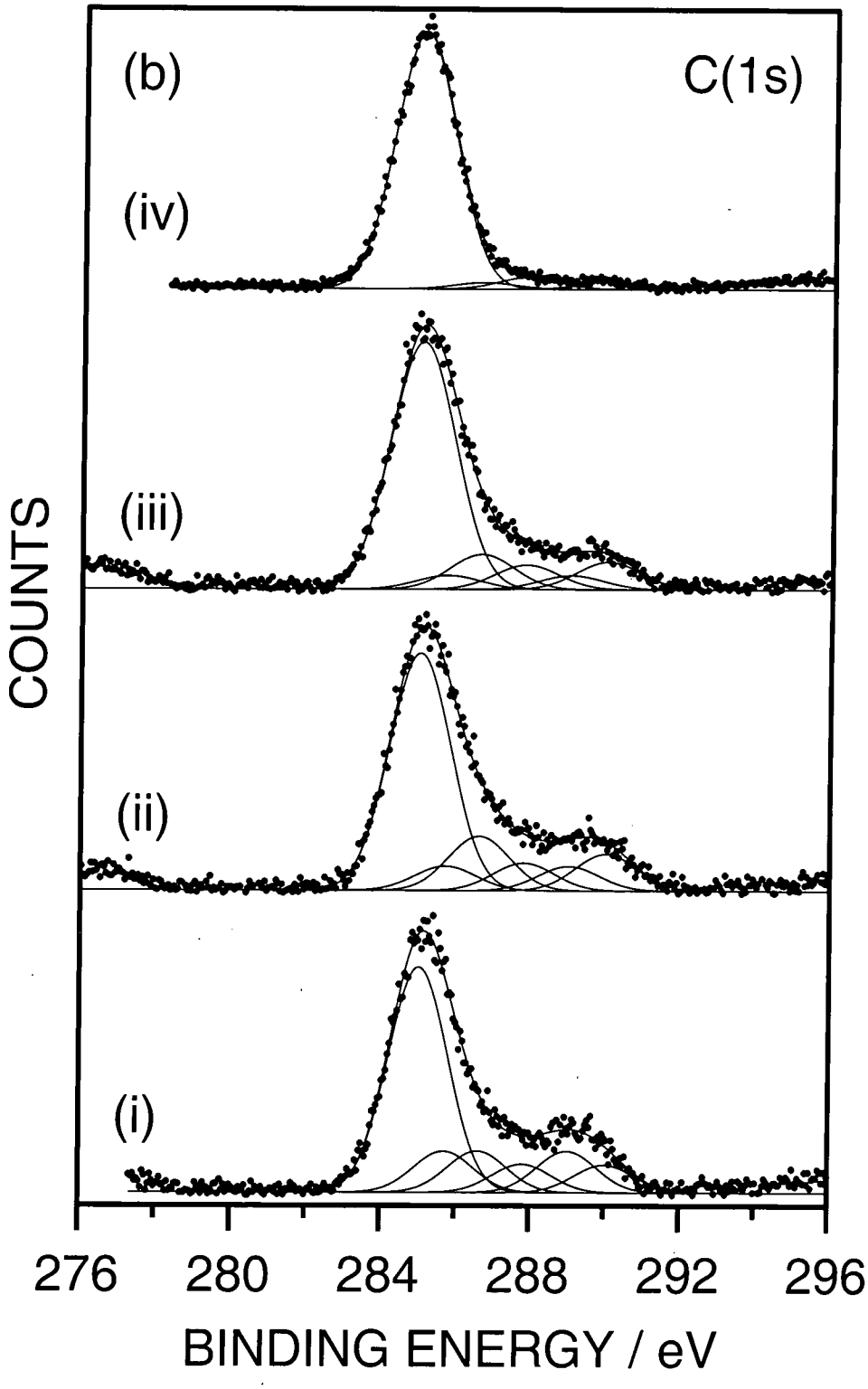

Figure 5b: C(1s) XPS spectra of 2.5% $A_{30}B_{30}A_{30}$ copolymer doped polyethylene blend: (i) O_2 pulsed plasma treatment (P_p = 20 W, t_{on} = 120 μs, t_{off} = 1360 μs, substrate heated to 80 °C); (ii) annealing of (i) at 80 °C for 10 min: (iii) annealing of (i) at 80 °C for 30 min; and (iv) annealing of (i) at 80 °C for 41 hours. (Note that the XPS peak areas have been normalised to 100%).

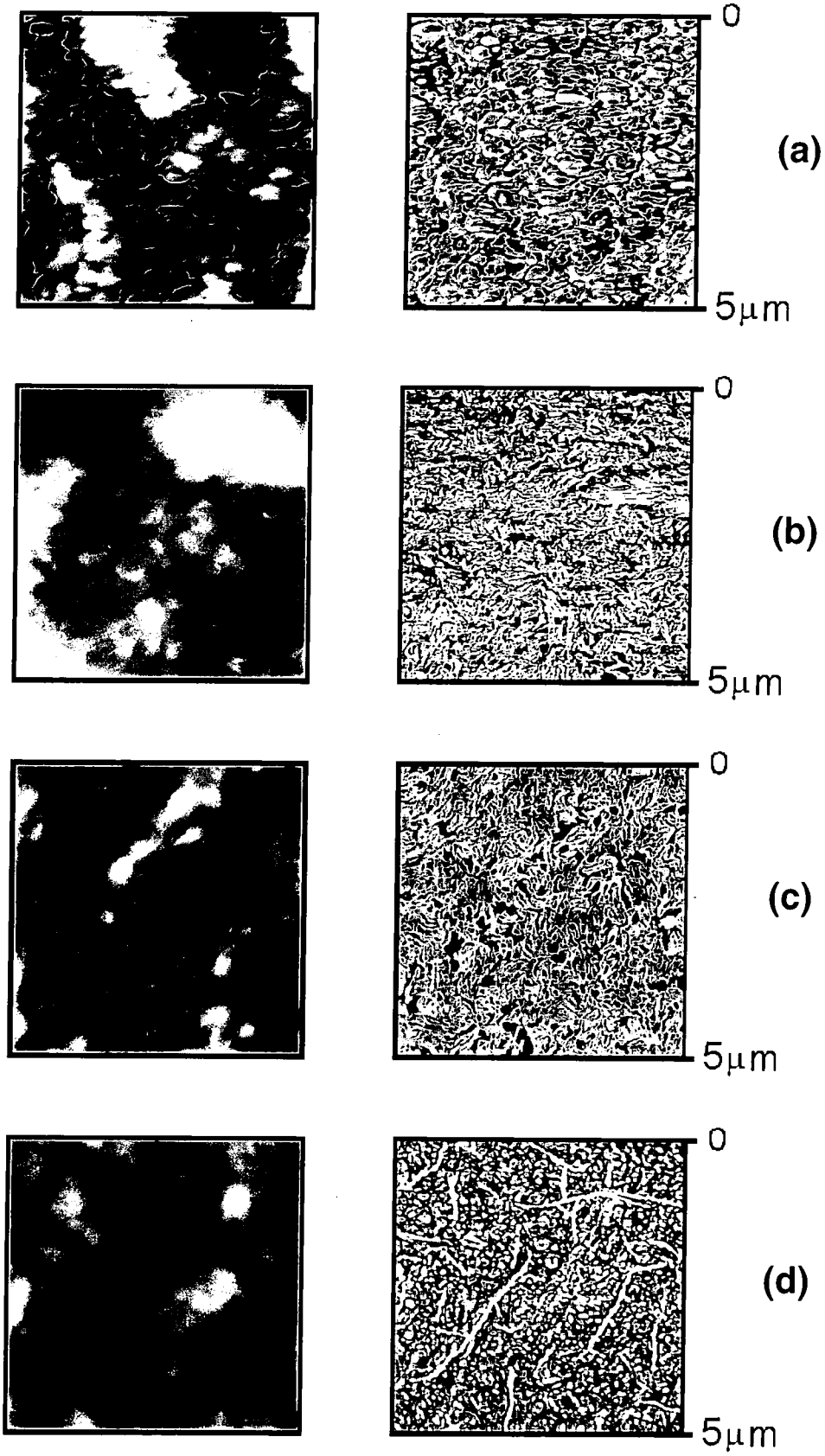

Figure 6: Atomic force micrographs of 2.5% $A_{30}B_{30}A_{30}$ copolymer doped polyethylene blend: (a) solvent washed; (b) solvent washed and annealed at 80 °C for 30 min; (c) solvent washed followed by O_2 pulsed plasma treatment (P_p = 20 W, t_{on} = 120 μs, t_{off} = 1360 μs, substrate heated to 80 °C); and (d) annealing of (c) at 80 °C for 30 min.

Table 2: XPS analysis summarising changes in elemental composition at the surface of the pulsed plasma oxidised $A_{30}B_{30}A_{30}$ doped polyethylene upon annealing.

Treatment	%C	%Si	%O	O/Si
washed and annealed	63.7	18.1	18.2	1.0
20 W O_2 pulsed plasma (h.s) t_{on} = 120 μs, t_{off} = 1360 μs (1)	26.1	21.4	52.6	2.5
(1) + heating at 80 °C for 10 min	31.6	19.1	49.2	2.6
(1) + heating at 80 °C for 30 min	32.9	20.1	47.1	2.3
(1) + heating at 80 °C for 41 hours	53.8	19.6	26.6	1.4

Table 3: Water contact angle measurements of $A_{30}B_{30}A_{30}$ doped polyethylene blend surfaces.

Treatment	Contact angle / deg		
	$A_{30}B_{30}A_{30}$/PE	PDMS	PE
As received	107.0 ± 1.0	116.0 ± 2.0	102.8 ± 0.5
Washed and annealed at 80 °C for 30 min	109 ± 1.0	-	-
20 W O_2 pulsed plasma (h.s) t_{on} = 120 μs, t_{off} = 1360 μs (1)	0.0 ± 0.0	0.0 ± 0.0	61.8 ± 1.0
(1) + 1 week at room temperature	46.0 ± 2.5	43.8 ± 1.7	76.2 ± 1.8
(1) + annealed at 80 °C for 30 min	43.5 ± 3.5	-	-

change was apparent in the corresponding height scan. No discernible change in surface morphology was noted following pulsed plasma oxidation at elevated substrate temperature, this can be taken as being consistent with a very thin layer of SiO_x-like material being formed at the polymer blend surface. Subsequent annealing gave rise to the appearance of cracks and small droplet-like regions of PDMS-containing material. This correlates to the emergence of PDMS moieties in the Si(2p) XPS envelope, Figure 5.

The optimum pulsed plasma oxidised polymer blend surfaces produced a completely wettable surface towards water, which underwent partial hydrophobic recovery to 46° over the period of a week, Table 3. Hydrophobic recovery occurred at a faster rate if the oxidised polymer blend film was annealed at elevated temperature, Table 3. A comparison with corresponding plasma treatments performed on bulk PDMS elastomer and pure polyethylene substrates indicated that the polymer blend surface was behaving in an analogous fashion to pure PDMS.

3.4 DISCUSSION

On the basis of the lower surface tension PDMS segment contained in the PE-co-PDMS-co-PE block copolymer, one would expect this additive to migrate towards the air-polyethylene interface.[10] XPS analysis of the washed and annealed polymer blend surface confirmed this to be the case, Table 1. The PDMS segments can be envisaged as forming a looplike structure at the air-solid interface, with the polyethylene ends embedded into the polyethylene bulk.[22] The stoichiometry of the segregated polymer blend surface was less than the elemental composition of pure PDMS (50% C, 25% Si, 25% O), and was therefore taken as being indicative of incomplete coverage of the polyethylene surface by PDMS segments (this is consistent with the AFM phase image, Figure 6). Contact angle analysis also supported this description, since the polymer blend surface (after washing and annealing) gave lower water contact angle values compared to pure PDMS films, Table 3.

In the case of 2W continuous wave (CW) plasma treatment, maintaining the substrate at room temperature produced more SiO_x compared to heating the film during plasma treatment, Table 1. Whereas the converse was true for pulsed plasma exposure. These differences can be explained in terms of PDMS being allowed to thermally segregate to the surface during the off-period of the pulsed plasma duty cycle. Whereas the continuous bombardment of the substrate by energetic plasma species during CW heated conditions will lead to greater PDMS chain scission and ablation, i.e. less probability for the formation of extended. SiO_x networks.

Examination of the pulsed/heated oxygen plasma treated films by XPS and contact angle measurements showed that the polymer blend surface was highly oxidised and fully wettable immediately after plasma treatment. A small

degree of hydrophobic recovery was observed over time. Diffusion of unreacted copolymer chains contained in the sub-surface region towards the air-solid interface accounts for this behaviour. AFM analysis indicated the presence of cracks in the SiO_x surface, which facilitate the transport of PDMS containing moieties towards the air-solid interface.

3.5 CONCLUSIONS

Pulsed plasma oxidation of polyethylene-polydimethylsiloxane (ABA) doped polyethylene films at elevated temperatures gives rise to the formation of a well-adhered hydrophilic layer of SiO_x.

3.6 REFERENCES

1 Yasuda, T.; Yoshida, K.; Okuno, T. *J. Polym. Sci, Part B: Polym. Phys.* **1988**, *26*, 2061

2 Wang, J. H.; Chen, J. J.; Timmons, R. B. *Chem. Mater.* **1996**, *8*, 2212

3 Tan, K.L.; Woon, L.L.; Wong, H.K.; Kang, E.T.; Neoh, K.G. *Macromolecules* **1993**, *26*, 2832.

4 Mailhot, B.; Gardette,J.-L. *Macromolecules* **1992**, *25*, 4119

5 Bates, F. S. Science 1991, 251, 898.

6 Zhao, J.; Rojstaczer, S. R.; Chen, J.; Xu, M.; Gardella J. A., Jr. *Macromolecules* **1999**, *32*, 455.

7 Ndoni, S.; Jannasch, P.; Larsen, N. B.; Almdal, K. *Langmuir* **1999**, *15*, 3859.

8 Smith, S. D.; Wnuk, A. J.; Gerber, M. S. U.S. Pat. 5,476,901, 1995.

9 *Polymer Handbook*; Brandrup, J., Immergut, E. H., Eds.; John Wiley & Sons: New York, 1989.

10 Garbassi, F.; Morra, M.; Occhiello, E. In *Polymer Surfaces - From Physics to Technology*; Wiley: Chichester, 1994.

11 Inoue, H.; Matsumoto, A.; Matsukawa, K.; Ueda, A.; Nagai, S. *J. Appl. Polym. Sci.* **1990**, *41*, 1815.

12 Wen, J.; Somorjai, G.; Lim, F.; Ward, R. *Macromolecules* **1997**, *30*, 7206.

13 LeGrand, D. G.; Gaines, G. L., *Jr. Polym. Prepr. Am. Chem. Soc., Div. Polym. Chem.* **1979**, *11*, 442.

14 Chen, X.; Gardella, J. A., Jr. *Macromolecules* **1994**, *27*, 3363.

15 Johanson, G.; Hedman, J.; Berndtsson, A.; Klasson, M.; Nilsson, R. *J. Electron Spectr.* **1973**, *2*, 295.

16 Zhong, Q.; Innis, D.; Kjoller, K. Elings, V.B. *Surf. Sci.* **1993**, *14*, 3045.

17 Magonov, S. N.; Elings, V. B.; Whangbo, M. H. *Surf. Sci.* **1997**, *375*, L385.

18 Clark, D. T.; Thomas, H. R. *J. Polym. Sci. Chem. Ed.* **1977**, *15*, 2843.

19 Alfonsetti, R.; Lozzi, L.; Passacantado, M.; Picozzi, P.; Santucci, S. *Applied Surface Science* **1993**, *70/71*, 222.

20 Beamson, G.; Briggs, D. In *High Resolution XPS of Organic Polymers: The Scienta ESCA300 Database*; Wiley: New York, 1992.

21 Schonherr, H.; Shetivy, D.; Vancso, G.J Polym. Bull. **1993**, *30,* 567.

22 Hariharan, A.; Harris, J. G. *J. Phys. Chem.*, **1995**, *99*, 2788.

CHAPTER 4

ELECTRON BEAM CURING OF AMINOSILANE/ACRYLATE/ITACONIC ACID COATINGS

4.1 INTRODUCTION

Electron beam (EB) curing describes the use of fast electrons, in the range between 120 – 300 keV, for polymerising and / or cross-linking a combination of monomers and oligomers onto a substrate.[1] Electron beam accelerators[2] are used to generate the electron stream capable of curing thicker coatings than UV curing due to more penetrative nature of the electrons through matter; in contrast with photons of light, which tend to be absorbed mainly at the surface of materials.

Acrylates, methacrylates and their prepolymers show typical free radical addition polymerisation through their carbon double bonds after electron irradiation.[3,4] In addition, at increasing monomer conversion cross-linking of the polymer chains occurs. The final result is the formation of a tight three-dimensional network. In order to attain adequate cross-linking at reduced radiation dose levels, bifunctional and polyfunctional acrylates[5] are employed as in this work, Structure 1.

Free radical polymerisation and cross-linking processes are inhibited by oxygen. Oxygen reacts both with the initiating radicals and with the propagating free-radical chain, thus preventing chain propagation or terminating the propagating chain. Purging the irradiation zone with inert gas lowers the oxygen concentration and prevents inhibition by oxygen. Another way to eliminate oxygen-inhibition is by reacting primary or secondary amines with multifunctional acrylates.[6,7] These addition products were found to undergo more rapid and complete polymerisation. In addition, the ratio of primary to secondary amines in the curable composition provides a means for controlling the viscosity of the product. Use of amines, and more preferably amine adducts produced from polyamines and epoxides or acrylates, as curing agents with no need for irradiating the coating has been reported in the past.[8] When enhanced wetting and adhesion properties are required for the coatings, aminosilanes can also be used, Structure 2.

Finally, formation of polyamides from itaconic acid, Structure 3, and diamines has previously been reported.[9]

In this chapter, a correlation between the oxygen gas barrier properties and the surface chemistry of curable coatings, prepared from an aminosilane, an acrylate, and an α,β-unsaturated dicarboxylic acid, is described.

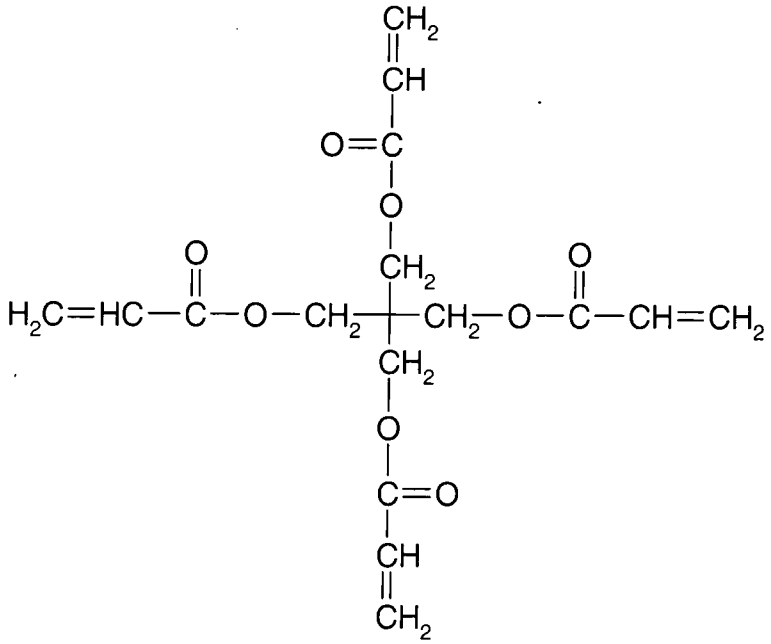

Structure 1: Pentaerythritol tetracrylate (PETA)

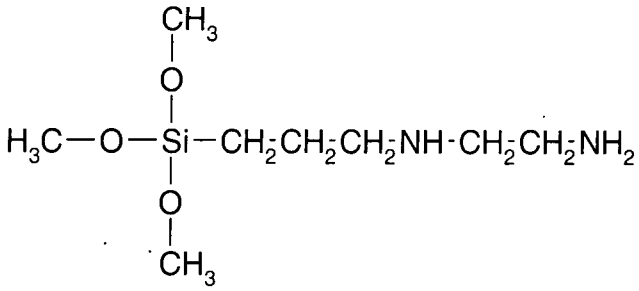

Structure 2: 3-(-2-aminoethylamino) propyltrimethoxy-silane (Z-6020)

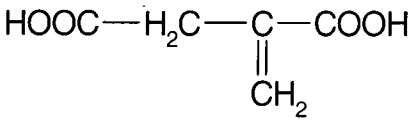

Structure 3: Itaconic acid (ITA)

4.2 EXPERIMENTAL

The coatings were freshly prepared by adding 3-(-2-aminoethylamino) propyltrimethoxy-silane (Z-6020 Dow Corning) to pentaerythritol tetracrylate (PETA) dissolved in propan-2-ol in a molar ratio of 4 : 1. They were left to react for 30 min via conjugate nucleophilic addition to α,β-unsaturated carbonyl groups. This corresponds to complete consumption of the acrylate double bonds, Scheme 1. The secondary amine group located at the third carbon atom from silicon is considered to be virtually inert in the case of amino-organofunctional silanes dissolved in polar solvents (e.g. alcohols). This can be attributed to hydrogen bonding with the silyl oxygen to form an internal cyclic structure,[10] Scheme 2; or alternatively there can be intramolecular interaction between the silicon and nitrogen centres present in the aminosilane,[11] Scheme 3.

Scheme 1: Conjugate nucleophilic addition to α,β-unsaturated carbonyl groups.[12]

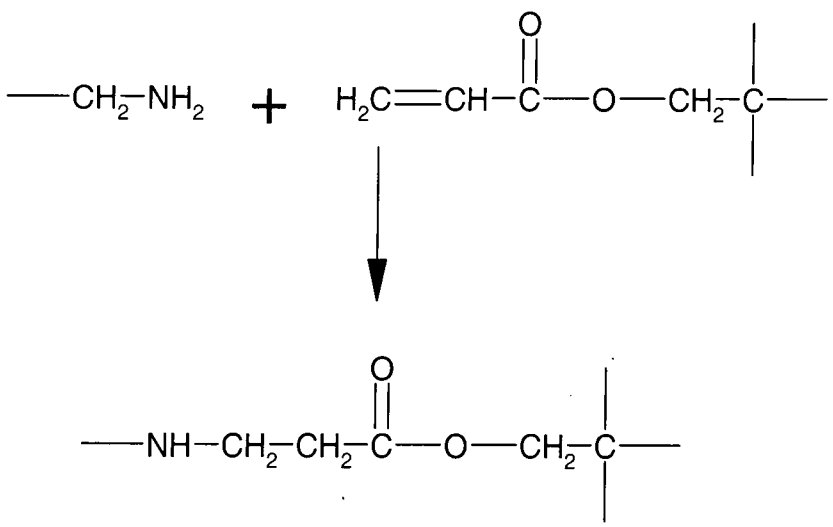

Scheme 2: Hydrogen bonding between secondary amine group and silyl oxygen.

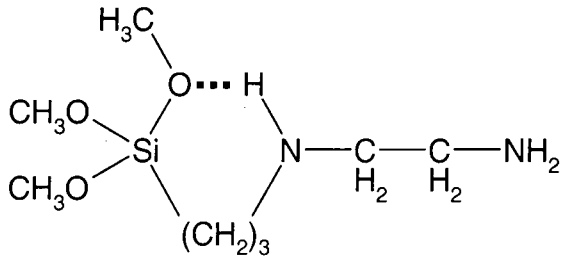

Scheme 3: Interaction between the silicon and nitrogen centres in the aminosilane.

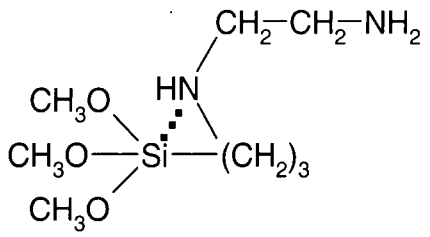

Itaconic acid (ITA) was then added in excess to this mixture as a cross-linking precursor (the overall molar ratio being 4 : 1 : 10.4 aminosilane : PETA : ITA, 20% wt/v in IPA). This solution was then coated onto 30 μm oriented polypropylene films (UCB) and allowed drying at room temperature in air.

Small strips of coated sample were then rinsed in cyclohexane for 30 s prior to XPS and ATR-IR analysis.

These coatings were also treated in a number of different ways, as described in Table 1.

Table 1: Coating treatments and oxygen transport rates (OTR) at 0% humidity level.

Coatings Treatment	OTR (cm^{-3} m^{-2} day^{-1})
Polypropylene substrate	1500
(i) air-dried	4
(ii) as (i) + heating at 100 °C for 2 days.	15
(iii) as (i) + e-beam (10 Mrad / 170 kV)	2
(iv) as (ii) + e-beam (10 Mrad / 170 kV)	19

Electron beam treatment was performed by using a CB150 Electrocurtain EB processor from Energy Science Inc. The sample was attached to a tray using an adhesive tape and went through the machine on a conveying belt at a given speed. The belt speed and the machine amperage were adjusted in such way to give the sample the correct exposure (10 Mrad). The standard voltage for treatment of these films was 170 kV.

A Kratos ES300 electron spectrometer equipped with a Mg Kα X-ray source (1253.6 eV), and a concentric hemispherical analyser was used for XPS analysis. Photo-emitted electrons were collected at a take-off angle of 30° from the substrate normal, with electron detection in the fixed retarding ratio (FRR, 22:1) mode. XPS spectra were accumulated on an interfaced PC computer and fitted using a Marquardt minimisation algorithm with Gaussian peaks all having the same full-width-at-half-maximum (FWHM).[13] Instrument sensitivity factors using reference chemical standards were taken as C(1s) : O(1s) : Si (2p) : N (1s) equals 1.00 : 0.57 : 0.72 : 0.74.

ATR-FTIR spectra were acquired over the 600-4000 cm^{-1} wavenumber range at a resolution of 4 cm^{-1} using a Mattson Polaris spectrometer fitted with Greasby Specac Golden Gate ATR accessory. Spectra were averaged over 32 scans, in conjunction with background subtraction. Solution state FTIR spectra were also obtained on a Mattson Polaris spectrometer. The optical pathlength of the empty sample cell was calculated to be 42 μm.

Solid state NMR spectra were recorded using a Varian Unityplus spectrometer (75.43 MHz ^{13}C, 59.58 MHz ^{29}Si, 30.41 MHz ^{15}N) and a Doty Scientific MAS probe with 7 mm o.d. rotor. A cross-polarisation magic-angle spinning experiment with high-power proton decoupling was used.

C-13 solution state NMR were obtained using a Varian VXR-400S (100.58 MHz ^{13}C) with 60 pulse, continuous proton decoupling, and 3 s relaxation delay. Si-29 solution spectra were carried out on a Bruker AMX-500 (99.36 MHz ^{29}Si) with 30 pulse, universe gated decoupling, 30 s relaxation delay, and 1815 repetitions.

Optical micrographs were recorded on an Olympus BX40 microscope operated in transmission light mode.

Oxygen permeability was measured using an OXTRAN 2/20 MH instrument from MOCON. The films were typically exposed to 3% H_2/nitrogen on both sides for 4-6 hours to flush out all air entrapped in the chambers, a baseline was measured and then one side of the film was exposed to either air (21% O_2) or 100% O_2 on one side, the other side still being 3% H_2/nitrogen. Once the films have been conditioned (4-6 hours again), the measurements of OTR were made until equilibration (less than 5 % variation between 2 consecutive measures). The oxygen detector is a coulometric detector that generates a current when reached by a certain amount of oxygen and hydrogen. The hydrogen was provided by the nitrogen flow.

4.3 RESULTS

4.3.1 Infrared analysis

Infrared analysis of the as-dried coatings reveals the presence of Si-O-C / Si-O-Si bonds at 1113 cm^{-1} (aminosilane and condensation of alkoxy silane sites), carbon - carbon double bonds at 1632 cm^{-1} (itaconic acid), and carboxylic acid / ester groups at 1693 - 1715 cm^{-1} (ν C=O stretching vibrations from itaconic acid and PETA ester linkages), Figure 1.

Table 2: IR absorption assignments.[14,15,16]

Wavenumber / cm^{-1}	Assignment	Symbol
3450	O-H / N-H stretching vibrations.	
2930	C-H stretching vibrations	
1693-1715	C=O stretching vibrations.	
1634-1665	Amide I band	
1628-1634	C=C stretching vibrations.	■
1537-1559	Asymmetrical CO_2^- stretching vibrations.	◆
1389-1446	CH_2 scissoring and / or C-O-H bending vibrations.	
1373-1397	Symmetrical CO_2^- stretching vibrations.	◆
1302	CH in plane bending vibrations / C-O stretching	
1161-1167	C-C(=O)-O stretching vibrations	
1074-1113	Si-O-Si / Si-O-C stretching vibrations	
897-943	CH_2= wagging / O-H out of plane vibrations	

Also, there is evidence for the formation of carboxylate anions by virtue of the presence of the absorption bands at 1539 cm^{-1} (ν_a CO_2^-) and 1395 cm^{-1} (ν_s CO_2^-). These observations are consistent with previously reported studies which show that the C=O stretching vibrational frequency at 1699 cm^{-1} of

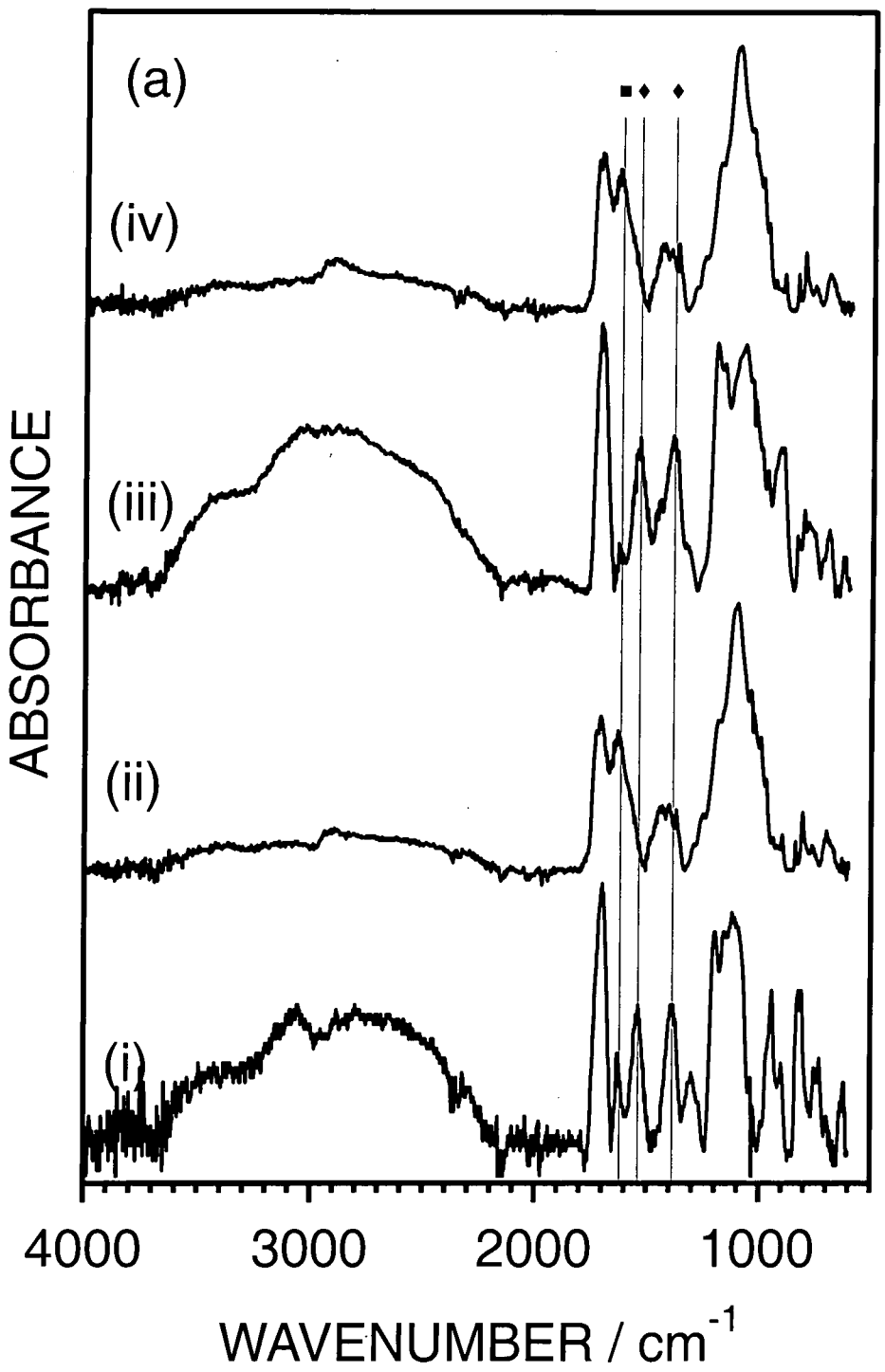

Figure 1: ATR-FTIR spectra of aminosilane / acrylate / itaconic acid 4 / 1 / 10.4 coatings: (i) dried at room temperature; (ii) heating of (i) at 100 °C; (iii) e-beam treatment of (i); and (iv) e-beam treatment of (ii).

un-ionised COOH shifts towards lower wavenumbers, broadens and reduces in intensity with increasing degree of ionisation, in conjunction with the emergence of COO^- bands at 1539 cm^{-1} and 1395 cm^{-1}.[17]

The exact location of carboxylate anion absorption bands was confirmed by examining a 1 : 1 aminosilane / itaconic coating prepared from methanol solution, Figure 2. It can be seen, that the absorption band due to COOH (1694 cm^{-1}) is virtually absent and two strong absorption bands at 1537 cm^{-1} (ν_a CO_2^-) and 1373 cm^{-1} (ν_s CO_2^-) dominate the spectrum indicating carboxylate anion formation (i.e. both carboxylic acid groups contained in itaconic acid have undergone reaction with the amine groups from the aminosilane).

In the case of the 4 : 10.4 aminosilane / ITA mixture, un-ionised COOH (1694 cm^{-1}) as well as CO_2^- (1537 cm^{-1} and 1385 cm^{-1}) is evident due to an excess of ITA being present, Figure 2.

Infrared analysis of aminosilane / PETA / ITA solutions, with different molar ratios, in propan-2-ol (prepared by varying the concentration of the itaconic acid component) shows that for four aminosilane molecules (eight amine groups) only four carboxylic groups out of eight in total participate in acid-base reactions, Figure 3, Table 3. Hence, it can be concluded that there are still unreacted amine centres present in the solution. However, addition of excess itaconic acid results in no further reaction.

Table 3: amount of un-ionised COOH and ionised COO^- present in the solutions. The relative percentages were calculated by peak fitting the following absorption bands: PETA at 1742 cm^{-1}; COOH from ITA at 1714 cm^{-1}; and COO^- from ITA at 1563 cm^{-1}.

Z6020 : PETA : ITA (molar ratio) 20% w/w solution in IPA	% COOH	% COO^-	Z6020 : PETA : COO^- (molar ratio)
4 : 1 : 4	24.8	75.2	4 : 1 : 3
4 : 1 : 6	62.1	37.9	4 : 1 : 2
4 : 1 : 8	73.3	26.6	4 : 1 : 2
4 : 1 : 10	82.2	17.8	4 : 1 : 2

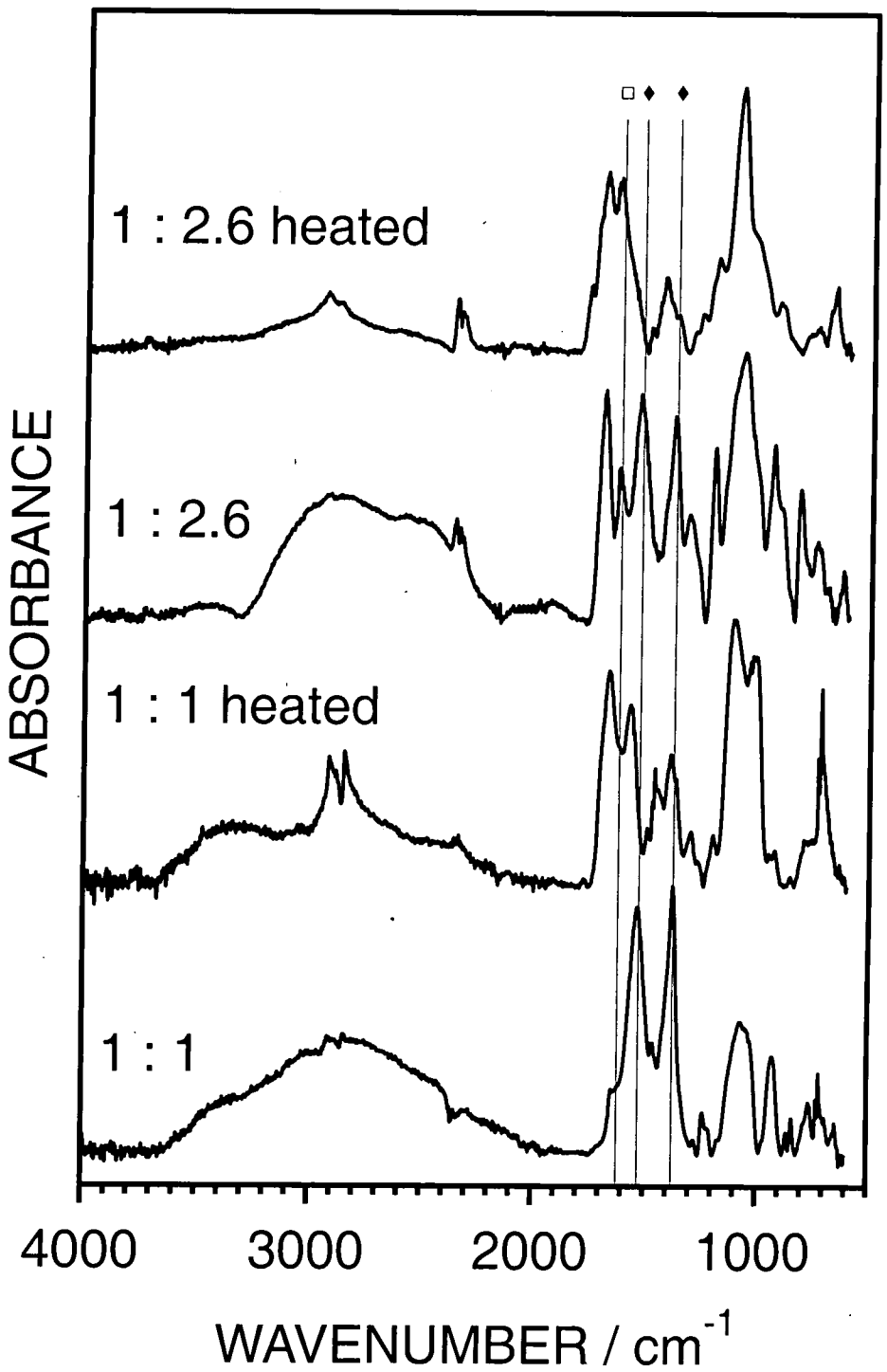

Figure 2: ATR-IR spectra of Z-6020 / ITA samples with different molar ratios prepared in the lab.

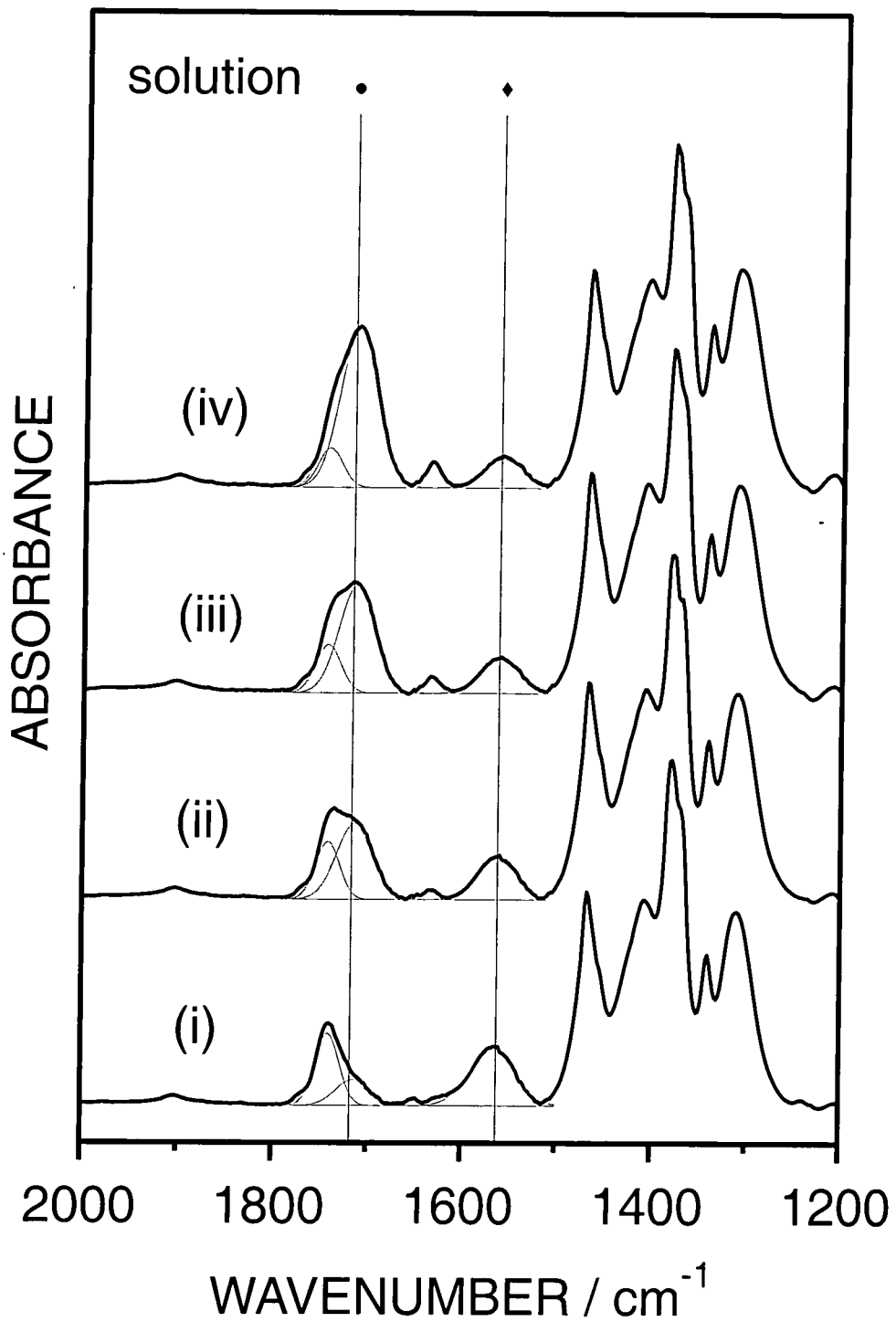

Figure 3: IR spectra for 20% w/w Z-6020 / PETA / ITA solution mixtures with different molar ratios in methanol: (i) 4 : 1 : 4; (ii) 4 : 1 : 6; (iii) 4 : 1 : 8; and (iv) 4 : 1 : 10.

The peak at 1628 cm^{-1} confirms the presence of carbon - carbon double bonds. These bonds can be mainly attributed to the itaconic acid component, since all the double bonds from the PETA will have been consumed during conjugate nucleophilic addition to α,β-unsaturated carbonyl groups reactions with the $-NH_2$ groups of the aminosilane (section 4.3.3).

Heating of the air-dried aminosilane-rich sample caused the disappearance of the bands associated with the presence of a carboxylic salt (peaks at 1539 cm^{-1} and 1395 cm^{-1}). Decrease in the intensities of the following peaks at 2500 cm^{-1} - 3600 cm^{-1} (O-H) and 1713 cm^{-1} (C=O) indicates a decrease in the amount of carboxylic acid groups present at the coating. This can be explained either by decarboxylation[18] or more likely by amide formation.[19] Amide formation is evident from the appearance of a new peak associated with amide group at 1665 cm^{-1} (amide I band) in the ATR-IR spectrum of the heated 1 : 1 aminosilane / ITA coating, Figure 2. In the case of 4 : 1 : 10.4 mixture this absorption band can be seen shifted to lower frequency (1634 cm^{-1}). This absorption can be positively assigned to amide groups and not to C=C double bonds due to near complete absence of peaks in the 897 cm^{-1} – 943 cm^{-1} region. So, in addition to possible formation of amide groups, heating causes the opening of carbon-carbon double bonds. This type of reaction for primary amines has been reported previously,[9] Scheme 4.

Scheme 4: Possible reaction of 1 : 1 aminosilane / itaconic acid during heating

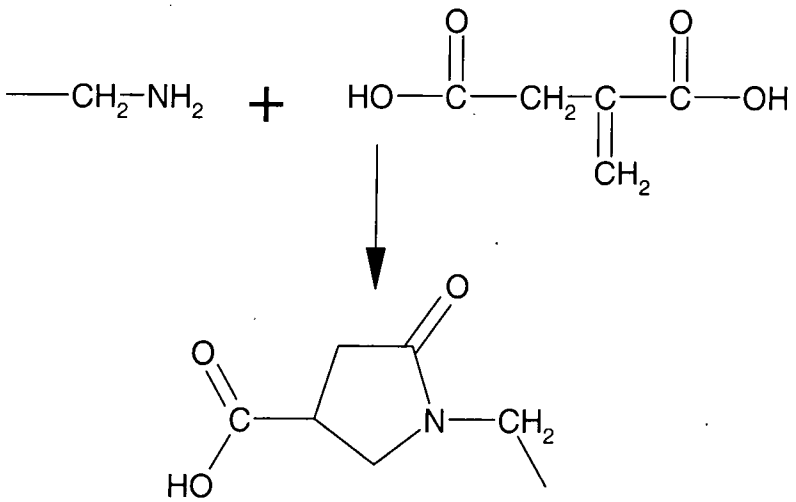

No change in carboxylic salt (bands at 1539 cm^{-1} and 1397 cm^{-1}) is observed upon e-beam radiation of the air-dried coatings. However, a decrease in the intensity of the C=C vibrational stretching band (1628 cm^{-1}) suggests possible polymerisation or cross-linking of the itaconic acid to yield a salt phase attached to a polymerised itaconic acid network.

A comparison between the IR spectra of the heated and heated / e-beamed, samples Figure 1, shows that e-beam treatment does not cause any change to the chemistry of the coating following heating. The IR spectra of both samples are identical. Hence the heating process prohibits subsequent cross-linking of the itaconic acid species.

4.3.2 XPS analysis

The presence of carboxylic salt in both untreated and air-dried / e-beamed coatings can be seen from the N(1s) spectra, Figure 4, (the exact location of the peaks due to N-C at 400.1 ± 0.3 eV and N^{+}-C at 402.0 ± 0.3 eV were determined from XPS analysis of 1 : 1 aminosilane / ITA sample, Figure 5).

Heating of the air-dried coating shifts the N(1s) peak towards lower binding energies indicating changes in the chemical environment around nitrogen atoms, Figures 4 and 5. Unfortunately in this case, XPS can not clarify if heating converts the ammonium salt to amine or amide type species (amine binding energies: 399.1 - 400.2 eV; amide binding energies: 399.8 - 400.0 eV)[20].

Deconvolution of the N(1s) envelope shows that there is significantly less ammonium salt in the case of heated coatings, Table 4.

The possibility of decarboxylation/amide formation of the itaconic acid component in the air-dried aminosilane-rich mixture upon heating can be evident from the C(1s) spectra, Figure 6. Peak fitting shows that the following carbon moieties are present in the coating; C_xH_y at 285.0 eV, C-CO_2 at 285.7 eV, C-O- / C-N at 286.6 eV, C=O / N-C=O at 287.9 – 288.2 eV, and -O-C=O at 288.9 –289.2 eV. The relative intensity of the (-O-C=O) peak decreases upon heating, thereby suggesting that the decarboxylation/amide formation are viable reaction pathways.

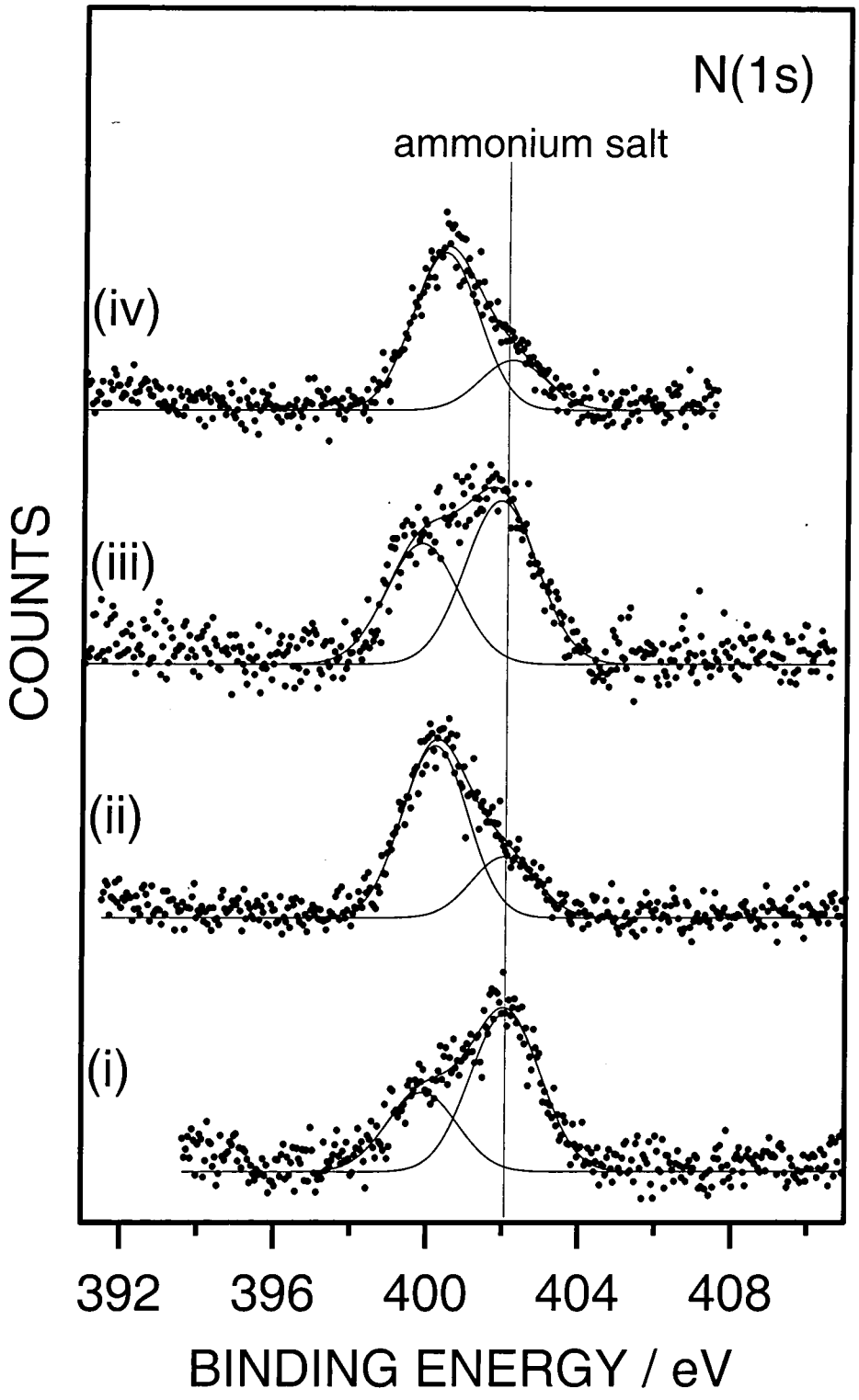

Figure 4: N(1s) XPS spectra of aminosilane / acrylate / itaconic acid 4 / 1 / 10.4 coatings: (i) dried at room temperature; (ii) heating of (i) at 100 °C; (iii) e-beam treatment of (i); and (iv) e-beam treatment of (ii).

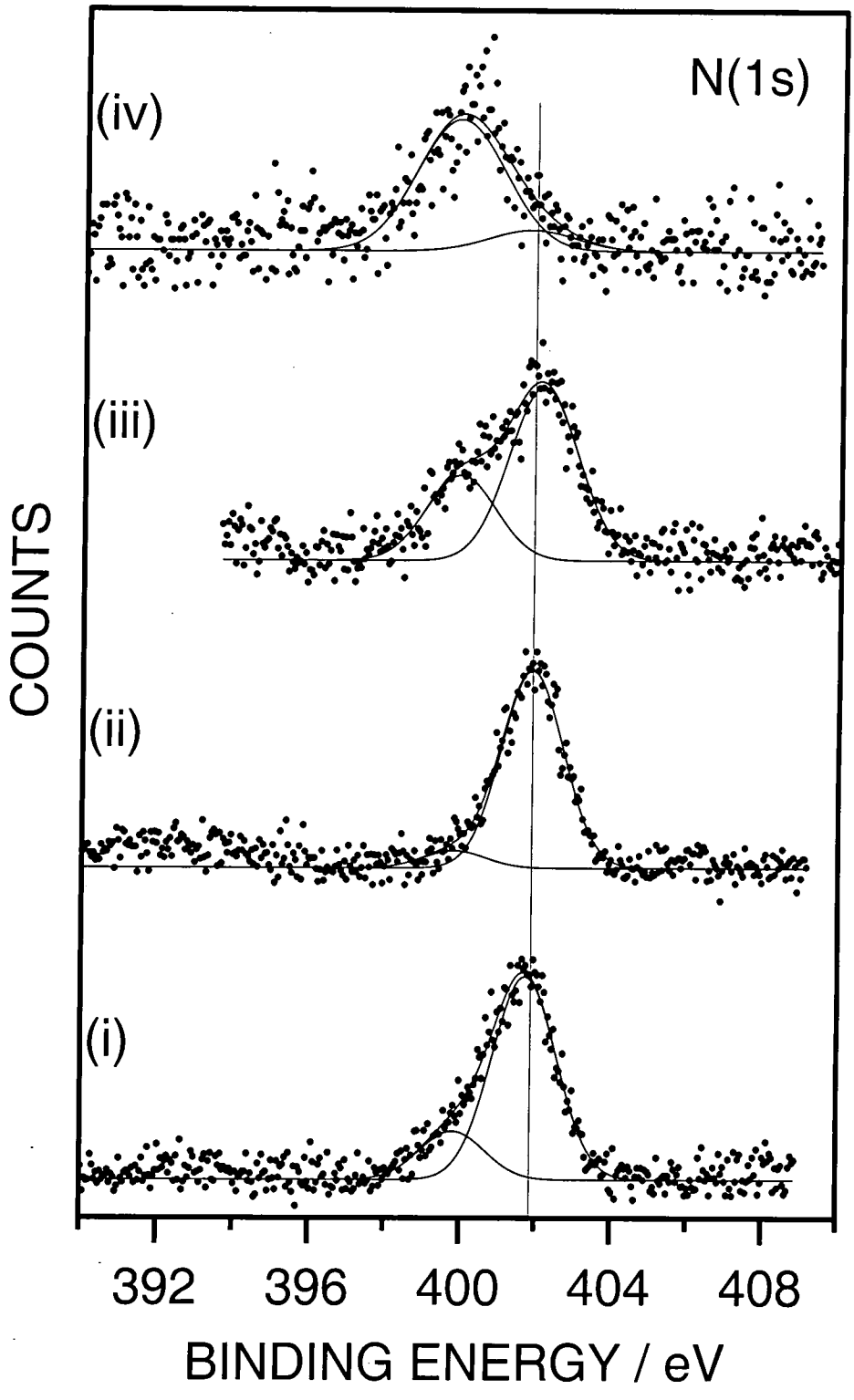

Figure 5: N(1s) XPS spectra of: (i) 1 : 1 Z-6020 / ITA; (ii) 1 : 2.6 Z-6020 / ITA; (iii) 4 : 1 : 10.4 Z-6020 / PETA / ITA; (iv) 1 : 2.6 Z-6020 / ITA heated.

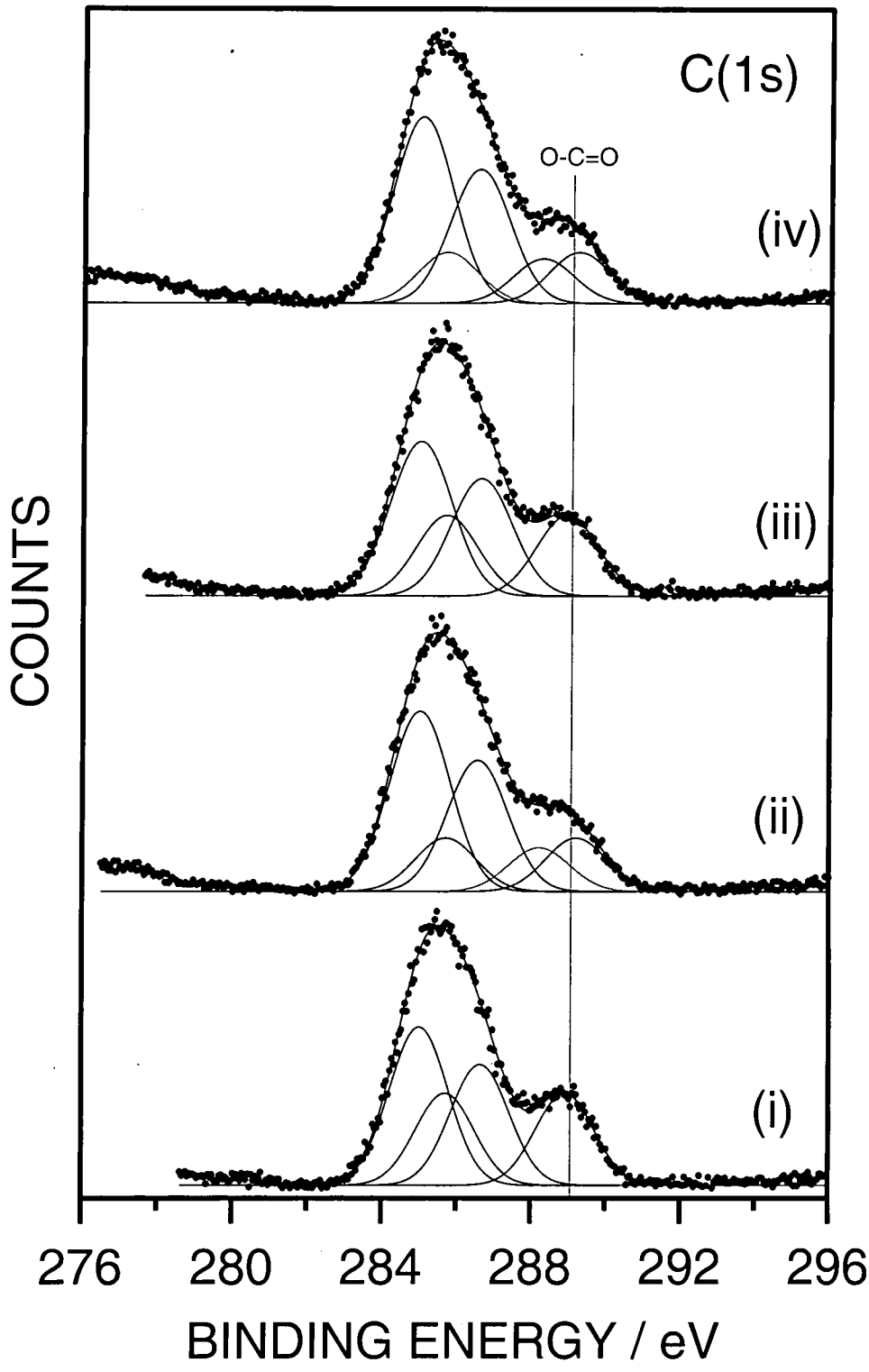

Figure 6: C(1s) XPS spectra of aminosilane / acrylate / itaconic acid 4 / 1 / 10.4 coatings: (i) dried at room temperature; (ii) heating of (i) at 100 °C; (iii) e-beam treatment of (i); and (iv) e-beam treatment of (ii).

Table 4: Summary of changes in elemental composition of the coating surfaces.

Treatment	% C ± 0.8	% Si ± 0.1	% O ± 0.6	% N ± 0.3	% N in salt form ± 0.3
Theoretical	57.4	2.3	35.5	4.7	
(i)	62.0	3.7	27.8	6.6	4.4
(ii)	61.9	4.4	26.9	6.9	1.7
(iii)	61.7	3.7	28.0	6.7	3.8
(iv)	61.5	4.9	27.2	6.4	1.5

4.3.3 NMR analysis

The NMR chemical shifts for the Z-6020, PETA, and ITA are given in Table 5.

Table 5: C-13 NMR peak shifts (strong peaks at 25 and 65 ppm are due to IPA solvent).

Aminosilane		PETA		ITA	
Unit	δ (ppm)	Unit	δ (ppm)	Unit	δ (ppm)
Si-C	5.5, 6.9	-CH2-	34.1, 35.1	$-CH_2-$	37.0
$-CH_2-$	22.1	-CH2-O-	63.3	=C	131.7
$-CH_2-NH_2$	40.6	=CH-	128.5	=CH2	135.9
$-CH_2-NH$	49.1	=CH2	131.6	=C-C*OOH	172.2
CH_3-O	51.2	=C-C*OOR	165.6	-COOH	179.5
$CDCl_3$	77.2	=C-C*OOH	171.2		

NMR analysis provided a means for determining the origin of the carbon - carbon double bonds present in the air-dried aminosilane-rich coating. Figure 7a-iv clearly shows that all the carbon - carbon double bonds from the PETA

are consumed during reaction with aminosilane (conjugate nucleophilic addition to α,β-unsaturated carbonyl groups reaction). This is evident from the absence of peaks at 131.6 ppm and 128.5 ppm associated with carbon – carbon double bonds in PETA, Figure 7a-ii.

A shift of the two ITA carboxylic groups (-COOH at 179.5 ppm and =C-C*OOH at 172.3 ppm) upfield to 175.4 ppm and 171.0 ppm indicates the formation of carboxylate anion, Figure 7a-v and 7a-vii; confirmation of this assignment was made by running the C-13 NMR spectrum of the 1 : 1 aminosilane / ITA reference sample (gives ammonium salt), Figure 8 (i). The C-13 NMR spectrum of the 1 : 2.6 aminosilane / ITA sample also showed that salt is formed, Figure 8 (ii).

It was found that no interaction between PETA and ITA occurs, Figure 7a-vi (the NMR spectra correspond to just a two component mixture).

Solid itaconic acid does not undergo e-beam polymerisation since the C-13 NMR spectrum of ITA before and after e-beam exposure are identical, Figure 7b-iii and Figure 7a-iii. But e-beam induced polymerisation or cross-linking of ITA does take place in the presence of aminosilane. This is evident from the disappearance of C-13 NMR features associated with the ITA carbon - carbon double bonds contained in the ITA / aminosilane reference mixture, Figure 7b-v and 7b-vii.

The C-13 NMR spectrum of the e-beamed 1 : 10.4 PETA / ITA mixture (Figure 7b-vi) exhibits broad absorption peaks mainly due to ITA, and no information of any possible interaction between PETA and ITA could be extracted.

Si-29 NMR spectra show that the alkoxy groups of the aminosilane undergo condensation, Figure 9. The extent of upfield shift is a measure of the level of condensation. As it can be seen in Figure 9, e-beam treatment does not give rise to further formation of T2 [$Si(OSi)_2OR$] and T3 [$Si(OSi)_3$] condensation products. Approximate chemical shifts of aminosilanes at different condensation levels are given in the Table 6.

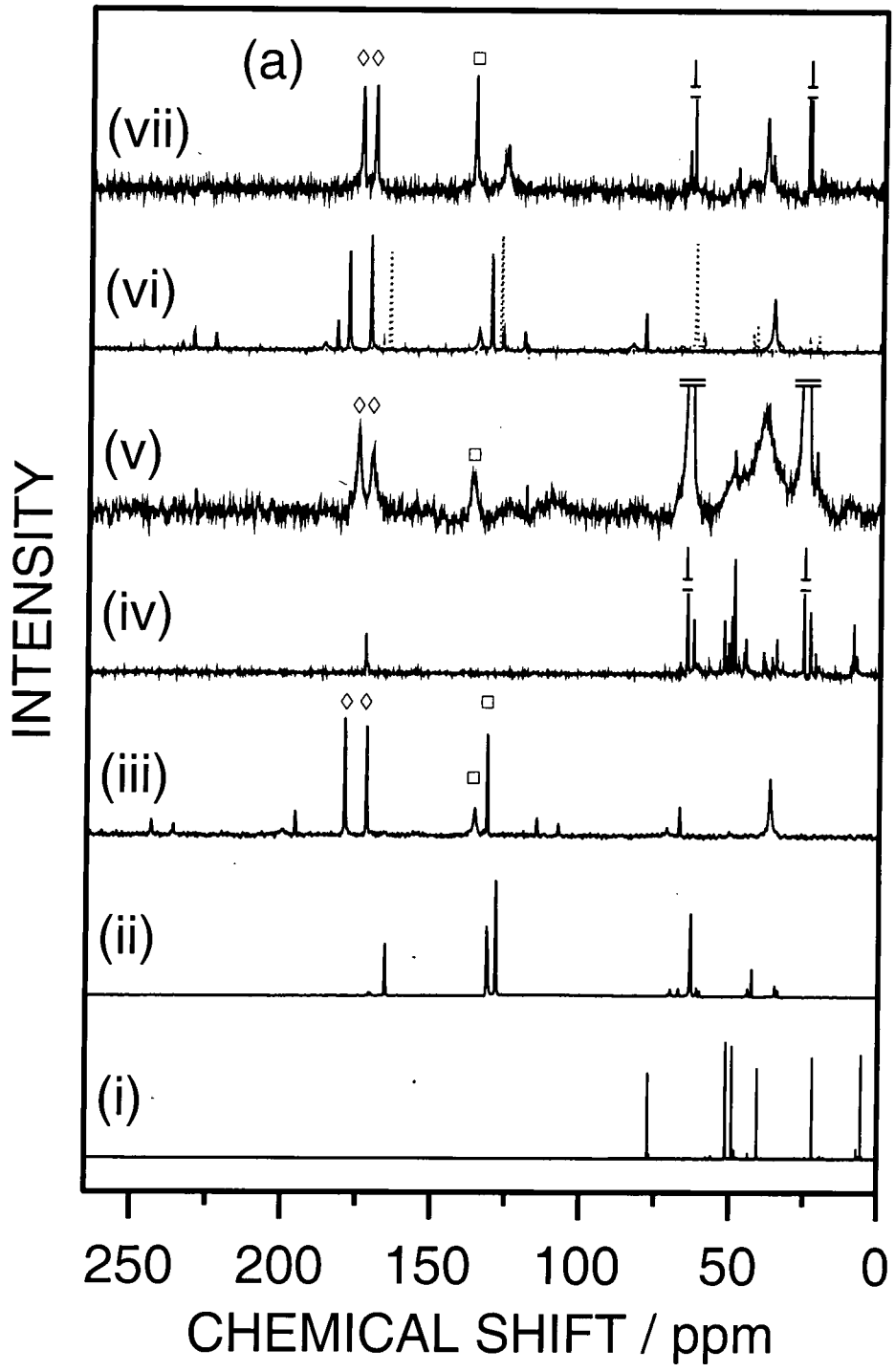

Figure 7a: C-13 NMR spectra of air-dried samples: (i) aminosilane; (ii) acrylate; (iii) itaconic acid; (iv) aminosilane / acrylate 4 / 1 mixture; (v) aminosilane / itaconic acid 1 / 2.6 mixture; (vi) acrylate (dashed line) / itaconic acid (solid line) 1 / 10.4 mixture; and (vii) aminosilane / acrylate / itaconic acid 4 / 1 / 10.4 mixture.

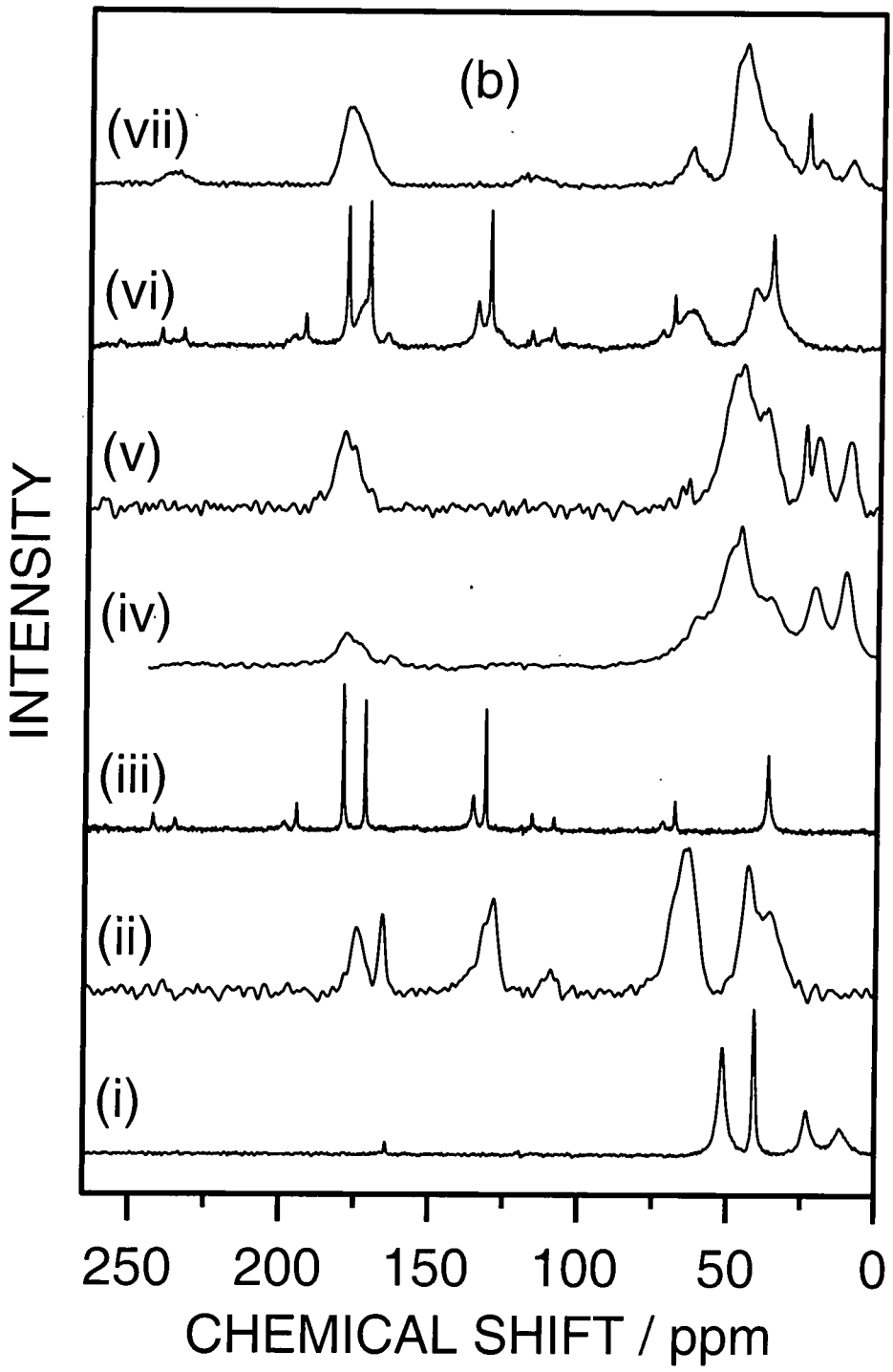

Figure 7b: C-13 NMR spectra of e-beamed samples: (i) aminosilane; (ii) acrylate; (iii) itaconic acid; (iv) aminosilane / acrylate 4 / 1 mixture; (v) aminosilane / itaconic acid 1 / 2.6 mixture; (vi) acrylate (dashed line) / itaconic acid (solid line) 1 / 10.4 mixture; and (vii) aminosilane / acrylate / itaconic acid 4 / 1 / 10.4 mixture.

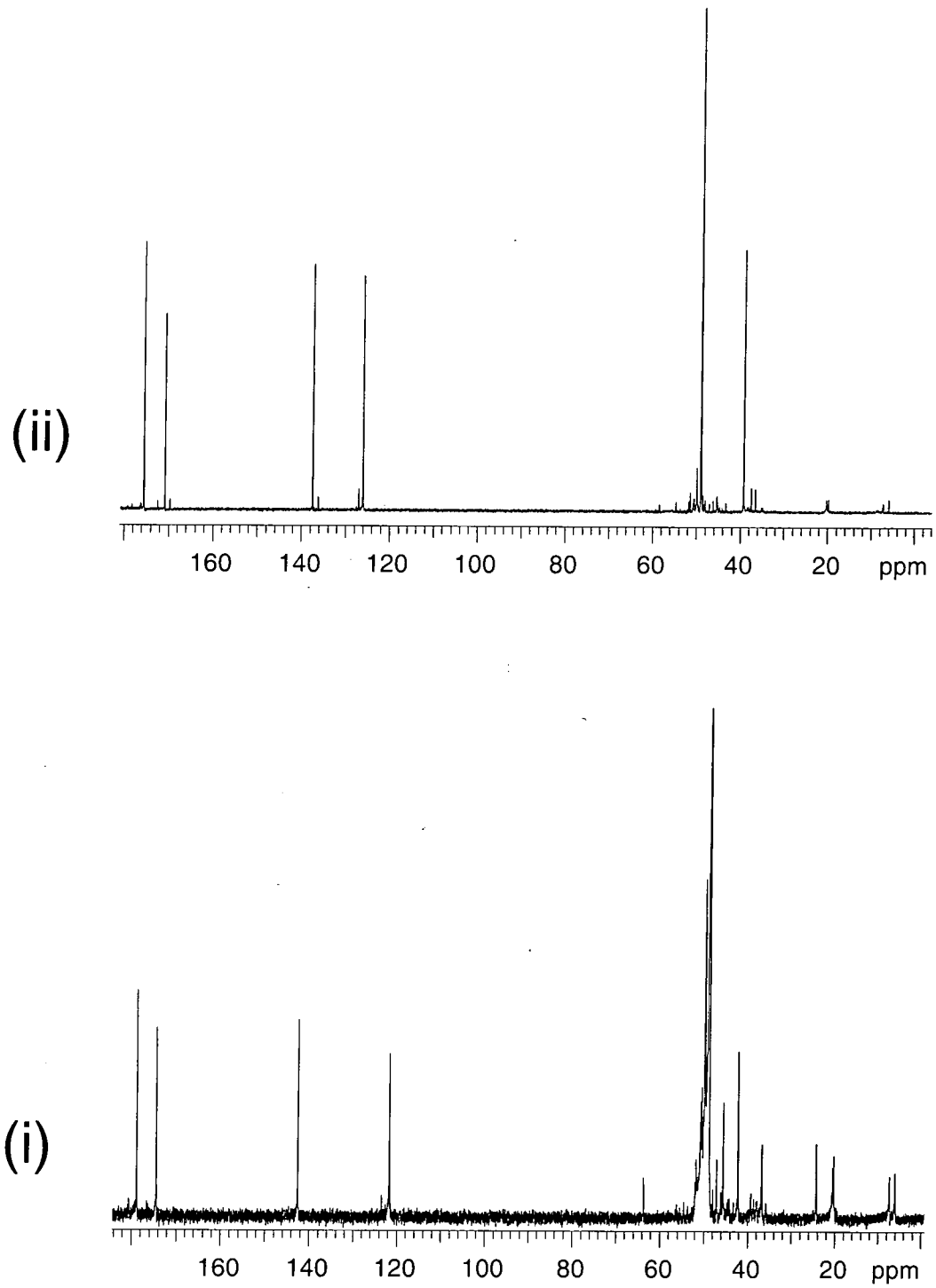

Figure 8: C-13 NMR spectra of: (i) 1 : 1 and (ii) 1 : 2.6 Z-6020 / ITA samples.

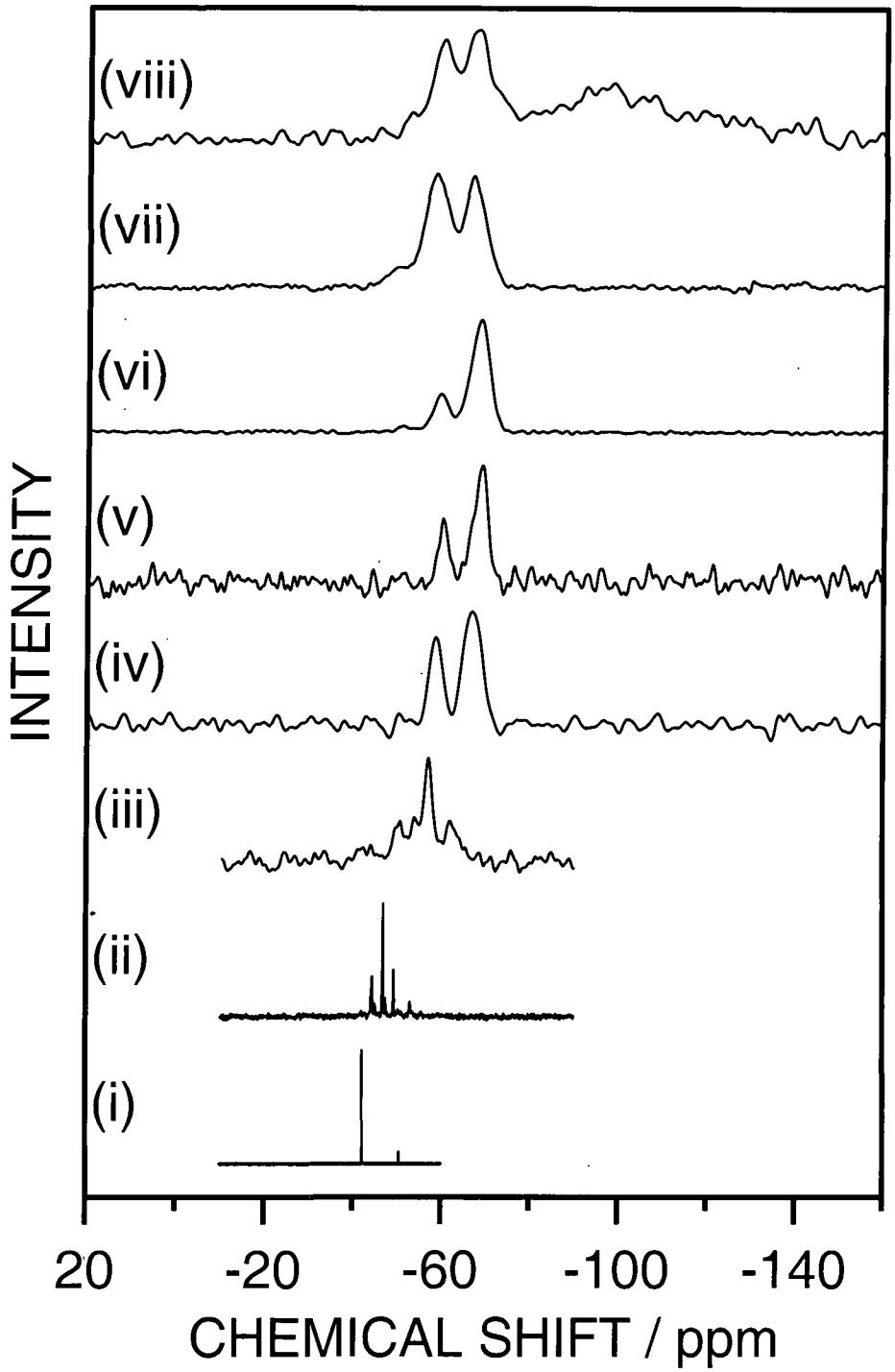

Figure 9: Si-29 NMR spectra of: (i) aminosilane; (ii) aminosilane / acrylate 4 / 1 mixture; (iii) aminosilane / itaconic acid 1 / 2.6 mixture; (iv) aminosilane / acrylate / itaconic acid 4 / 1 / 10.4 mixture; (v) e-beam treatment of (i); (vi) e-beam treatment of (ii); (vii) e-beam treatment of (iii); and (viii) e-beam treatment of (iv).

Table 6: Si-29 NMR chemical shifts of aminosilanes at different condensation levels.

Unit type	δ (ppm)
$R\text{-}Si(OR)_3$	-40
$R\text{-}Si(OR)_2O_{1/2}$	-50
$R\text{-}Si(OR)O_{2/2}$	-58 to -60
$R\text{-}SiO_{3/2}$	-66 to -70

From the N-15 NMR spectrum of the heated 4 : 1 : 10.4 aminosilane : PETA : ITA coating, the presence of the peak at -256.5 ppm clearly indicates amide formation[21] upon heating, Figure 10. The peak at -337.6 ppm can be assigned to the presence of ammonium salt and / or amine.

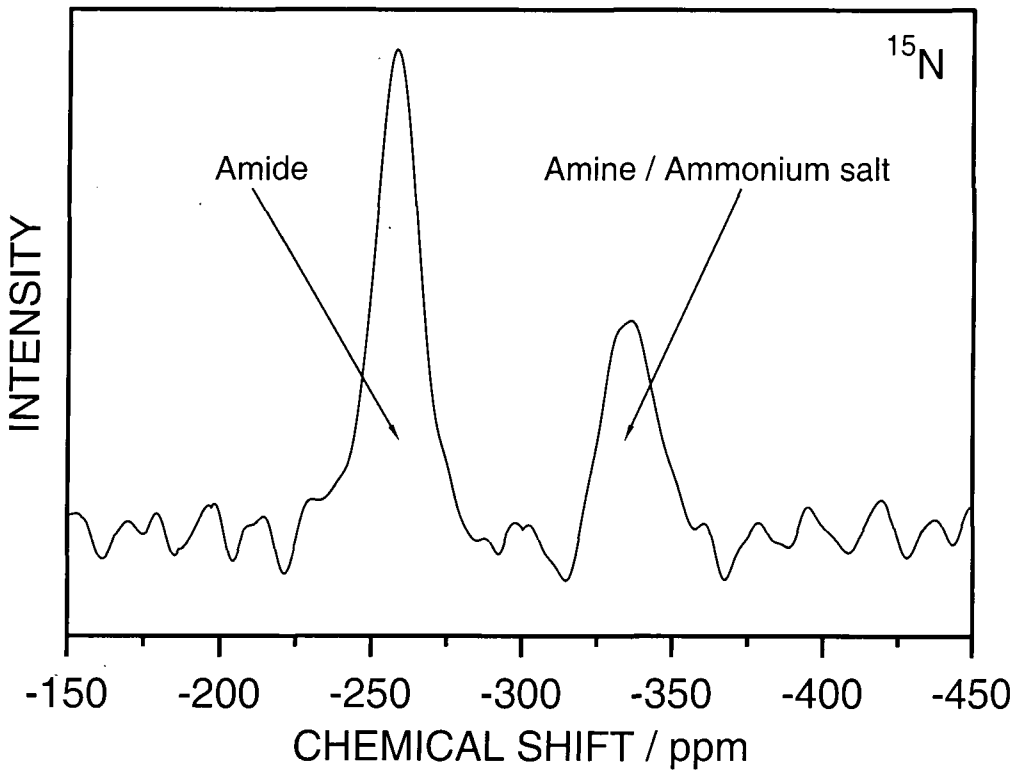

Figure 10: N-15 NMR spectrum of aminosilane / acrylate / itaconic acid 4 / 1 / 10.4 mixture after being heated at 100 °C for two days.

4.3.4 Optical Microscopy

Pure itaconic acid coating forms crystallites, Figure 11. In contrast, the formation of itaconic acid crystallites was not observed in the case of the air-dried aminosilane / acrylate / itaconic 4: 1: 10.4 coating, Figure 12.

This observation may explain the difference in polymerisation behaviour of itaconic acid. ITA does not undergo e-beam polymerisation in the solid state due to its crystal structure, but does undergo e-beam polymerisation when grafted in a medium of high viscosity.[22] In contrast, as previously stated in sections 4.3.1 and 4.3.3, the excess itaconic acid present in the air-dried samples, might have polymerised during e-beam irradiation. This behaviour can be attributed to the fact that ITA molecules in the aminosilane-rich mixture are "trapped" in an amorphous medium, which prevents them from forming crystallites. Therefore the ITA molecules can enjoy more freedom of motion, leading to a better arrangement of the molecules for polymerisation during the e-beam treatment.

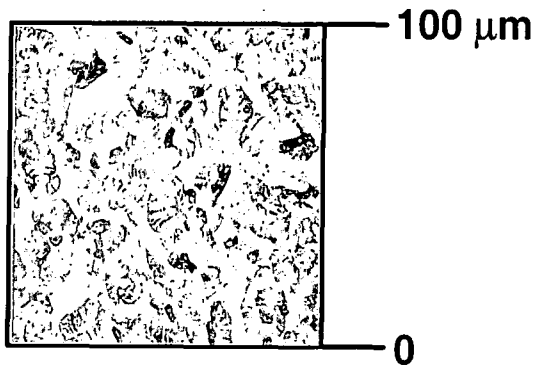

Figure 11: Optical micrograph of the ITA coating.

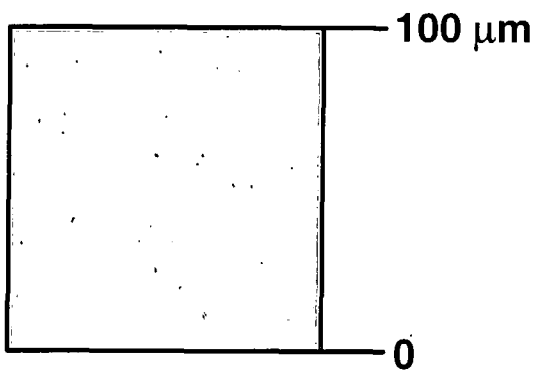

Figure 12: Optical micrograph of the 4 : 1 : 10.4 aminosilane / PETA / ITA coating.

4.4 DISCUSSION

Aminosilane undergoes nucleophilic addition with PETA selectively at the terminal amine group. Subsequent reaction with ITA leads to formation of ammonium carboxylate salt. Heating of this structure results in conversion of the ammonium carboxylate centres to amide linkages and opening of the carbon - carbon double bonds of the itaconic acid. This consumption of the double bonds can not be explained from the aforementioned mechanism, Scheme 4, since there are only secondary amine groups present in the resulting system, Scheme 1. Therefore, oligomerisation/cross-linking, and decarboxylation reactions might take place upon heating. This explanation is in contradiction with previously reported findings,[23] where polymerisation of itaconic acid occurs only at temperatures higher than 120°, but can be supported on the basis of the higher conformational mobility of the ITA molecules as described in Section 4.1.4. E-beam treatment results in polymerisation/cross-linking of the alkene bonds contained within the itaconic acid constituent but without the loss of ammonium salt species.

Furthermore, condensation reactions between aminosilane units lead to formation of siloxane-type networks.

4.5 CONCLUSIONS

Coating curable compositions onto polypropylene films was found to enhance the oxygen gas barrier properties of the latter. The observed improvement was attributed to the formation of ammonium salt, C-C crosslinked itaconic species, and siloxane networks, and found to be dependent upon the type of the treatment.

4.6 REFERENCES

1 *Radiation curing of polymeric materials*; Hoyle, C. E.; Kinstle, J. F., Eds.; ACS: Washington, D.C, 1990.

2 Tartz, M.; Hartmann, E.; Lenk, M.; Mehnert, R. *Nucl. Instrum. Meth. A* **1999**, *427*, 261.

3 Mehnert, R. *Nucl. Instrum. Meth. B.* **1995**, *105*, 348.

4 Glauser, T.; Johansson, M.; Hult, A. *Polymer* **1999**, *40*, 5297.

5 Batten, R. J.; Davidson, R. S.; Ellis, R. J.; Wilkinson, S. A. *Polymer* **1992**, *33*, 3037.

6 Gaske, J. E. US 3925349, 1975.

7 Banik, I.; Dutta, S. K.; Chaki, T. K.; Bhowmick, A. K. *Polymer* **1999**, *40*, 447.

8 Curatolo, B. S.; Apicella, F. V., Jr.; Richardson, T. W., Sr. US 5536775, 1996.

9 Morello, E. F. US 4420608, 1983.

10 Plueddeman, E. P., In *Silane Coupling Agents*; Plenum Press: New York, 1991.

11 Saratov, I. E.; Shpak, I. V.; Reikhsfel'd, V. O. *Zh. Obshch. Khim.* **1981**, *51*, 405.

12 McMurry, J. In *Organic Chemistry*; Brooks/Cole: Pacific Grove, 1988, pp 690.

13 Johanson, G.; Hedman, J.; Berndtsson, A.; Klasson, M.; Nilsson, R. *J. Electron Spectr.* **1973**, *2*, 295.

14 Silverstein, R. M.; Bassler, G. C.; Morrill, T. C. In *Spectroscopic Identification of Organic Compounds*; John Wiley & Sons: Singapore, 1991.

15 Lin-Vien, D.; Colthup, N. B.; Fateley, W. G.; Grasselli, J. G. In *The Handbook of Infrared and Characteristics of Organic Molecules*; Academic Press: San Diego, 1991.

16 Bellamy, L. J. In *The Infrared Spectra of Complex Molecules*; Chapman and Hall: London, 1975; Vol. 1.

17 Kawaguchi, S.; Kamata, M.; Koichi, I. *Polymer Journal* **1992**, *24*, 1229.

18 Tate, B. E. *Die Makromolekulare Chemie* **1967**, *109*, 176.

19 March, J. In *Advanced Organic Chemistry*; John Wiley & Sons: New York, 1991.

20 Beamson, G.; Briggs, D. In *High Resolution XPS of Organic Polymers: The Scienta ESCA300 Database*; Wiley: New York, 1992.

21 Martin, G. J.; Martin, M. L.; Gouesnard, J. P. In *NMR, Basic Principles and Progress - 15N-NMR Spectroscopy*, Diehl, P.; Fluck, E.; Kosfeld, R., Eds.; Springer-Verlang: Berlin Heidelberg, 1981; Vol. 18, pp 5.

22 Tate, B. E. *Adv. Polymer Sci.* **1967**, *5*, 214.

23 Higuchi, T: Tsutsui, K.; Shimada, A.; Bando, Y.; Minoura, Y. *Polymer J.* **1978**, *10*, 111.

CHAPTER 5

PULSED PLASMA CO-DEPOSITION OF MONOMERS CONTAINING CARBOXYLIC, AMINE, AND ANHYDRIDE FUNCTIONALITIES

5.1 INTRODUCTION

Low temperature plasma polymerisation/deposition[1] of volatile organic compounds provides an alternative way of modifying the surface properties of polymer substrates.[2] The non-penetrative nature of this process allows the alteration of the chemical and physical properties of the surface without affecting the bulk properties of the substrate. One of the most desirable targets in plasma polymerisation chemistry is control over the structural retention of the precursor molecule. This in turn leads to the production of highly functionalised coatings with a great degree of chemical specificity. It has been widely recognised that the discharge input power and the nature/reactivity of the organic monomer (precursor) are among the critical parameters for controlling the stoichiometry of the plasma polymers. In general, low powers and monomers that can undergo conventional polymerisation reactions produce polymer networks that closely resemble the precursor molecule.[3] Examples of such monomers are the compounds used in this work, Structures 1, 2, and 3. Plasma deposition of acrylic acid,[4,5,6,7] allylamine,[7,8] and maleic anhydride[9] has been studied in the past.

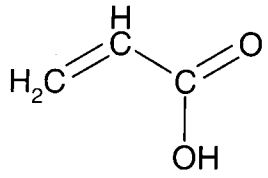

Structure 1: Acrylic acid

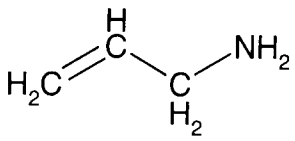

Structure 2: Allylamine

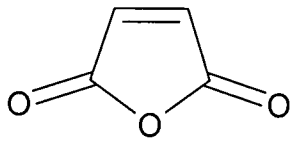

Structure 3: Maleic Anhydride

Pulsing of the applied RF voltage provides a means for lowering the input power below the lowest level possible using continuous wave plasma. This reduces excessive fragmentation of the precursor moieties, cross-linking processes, film ablation, and functional group diversity during plasma polymerisation. In addition, it has been shown that conventional polymerisation mechanisms can take place during the off-time at reactive sites generated within the on-period of the pulse cycle.[9,10,11]

Plasma co-polymerisation has also been explored for controlling the amount of functional groups present in the plasma polymer.[12,13] This was achieved by introducing a hydrocarbon diluent into the monomer feed.

In this chapter the plasma co-polymerisation of monomers containing carboxylic, amine, and anhydride groups is described. In addition, the influence of a non-polymerisable precursor in the co-deposited mixture has been explored. The gas barrier properties for some of the plasma films have also been investigated.

5.2 EXPERIMENTAL

Acrylic acid, "AA", (Aldrich, 99% purity), allylamine, "AL", (Aldrich, 99% purity), and maleic anhydride, "MA", (Aldrich, 99% purity) monomers were loaded into monomer tubes, and further purified by multiple freeze-pump-thaw cycles. Ammonia gas (Aldrich, 99% purity) was used as received. Pulsed plasma co-deposition of the pure monomers and their mixtures, Table 1, was carried out in a plasma reactor (described in chapter 2) for 10 min with t_{on}=100 μs, t_{off}=4000 μs, and peak power being set at 10 W. Continuous wave plasma deposition was performed for 7 min at 10 W. The total pressure during plasma co-polymerisation was varied between 3×10^{-2} and 4×10^{-2} mbar. The notation used throughout this chapter describes the sequence in which the two monomers were introduced into the plasma chamber and their pressure settings. For example, $AL_{0.2}AA_{0.1}$ means that the pressure was firstly set at 0.2 mbar with the introduction of the allylamine vapour alone and brought to a total 0.3 mbar (0.2+0.1) pressure with the incorporation of the acrylic acid monomer. The plasma polymers were deposited onto: (a) glass slides, ultrasonically cleaned in solvent mixture (1:1 cyclohexane/propan-2-ol), for XPS analysis; (b) potassium bromide powder for infrared analysis; and (c) oriented polypropylene films (UCB) for gas barrier measurements.

A Kratos ES300 electron spectrometer equipped with a Mg Kα X-ray source (1253.6 eV), and a concentric hemispherical analyser was used for XPS analysis. Photo-emitted electrons were collected at a take-off angle of 30° from the substrate normal, with electron detection in the fixed retarding ratio (FRR, 22:1) mode. XPS spectra were accumulated on an interfaced PC computer and fitted using a Marquardt minimisation algorithm with Gaussian peaks all having the same full-width-at-half-maximum (FWHM).[14] Instrument sensitivity factors using reference chemical standards were taken as C(1s) : O(1s) : Si (2p) : N (1s) equals 1.00 : 0.57 : 0.72 : 0.74.

Transmission infrared spectra were acquired over the 600-4000 cm^{-1} wavenumber range at a resolution of 4 cm^{-1} using a Mattson Polaris spectrometer. Spectra were averaged over 100 scans, in conjunction with background subtraction.

Plasma polymer deposition rates were measured with an oscillating AT cut quartz crystal (Kronos, Inc. QM-331 Film Thickness Monitor) placed at the centre of the plasma reactor.

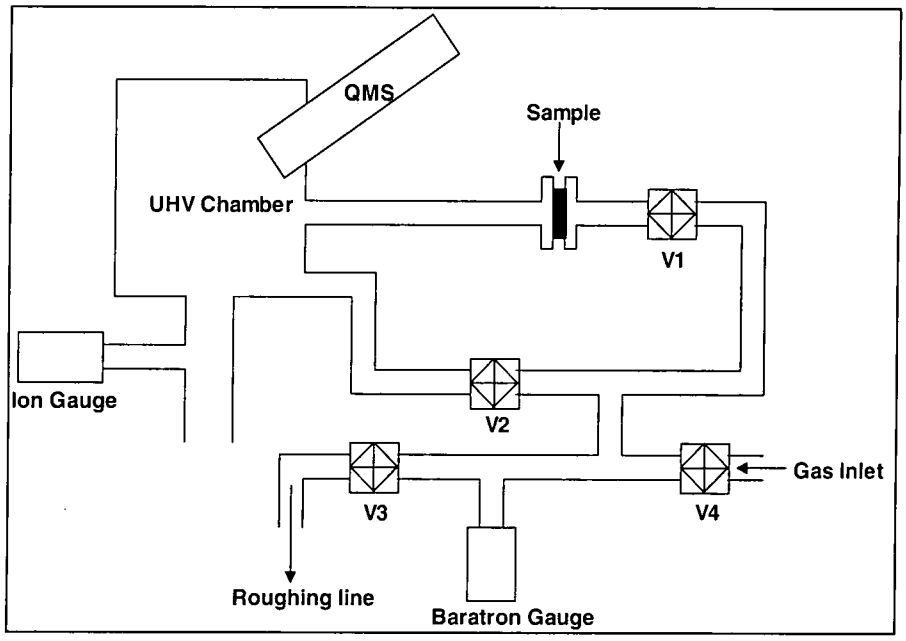

Figure 1: Experimental set up for permeability measurements.

The permeability measuring system, constructed around an ultra high vacuum (UHV) chamber, is represented schematically in Figure 1. The pressure in the chamber was monitored by using an ion gauge. A Vacuum Generators SX200 quadrupole mass spectrometer, interfaced to an IBM-compatible personal computer running data accumulation and analysis software developed in-house, allowed compositional analysis of the gaseous species in the chamber by mass-to-charge ratio (m/e). Calibration experiments to determine the response of the quadrupole mass spectrometer to known pressures of gas were performed using oxygen gas (BOC, 99.6% purity) which was introduced into the chamber by means of a leak valve. Mass spectra were recorded at ion gauge indicated pressures of 4×10^{-7} Torr that were converted to meaningful quantities using ion gauge sensitivity factors. By correlating these pressures with the intensity of the m/e = 32 signal (O_2^+), the mass

spectrometer's response per unit pressure was calculated. Discs of the sample films were placed in the permeability probe with the coated/treated side facing the high-pressure gas supply (1000 Torr). Mean equilibrium permeant partial pressures (MEPPP's) of the oxygen gas were determined after suitable equilibration of the system and removal of ambient gases from the m/e trace. Measured gas permeation was in the steady-state regime where the concentration of permeant on either side of the film is constant and the flow of permeant through the film is allowed to reach equilibrium. It has to be noted that this technique does not measure permeability but a quantity proportional to it (MEPPP's).

5.3 RESULTS

5.3.1 XPS analysis

5.3.1.1 Acrylic acid and allylamine (pulsed plasma)

The highest amount of ammonium salt was observed for the $AA_{0.2}AL_{0.1}$ treatment. Certain conditions ($AL_{0.2}AA_{0.1}$) led to maximum conversion of amine groups to ammonium salt ones, Table 1. An intermediate behaviour was obtained for the $AA_{0.15}AL_{0.15}$ composition. A small amount of ammonium salt was also found to be present for the pure allylamine plasma deposited films due to post-treatment attack of atmospheric CO_2,[15,16] Figure 2 and Table 1. The relative amounts of the different nitrogen environments were estimated by fitting the N(1s) envelope:[17,18,19] $\underline{N}\text{-}C_{amine}$, $\underline{N}\text{-}C{=}O_{amide}$ at 399.4 – 400.3 eV, and $\underline{N}_{ammonium\ salt}$ at 401.4 – 401.7 eV, Figure 3. The C(1s) envelope was fitted with the following carbon functionalities:[17,18] $\underline{C}_xH_y$ at 285.0 eV, $\underline{C}\text{–}CO_2$ at 285.7 eV, $\underline{C}$–O–, $\underline{C}$-N at 286.2 – 286.6 eV, $\underline{C}$=O, N–$\underline{C}$=O at 287.8 eV, and O–$\underline{C}$=O at 288.9 – 289.4 eV, Figure 4. The relative intensity of the (O=C-O) peak at 289.0 eV, observed for the deposited mixtures, increased with increasing conversion to ammonium salt. The opposite trend was observed for the ($\underline{C}$=O, N–$\underline{C}$=O) peak at 287.8 eV (i.e. possible amide formation). The rise in the relative intensity of the latter peak was more prevalent in the case of the $AA_{0.15}AL_{0.15}$ monomer mixture, Figure 4.

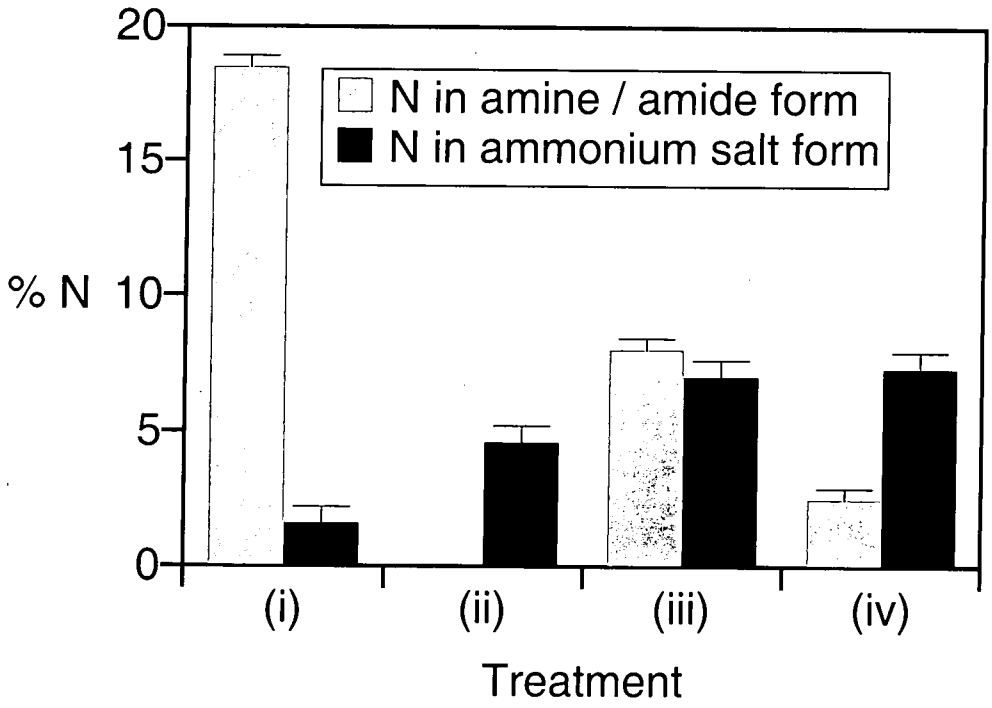

Figure 2: Relative amount of nitrogen associated with amine versus ammonium salt functionalities at the surface of the plasma coated glass slides: (i) allylamine alone P_{AL}=0.3 mbar; (ii) allylamine + acrylic acid (AA) with P_{AL}=0.2 and P_{AA}=0.1 mbar; (iii) P_{AA}=0.15 + P_{AL}=0.15 mbar; and (iv) P_{AA}=0.2 + P_{AL}=0.1 mbar.

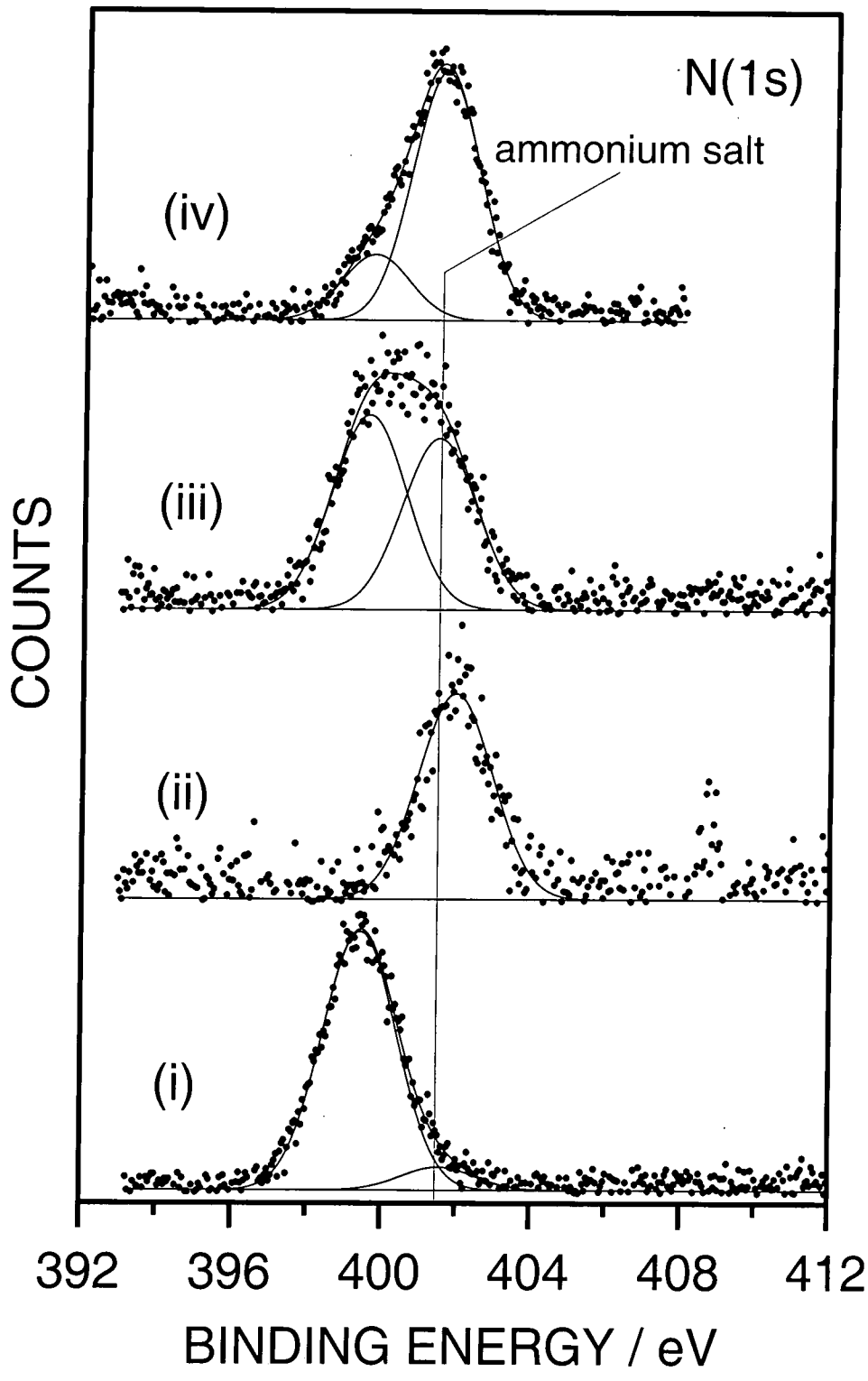

Figure 3: N(1s) XPS spectra of plasma coated glass slides: (i) allylamine alone P_{AL}=0.3 mbar; (ii) allylamine + acrylic acid (AA) with P_{AL}=0.2 + P_{AA}=0.1 mbar; (iii) P_{AA}=0.15 + P_{AL}=0.15 mbar; and (iv) P_{AA}=0.2 + P_{AL}=0.1 mbar.

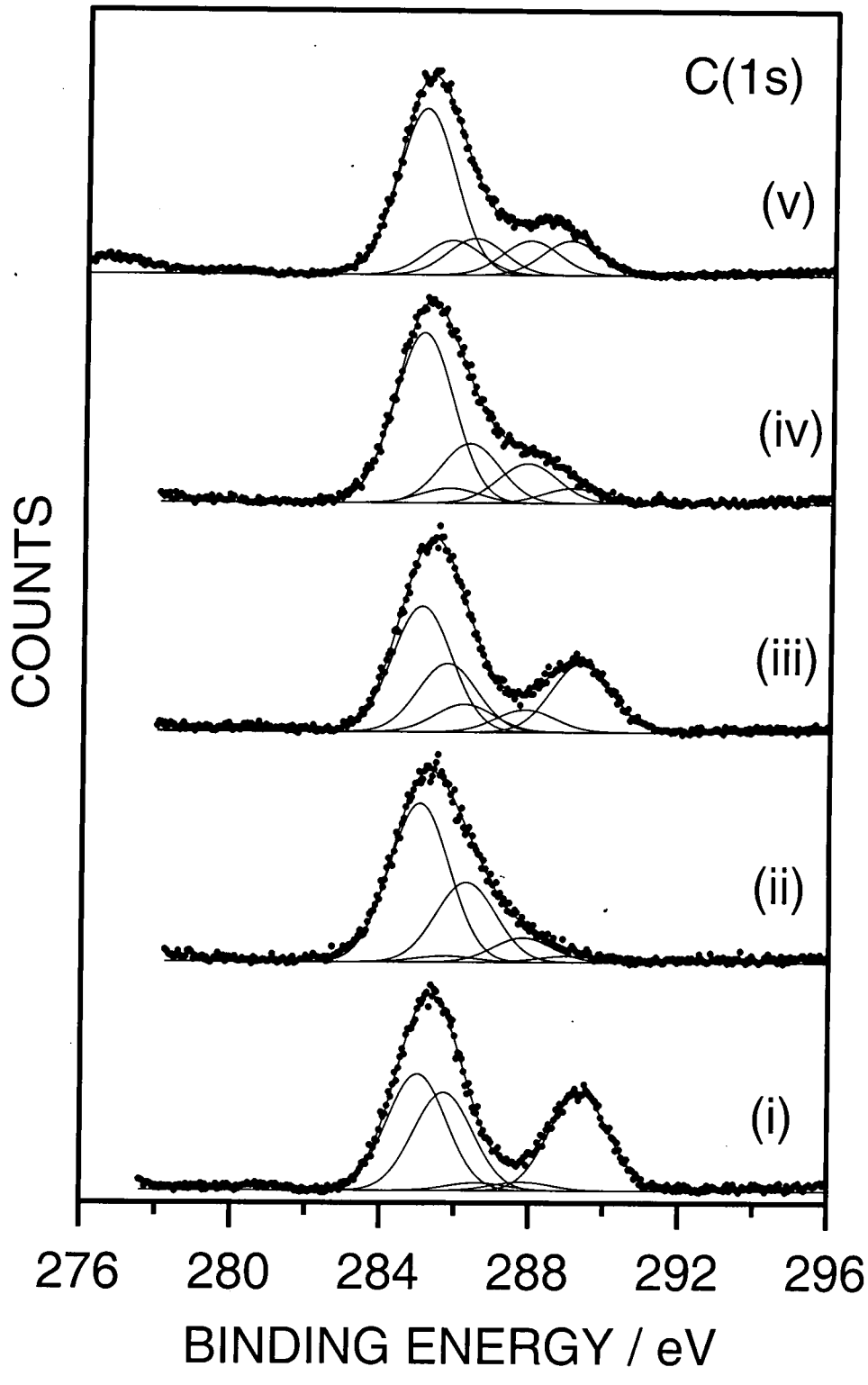

Figure 4: C(1s) XPS spectra of plasma coated glass slides: (i) acrylic acid alone P_{AA}=0.3; (ii) allylamine alone P_{AL}=0.3 mbar; (iii) allylamine + acrylic acid (AA) with P_{AL}=0.2 + P_{AA}=0.1 mbar; (iv) P_{AA}=0.15 + P_{AL}=0.15 mbar; and (v) P_{AA}=0.2 + P_{AL}=0.1 mbar.

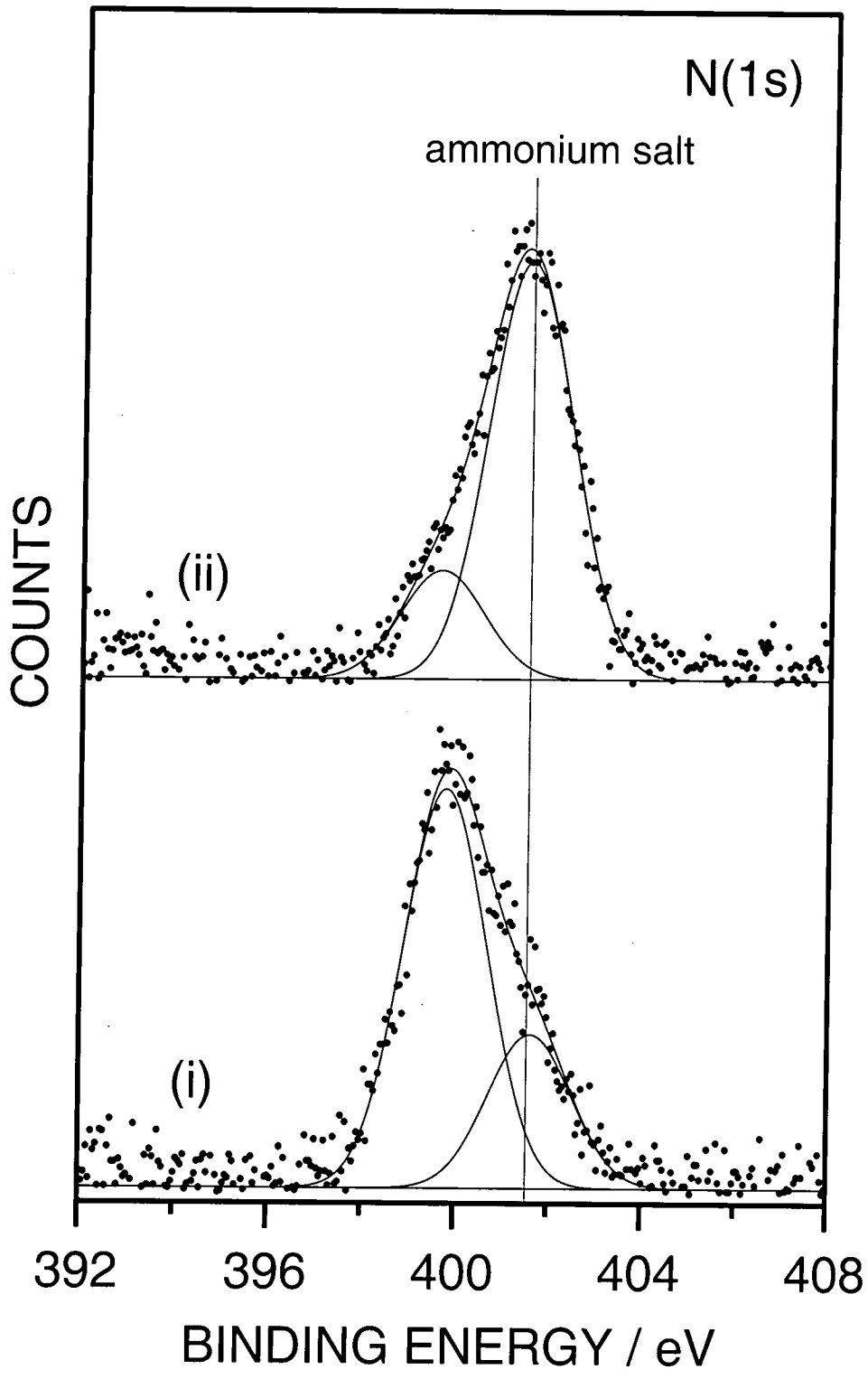

Figure 5: N(1s) XPS spectra of plasma coated glass slides: (i) CW plasma deposited acrylic acid + allylamine with P_{AA}=0.2 + P_{AL}=0.1 mbar; and (ii) pulsed plasma deposited acrylic acid + allylamine with P_{AA}=0.2 + P_{AL}=0.1 mbar.

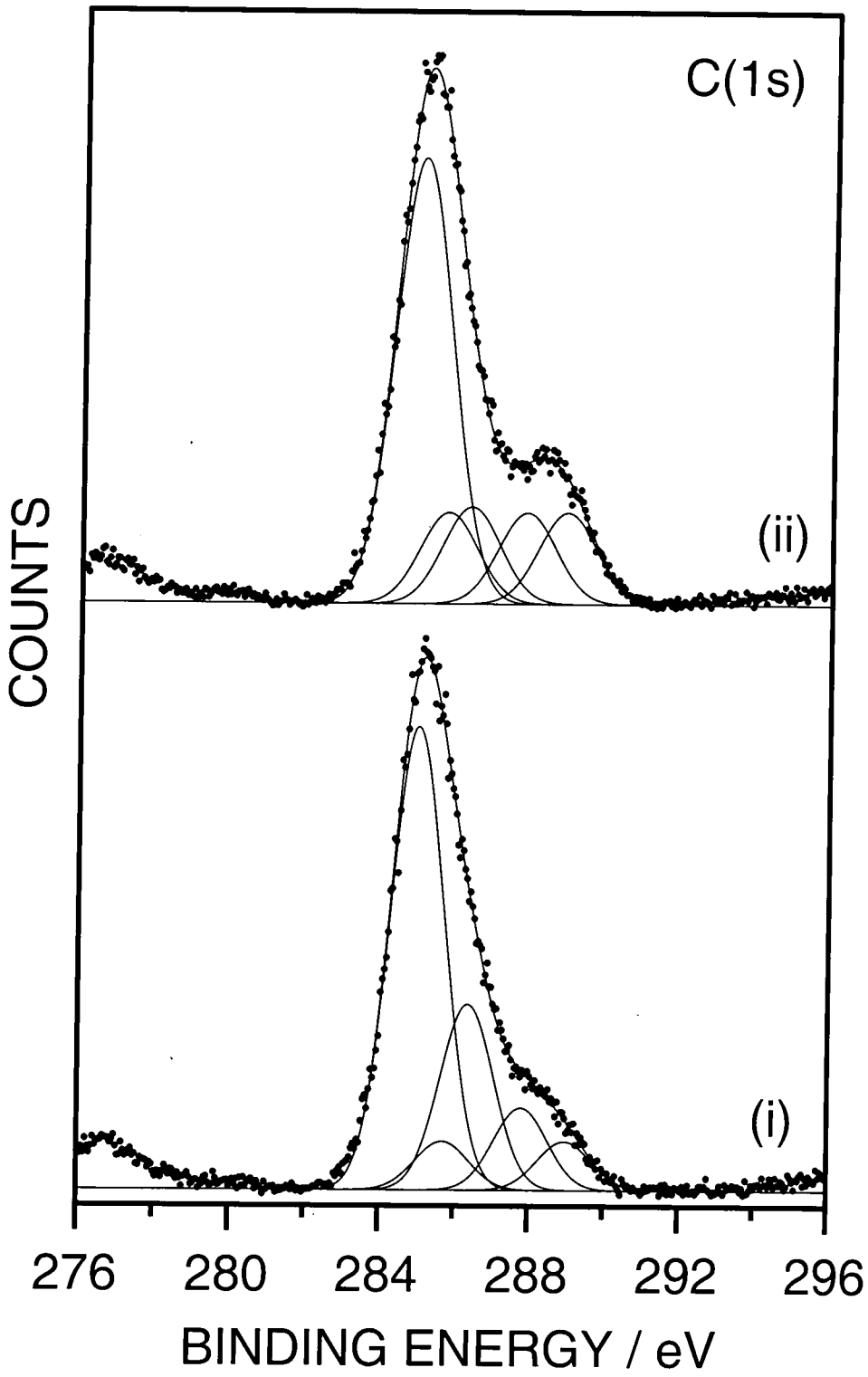

Figure 6: C(1s) XPS spectra of plasma coated glass slides: (i) CW plasma deposited acrylic acid + allylamine with P_{AA}=0.2 + P_{AL}=0.1 mbar; and (ii) pulsed plasma deposited acrylic acid + allylamine with P_{AA}=0.2 + P_{AL}=0.1 mbar.

5.3.1.2 Acrylic acid and allylamine (continuous wave plasma)

The films produced under continuous wave plasma conditions were found to differ significantly from their pulsed deposited counterparts, Table 1. Continuous wave plasma deposition caused a shift in the N(1s) peak towards lower binding energies, Figure 5. This was accompanied by a reduction in the intensity of the (O=C-O) peak and an increase in the intensity of the (C–O–, C-N) and (C=O, N–C=O) peaks, Figure 6. These observations were consistent with the formation of less ammonium salt species for continuous wave discharges.

5.3.1.3 Acrylic acid and ammonia

Interestingly, the treatment with $AA_{0.2}NH3_{0.1}$ yielded a high amount of ammonium salt at the surface whereas the same was not observed for the composition $AA_{0.15}NH3_{0.15}$, Figure 7 and Table 1. In the latter case, detection of Si(2p) signal indicated that the glass slide was not fully covered with the deposited polymer film, Table 1. Excess of ammonia attenuated the deposition of polymeric material onto substrate, Table 1 and gave rise to the appearance of a significant amount of C=O and/or N–C=O species at the surface. This was confirmed by the observed increase in the intensity of the peak at 287.8 eV, Figure 8.

5.3.1.4 Maleic anhydride and ammonia

Again, high concentrations of ammonia present in the mixture ($MA_{0.1}NH3_{0.3}$) produced very thin coatings / incomplete coverage of the glass slides, Table 1. This was evident from the appearance of the peak at 293.9 eV in the C(1s) envelope, which arises from the potassium present in the glass and the observed Si(2p) signal. In the case of the $MA_{0.1}NH3_{0.3}$ mixture the virtue absence of the peak at 286.6 eV (C–O–, C-N) suggested possible amide formation due to apparent disappearance of amine species, Figure 9. Peak fitting of the N(1s) envelope was performed based on the findings from the C(1s) XPS spectra, Figure 10.

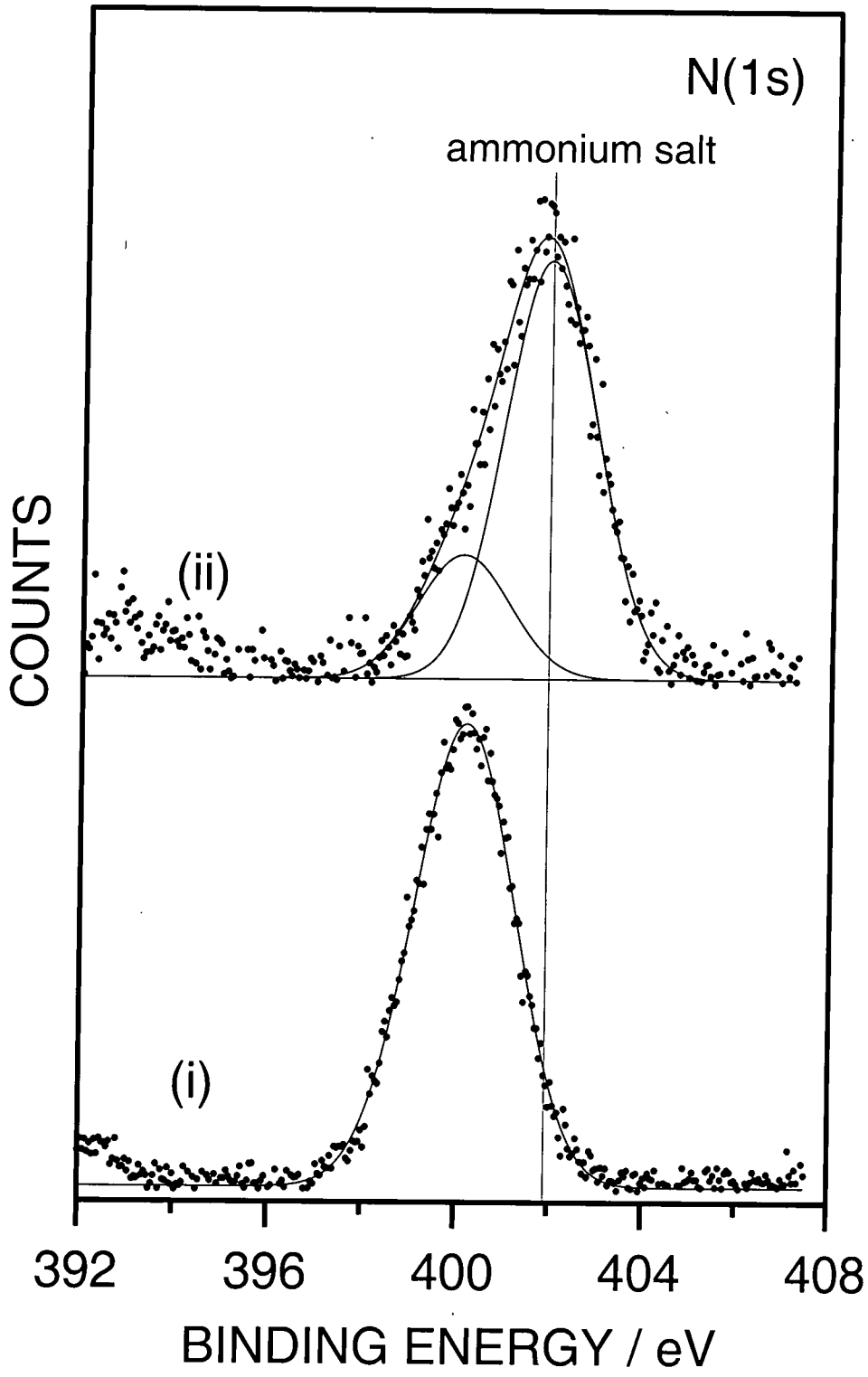

Figure 7: N(1s) XPS spectra of plasma coated glass slides: (i) acrylic acid + NH_3 with P_{AA}=0.15 and P_{NH3}=0.15 mbar; and (ii) P_{AA}=0.2 + P_{NH3}=0.1 mbar.

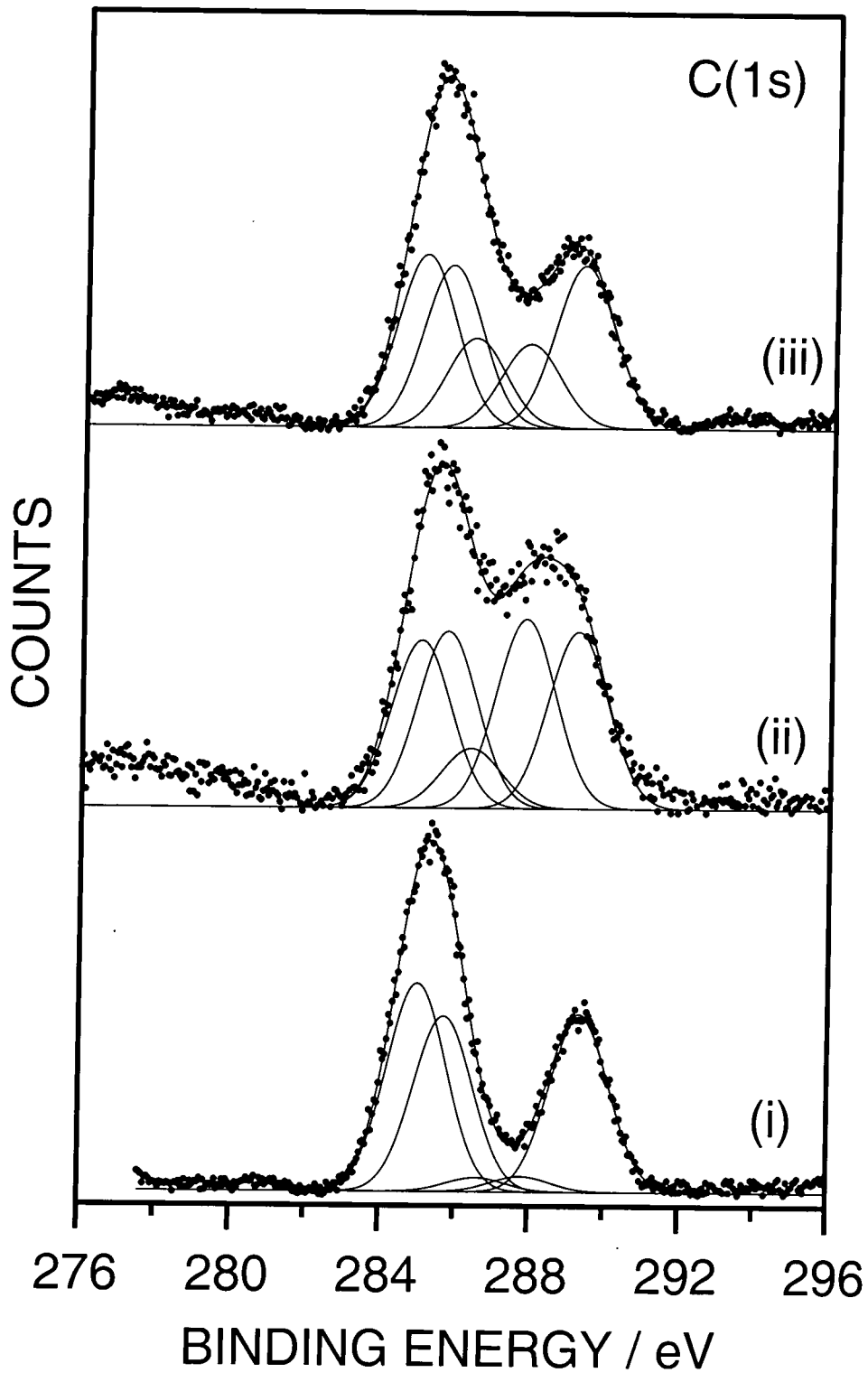

Figure 8: C(1s) XPS spectra of plasma coated glass slides: (i) acrylic acid alone P_{AA}=0.3 mbar; (ii) acrylic acid + NH_3 with P_{AA}=0.15 + P_{NH3}=0.15 mbar; and (iii) P_{AA}=0.2 + P_{NH3}=0.1 mbar.

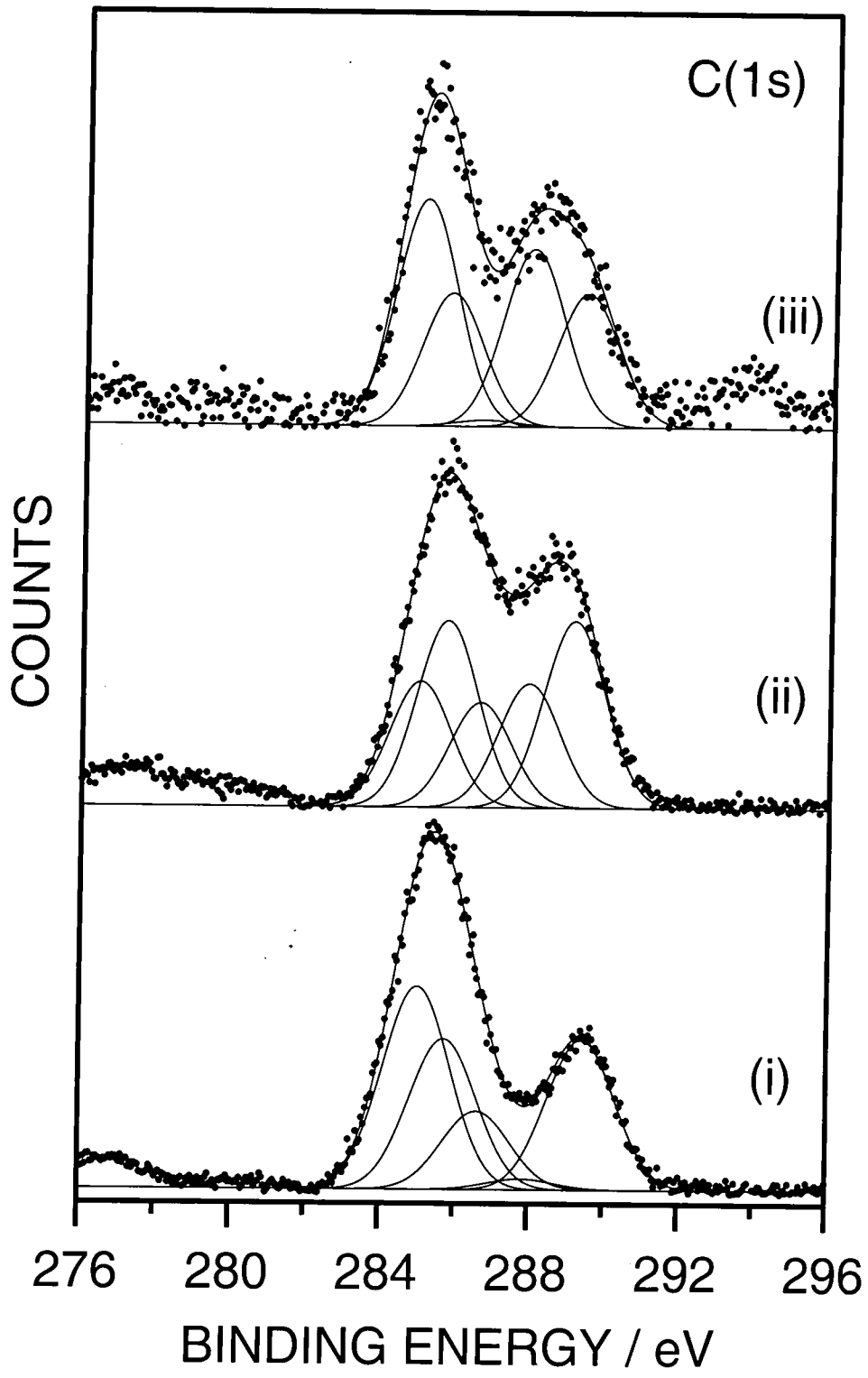

Figure 9: C(1s) XPS spectra of plasma coated glass slides: (i) maleic anhydride (MA) alone P_{MA}=0.1 mbar; (ii) MA + NH_3 with P_{MA}=0.1 + P_{NH3}=0.1 mbar; and (iii) P_{MA}=0.1 + P_{NH3}=0.3 mbar.

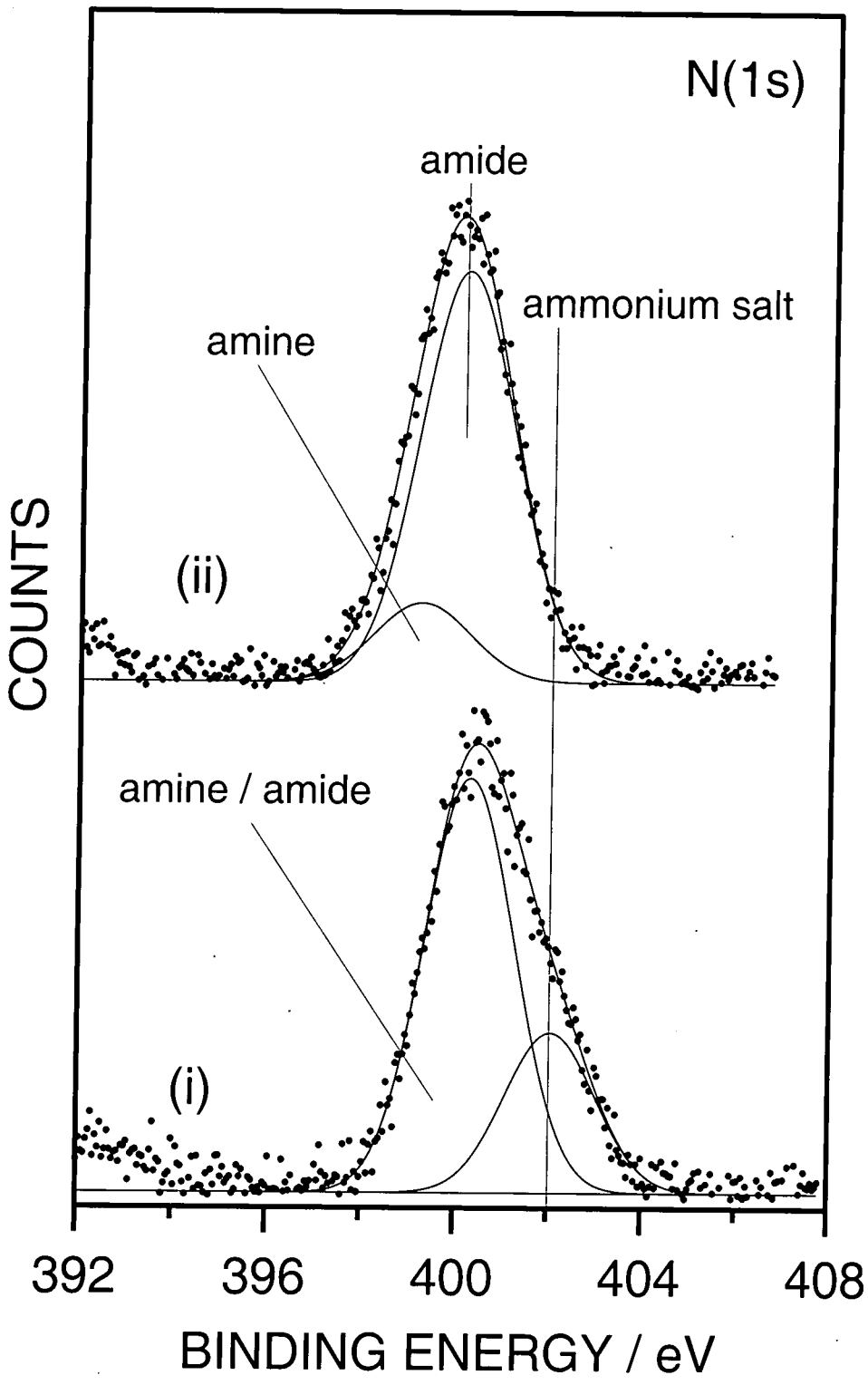

Figure 10: N(1s) XPS spectra of plasma coated glass slides: (i) maleic anhydride + NH_3 with P_{MA}=0.1 + P_{NH3}=0.1 mbar; and (ii) P_{MA}=0.1 + P_{NH3}=0.3 mbar.

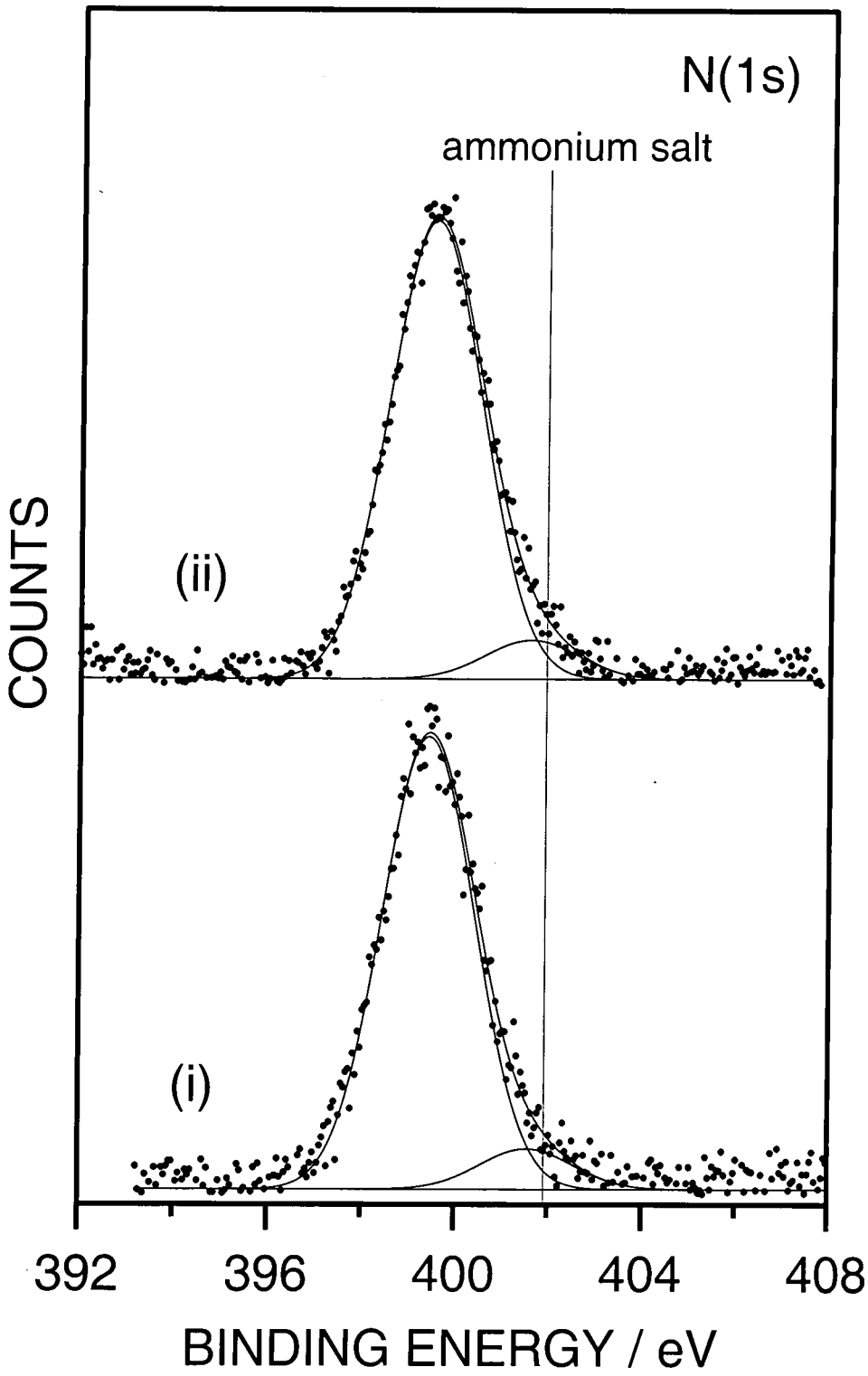

Figure 11: N(1s) XPS spectra of plasma coated glass slides: (i) allylamine alone P_{AL}=0.3 mbar; and (ii) MA + AL with P_{MA}=0.1 + P_{AL}=0.1 mbar.

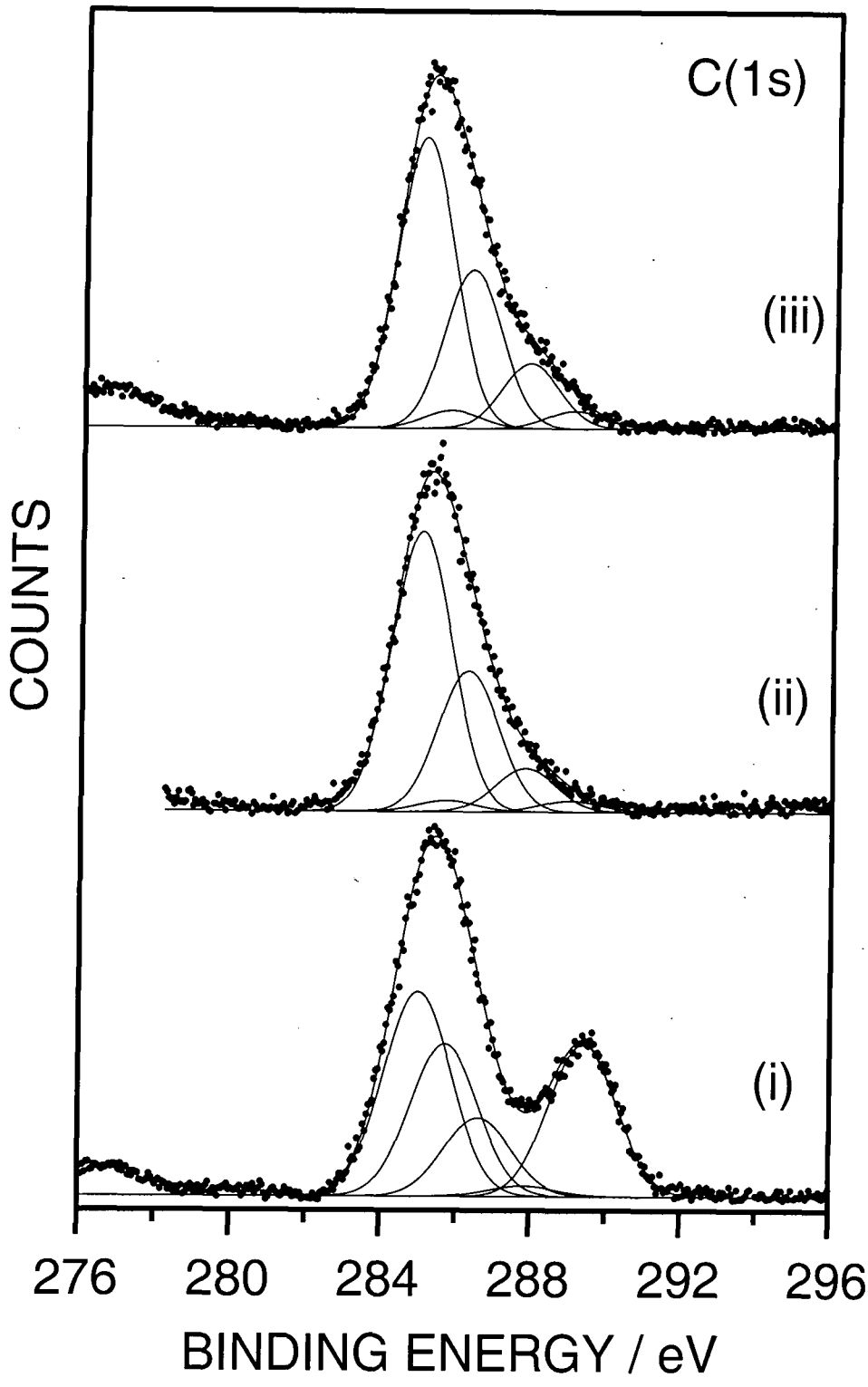

Figure 12: C(1s) XPS spectra of plasma coated glass slides: (i) maleic anhydride (MA) alone P_{MA}=0.1 mbar; (ii) allylamine alone P_{AL}=0.3 mbar; and (iii) MA + AL with P_{MA}=0.1 + P_{AL}=0.1 mbar.

Table 1: Summary of changes in elemental composition at the surface of the deposited films.

Plasma deposition	%C ± 3.0	%Si ± 0.1	%O ± 3.7	%N ± 0.6	% N amine/amide ± 0.4	%N ammonium salt ± 0.6
Acrylic acid (AA)	63.2	0.0	36.8	0.0	0.0	0.0
Allylamine (AL)	71.4	2.4	6.0	20.1	18.5	1.6
$AL_{0.2}AA_{0.1}$	64.5	0.0	31.0	4.6	0.0	4.6
$AA_{0.15}AL_{0.15}$	68.1	0.0	16.9	15.0	8.0	7.0
$AA_{0.2}AL_{0.1}$	66.9	0.0	23.3	9.8	2.5	7.3
$AA_{0.2}AL_{0.1}$ (CW)	73.2	0.0	14.8	12.0	8.7	3.3
$AA_{0.15}NH3_{0.15}$	46.2	5.4	19.0	29.4	29.4	0.0
$AA_{0.2}NH3_{0.1}$	57.9	0.0	31.8	10.3	2.3	8.0
$MA_{0.1}NH3_{0.1}$	55.4	0.0	29.1	15.4	11.1	4.3
$MA_{0.1}NH3_{0.3}$	28.1	17.0	36.4	18.5	18.5	0.0

5.3.1.5 Maleic anhydride and allylamine

This composition resulted in the deposition of pure allylamine films, Figures 11 and 12.

5.3.2 Infrared spectroscopy

Infrared spectroscopy showed that thin films deposited from acrylic acid bore more resemblance to the monomer precursor than those produced from allylamine under identical plasma conditions, Figure 13. In the latter case, a significant broadening of the peak at 1638 cm^{-1} (N-H) was observed. This can be attributed to contributions from several different nitrogen functionalities such as secondary amines, imines (N=C), and amides (N-C=O). Opening of carbon-carbon double bonds during plasma polymerisation was evident from the disappearance of absorption bands associated with alkene groups at 1636-1642 cm^{-1} (C=C), 986-995 cm^{-1} (trans CH= wag), and 912 cm^{-1} (CH_2= wag).

Table 2: IR absorption assignments.[20,21,22]

Wavenumber / cm^{-1}	Assignment	Symbol
1705-1720	C=O stretching vibrations.	■
1599-1638	N-H bending vibrations	
1636-1638	Amide I band.	
1636-1642	C=C stretching vibrations.	●
1638-1674	C=N stretching vibrations.	
1562-1576	Asymmetrical CO_2^- stretching vibrations.	◆
1454-1456	CH_2 bending vibrations.	
1435	C-O-H bending vibrations.	
1391-1406	Symmetrical CO_2^- stretching vibrations.	◆
1244-1300	C-O stretching vibrations	
986-995	Trans CH= wagging	●
912	CH_2= wagging	
831	NH_2 wagging	

The infrared spectra obtained from the CW and pulsed deposited $AA_{0.2}AL_{0.1}$ coatings were found to be very similar, Figure 13. The absorption band at 1705-1720 cm^{-1} (C=O) due to carboxylic groups from the acrylic acid was absent and two new peaks at 1562-1576 cm^{-1} (v_a CO_2^-) and 1391-1406 cm^{-1} (v_s CO_2^-) emerged. This provided an indication that carboxylate groups had formed. The intensity of these peaks relative to that of the methylene band at 1454-1456 cm^{-1} was higher in the case of the pulsed plasma polymers. This observation was in agreement with the findings from XPS analysis. Finally, both plasma depositions of the $AA_{0.2}AL_{0.1}$ vapour mixture lead to consumption of all the carbon-carbon bonds.

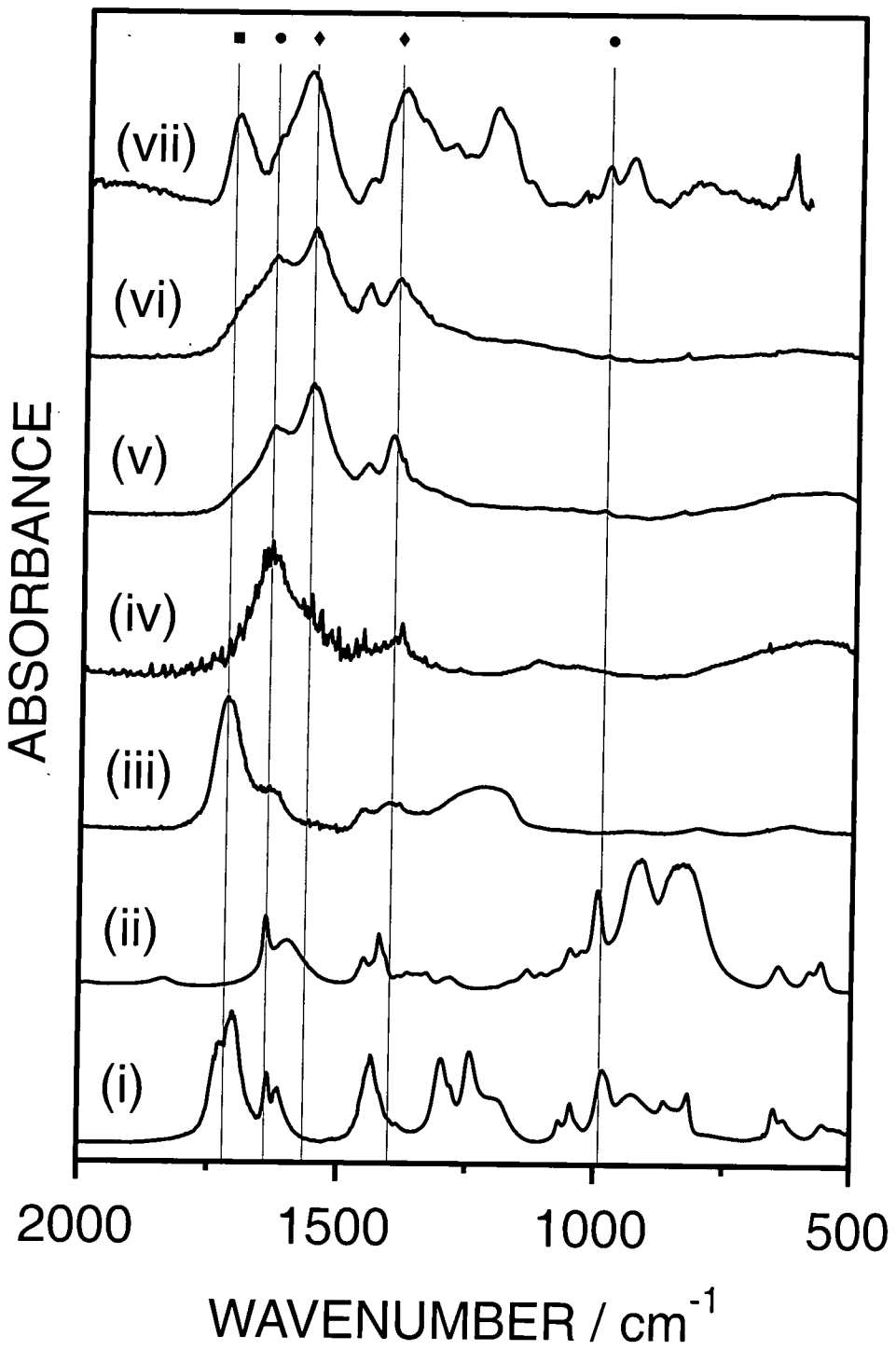

Figure 13: Infrared spectra: (i) acrylic acid; (ii) allylamine; (iii) pulsed plasma deposited acrylic acid; (iv) pulsed plasma deposited allylamine; (v) pulsed plasma deposited acrylic acid + allylamine with P_{AA}=0.2 + P_{AL}=0.1 mbar; (vi) CW plasma deposited acrylic acid + allylamine with P_{AA}=0.2 + P_{AL}=0.1 mbar; and (vii) neat acrylic acid and neat allylamine mixture (1:1 molar ratio).

Ionisation of the carboxylic groups was also found to occur in the case of the 1:1 acrylic acid / allylamine liquid mixture, Figure 13. A summary of the characteristic absorption bands for the pure monomers and plasma deposited polymers is presented in Table 2.

5.3.3 Gas barrier measurements

Oxygen gas barrier results for the different plasma deposited films are shown in Table 3. Pulsed plasma deposition of $AA_{0.2}AL_{0.1}$ produced the most oxygen impermeable films. Whereas the converse was true for continuous wave deposition of the same mixture. It was also found that the acrylic acid constituent has a greater influence on enhancing the gas barrier properties of the polypropylene films compared to allylamine. This observation is not conclusive due to very large difference in the thickness of the respective films as determined by deposition rate measurements. In addition, XPS data have suggested that pulsed deposition of allylamine lead to incomplete coverage of the substrate.

Table 3: Oxygen permeability measurements.

Sample	MEPPP (10^{-8})	BIF*	Relative thickness
o-PP (reference sample)	29.1 ± 1.3	-	-
pulsed deposited allylamine	18.6 ± 5.4	1.6	1
pulsed deposited acrylic acid	4.3 ± 2.7	6.8	×7
pulsed deposited $AA_{0.2}AL_{0.1}$	2.9 ± 1.8	10.0	×8
CW deposited $AA_{0.2}AL_{0.1}$	21.4 ± 3.3	1.4	×8

* *Barrier Improvement Factor*

5.4 DISCUSSION

Good structural retention was found to be the key factor for producing ammonium salt containing plasma films. This can be explained on the basis that an increase in the amount of the incorporated carboxylic and amine groups at the surface will give rise to an increased number of interactions between them. The highest amount of surface functionalisation occurred by pulsing the discharge power (i.e. reduced input power). This is in agreement with previously reported results.[23] The chemical and physical properties of the resulting plasma films were more strongly influenced by the plasma conditions affecting the deposition of the acrylic acid monomer. Excessive fragmentation of the allylamine monomer will still produce amine-containing functionalities, whereas the opposite is true in the case of acrylic acid.[4] This was supported by the observation that highly enriched in ammonium-salt plasma polymers were also deposited upon replacement of the allylamine precursor with ammonia gas in the monomer mixture. Continuous wave and pulsed plasma polymerised films were found to differ significantly in their outermost surface regions, but not to the same extent in their bulk. This can be attributed to a possible greater freedom of lateral movement of the amino and carboxylic groups at the surface.[24]

As anticipated, the ammonium salt content in the deposited polymer films was found to be strongly correlated with the composition of the precursor mixture. For instance, a large excess of one monomer will have a diluting effect towards the deposition of the other monomer and vice versa. From the results in this chapter, the existence of an optimum composition leading to maximum ammonium salt formation was confirmed, even though this was not precisely estimated, due to limitations in the experimental set-up.

The nature of the monomer precursor was also vital. Replacement of the acrylic acid with maleic anhydride may give rise to reaction pathways favouring formation of amides and not ammonium salt. This type of reaction has been reported in the past.[25,26]

Finally, ammonium salt formation at the surface of the plasma deposited polymers gave rise to good gas barrier properties on polypropylene substrates. This is possibly due to the intermolecular ionic interactions between amine and carboxylic groups present in the copolymer chains promoting more closely packed networks at the surface.

5.5 CONCLUSIONS

Plasma co-polymerisation of acrylic acid with allylamine and ammonia promoted ammonium salt formation at the surface. The same was not observed when the acrylic acid was replaced with maleic anhydride. Plasma conditions and mixture composition were found to be among the most important parameters controlling the chemistry of the plasma films. Finally, ammonium salt containing plasma coatings gave rise to good gas barrier properties.

5.6 REFERENCES

1 Yasuda, H. In *Plasma Polymerization*; Academic Press: London, 1985.

2 Garbassi, F.; Morra, M.; Occhiello, E. In *Polymer Surfaces - From Physics to Technology*; Wiley: Chichester, 1994.

3 López, G. P.; Ratner, B. D. *Langmuir* **1991**, *7*, 766.

4 Candan, S.; Beck, A. J.; O'Toole, L.; Short, R. D. *J. Vac. Sci. Technol. A*, **1998**, *16*, 1702.

5 O'Toole, L.; Beck, A. J.; Short, R. D. *Macromolecules* **1996**, *29*, 5172.

6 O'Toole, L.; Beck, A. J.; Ameen, A. P.; Jones, F. R; Short, R. D. *J. Chem. Soc. Faraday Trans.* **1995**, *91*, 3907.

7 Ko, T. M.; Cooper, S. L. *J. Appl. Polym. Sci.* **1993**, *47*, 1601.

8 Calderon, J. G.; Harsch, A.; Gross, G. W.; Timmons, R. B. *J. Biomed. Mater. Res.* **1998**, *42*, 597.

9 Ryan, M. E.; Hynes, A. M.; Badyal, J. P. S. *Chem. Mater.* **1996**, *8*, 37.

10 Badyal, J. P. S.; Hynes, A. M. *Chem. Mater.* **1998**, *10*, 2177.

11 Panchalingam, V.; Chen, X.; Savage, C. R.; Timmons, R. B.; Eberhart, C. *J. Appl. Polym. Sci.: Appl. Polym. Sym.* **1994**, *54*,123.

12 France, R. M.; Short, R. D.; Dawson, R. A.; MacNeil, S. *J. Mater. Chem.* **1998**, *8*, 37.

13 Beck, A. J.; Jones, F. R; Short, R. D. *Polymer* **1996**, *37*, 5537.

14 Johanson, G.; Hedman, J.; Berndtsson, A.; Klasson, M.; Nilsson, R. *J. Electron Spectr.* **1973**, *2*, 295.

15 Williamson, W. H. US 3961018, 1976.

16 Chakraborty, A. K.; Bischoff, K. B.; Astarita, G.; Damewood, J. R., Jr. *J Am. Chem. Soc.* **1988**, *110*, 6947.

17 Moulder, J. F.; Stickle, W. F.; Sobol, P. E.; Bomben, K. D. In *Handbook of X-ray Photoelectron Spectroscopy*; Chastain, J., Ed.; Perkin-Elmer Corporation: Minnesota, 1992.

18 Beamson, G.; Briggs, D. In *High Resolution XPS of Organic Polymers: The Scienta ESCA300 Database*; Wiley: New York, 1992.

19 Jousseaume, V.; Morsli, M; Bonnet, A.; Lefrant, S. *J. Appl. Polym. Sci.* **1998**, *67*, 1209.

20 Silverstein, R. M.; Bassler, G. C.; Morrill, T. C. In *Spectroscopic Identification of Organic Compounds*; John Wiley & Sons: Singapore, 1991.

21 Lin-Vien, D.; Colthup, N. B.; Fateley, W. G.; Grasselli, J. G. In *The Handbook of Infrared and Characteristics of Organic Molecules*; Academic Press: San Diego, 1991.

22 Bellamy, L. J. In *The Infrared Spectra of Complex Molecules*; Chapman and Hall: London, 1975; Vol. 1.

23 Hutton, S. J. Ph.D. Thesis, University of Durham, 2000.

24 Burns, N. L.; Holmberg, K., Brink, C. *J. Colloid Interface Sci.* **1996**, *178*, 116.

25 Kretov, A. E.; Kulchitskaya, N. E. *Jnl. Gen. Chem. USSR*, **1955**, *25*, 2363.

26 Adalsteinsson, H.; Bruice, T. C. *J. Am. Chem. Soc.* 1998, 120, 3440.

CHAPTER 6

PLASMA FLUORINATION OF POLYDIMETHYLSILOXANE DOPED POLYOLEFINS AND PURE POLYDIMETHYLSILOXANE COATINGS

6.1 INTRODUCTION

Fluorination of polymer surfaces by utilising non-equilibrium CF_4 plasmas[1,2] has been used in numerous cases in the past for producing polymers with enhanced hydrophobicity.[3] CF_4 glow discharge contains primarily fluorine atoms and in a small concentration CF, CF_2, and CF_3 radicals with the former being the most reactive component. This excess of fluorine radicals can lead to direct surface fluorination via hydrogen substitution by fluorine in the case of saturated polymers or via atomic fluorine addition at the carbon-carbon double bond in the case of unsaturated ones.[4]

In this chapter, the CF_4 plasma modification of the polydimethylsiloxane/ polyethylene (PDMS/PE), polydimethylsiloxane/polypropylene (PDMS/PP), and pure PDMS surfaces has been investigated as a function of discharge input power, treatment time, and in the case of pulsing conditions, on-time/off-time settings using X-ray photoelectron spectroscopy (XPS) and contact angle measurements.

6.2 EXPERIMENTAL

6.2.1 PDMS doped polyethylene/polypropylene

Linear polydimethylsiloxane (PDMS) containing a $-SiMe_2CH{=}CH_2$ endblock (Dow Corning, M_w = 500,000 and T_g = 146 K) was mixed with linear low density polyethylene / low density polyethylene (LLDPE / LDPE) or polypropylene (PP) during film extrusion via the bubble-film process.

The samples were ultrasonically cleaned in a 1:1 cyclohexane (BDH, 99.5 % purity) / propan-2-ol (BDH, 99.7 % purity) mixture for 30 s, followed by annealing in a vacuum oven (LTE, Qualivac) at 80 °C for 30 min. CF_4 gas (Air products, 99.7 % purity) plasma treatment of the polymer blend surfaces was carried out for 1s up to 5 min duration at powers ranging from 2 W up to 20W in a cylindrical glass reactor as described in Chapter 2.

6.2.2 Pure PDMS coatings

Pure PDMS surfaces were prepared by spin coating a 5% wv solution of PDMS gum (Fluorochem) in toluene onto nylon 6.6 substrates (Goodfellow). The coatings were vacuum-dried inside a desiccator for 1 day and then examined by

using XPS. Absence of N(1s) peak in the XPS spectra was indicative of the complete PDMS coverage of the nylon substrates.

Continuous wave CF_4 plasma treatment was carried out for 60 s at 0.2 mbar pressure for powers ranging from 5 - 40 W. In the case of the pulsed plasma exposure, the conditions comprised, t_{on} varying between 20 - 50000 μs, t_{off} varying between 250 - 20000 μs, and peak power set at 10 W (the CF_4 gas pressure and treatment time were kept the same as for continuous wave experiments).

6.2.3 Sample characterisation

A Kratos ES300 electron spectrometer equipped with a Mg Kα X-ray source (1253.6 eV), and a concentric hemispherical analyser (CHA) was used for XPS analysis. Photo-emitted electrons were collected at a take-off angle of 30° from the substrate normal, with electron detection in the fixed retarding ratio (FRR, 22:1) mode. XPS spectra were accumulated on an interfaced PC computer and fitted using a Marquardt minimisation algorithm assuming that all the peaks are Gaussian with equal full-width-at-half-maximum (FWHM).[5] Instrument sensitivity factors using reference chemical standards were taken as C(1s) : O(1s) : Si (2p) : F(1s) equals 1.00 : 0.57 : 0.72 : 0.67.

Contact angle measurements were taken with digital contact angle goniometer (VCA, 2500XE). At least six measurements were taken with high purity deionised water (0.04 μS) from different areas of the samples.

6.3 RESULTS

CF_4 plasma treatment of the washed and annealed PDMS doped polyolefin films resulted in surface fluorination, Table 1. This was accompanied by a significant reduction in the elemental concentration of all the other elements originally present at the surface of the films. As can be seen from the results in Table 1, CF_4 discharge led to complete disappearance of silicon species. Fluorination of the surface caused a shift of the C(1s) peak towards higher binding energies, Figures 1 and 2. Increase in the intensity of the high binding energy shoulder provided evidence for the presence of $>\underline{C}F_2$ and $-\underline{C}F_3$ groups at 291.2 and 293.6 eV, respectively.[6] A drop in the intensity of the hydrocarbon C(1s) shoulder (285.0 eV) was also noted. This suggested that plasma fluorination produced hydrocarbon-deficient surfaces.

The highest fluorination occurred at high glow discharge powers, Table1, Figures 1 and 2. The optimum duration of the CF_4 plasma treatment was found to be between 15 and 60 s, Table 2, Figure 3. A significant amount of oxygen incorporation was observed for prolonged treatments. Very short duration resulted in incomplete fluorination of the samples, Figure 3. Comparison between the blends and their respective host polyolefins showed that both behaved in a similar fashion upon CF_4 plasma treatment, Table 3.

The bulk loading in PDMS dopant appeared to have a very small effect on the extent of the surface fluorination, Figure 4. The highest surface concentration of fluorinated species corresponded to samples that contain none or minimum amount of PDMS in their bulk. Water contact angle measurements confirmed the existence of a highly fluorinated layer at the surface of the plasma treated films, Table 4.

CF_4 plasma treatment of pure PDMS coatings also produced highly fluorinated surfaces. In contrast with the polymer blends, larger amounts of fluorinated species were formed at low glow discharge powers, whereas the opposite trend was true for their oxidised counterparts, Figure 5. Reduction in the average input power, by pulsing the applied R.F. voltage, did not produce any significant increase in the relative amount of fluorine at the surface. Furthermore, it was found that very short t_{on} settings (below 1000 μs) led to incomplete fluorination together with a parallel increase in oxygen to silicon ratio, Figure 6. Similar behaviour was also observed in the case where long off-times (above 1000 μs) were utilised, Figure 7.

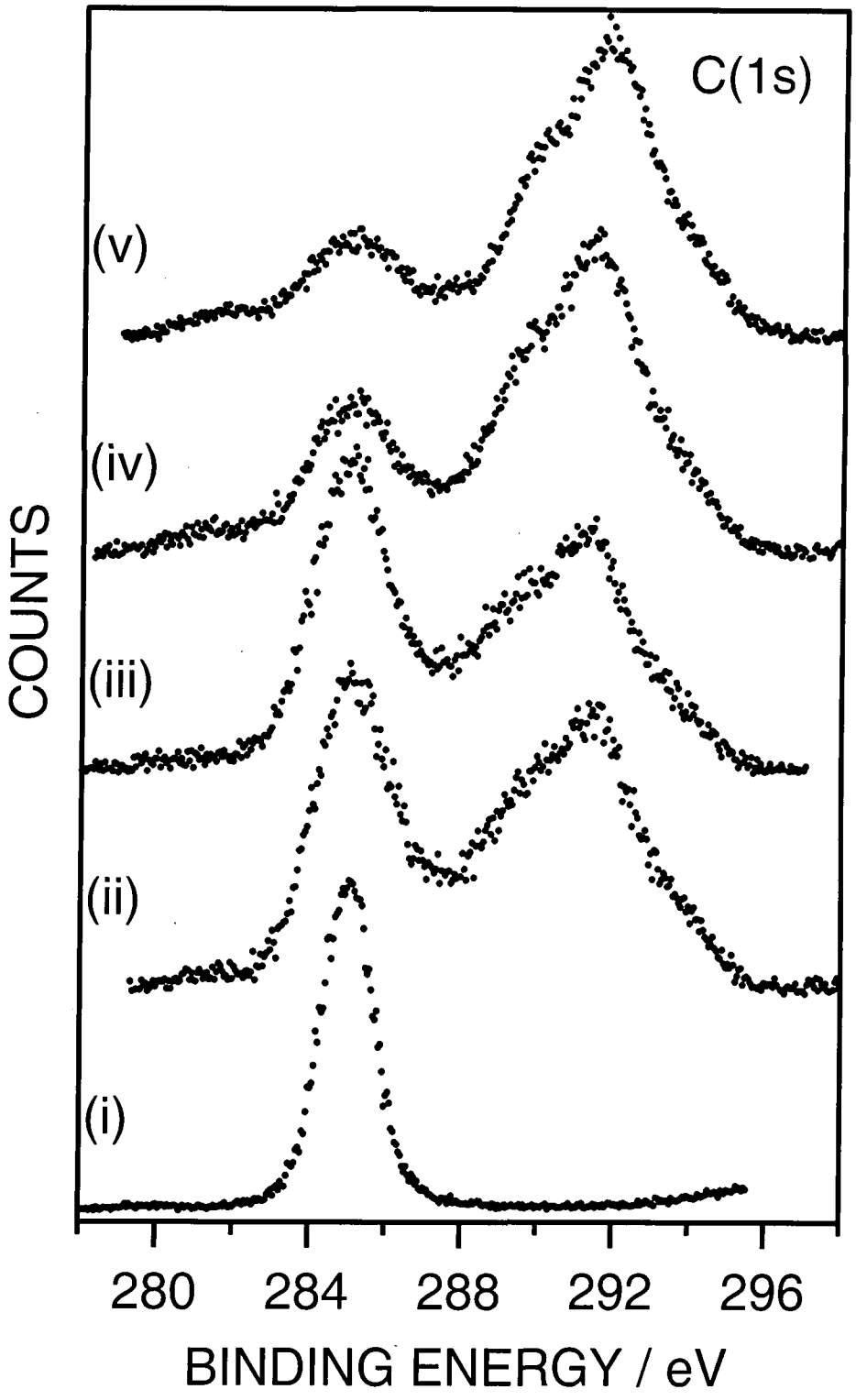

Figure 1: C(1s) XPS spectra of 2.5% PDMS doped polyethylene: (i) ultrasonically washed in 50 / 50 cyclohexane propan-2-ol solvent mixture, followed heating at 80 °C for 30 min; (ii) 2W CF_4 plasma treatment for 60 s; (iii) 5W CF_4 plasma treatment for 60 s; (iv) 10W CF_4 plasma treatment for 60 s; and (v) 20W CF_4 plasma treatment for 60 s.

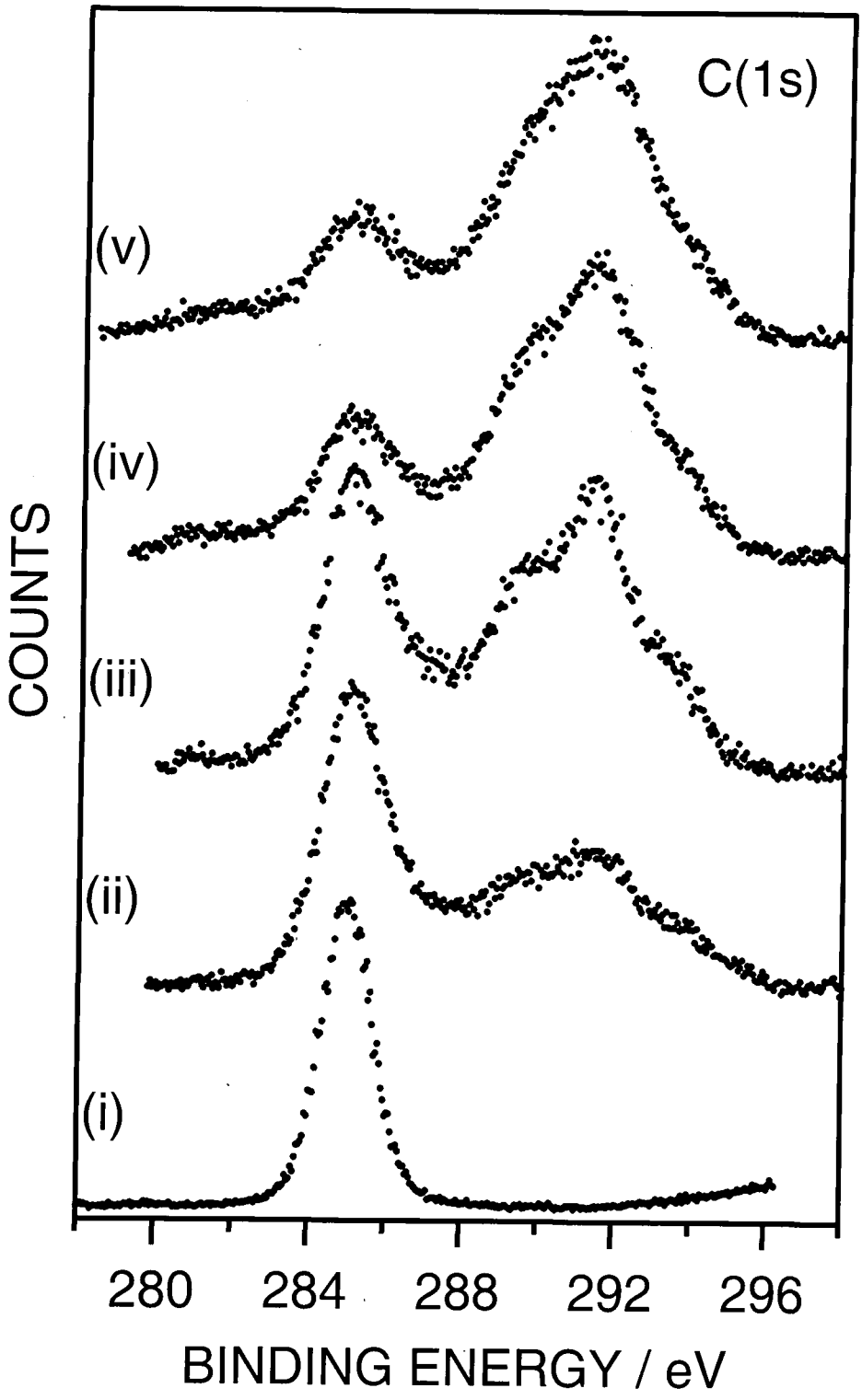

Figure 2: C(1s) XPS spectra of 2.5% PDMS doped polypropylene: (i) ultrasonically washed in 50 / 50 cyclohexane propan-2-ol solvent mixture, followed heating at 80 °C for 30 min; (ii) 2W CF_4 plasma treatment for 60 s; (iii) 5W CF_4 plasma treatment for 60 s; (iv) 10W CF_4 plasma treatment for 60 s; and (v) 20W CF_4 plasma treatment for 60 s.

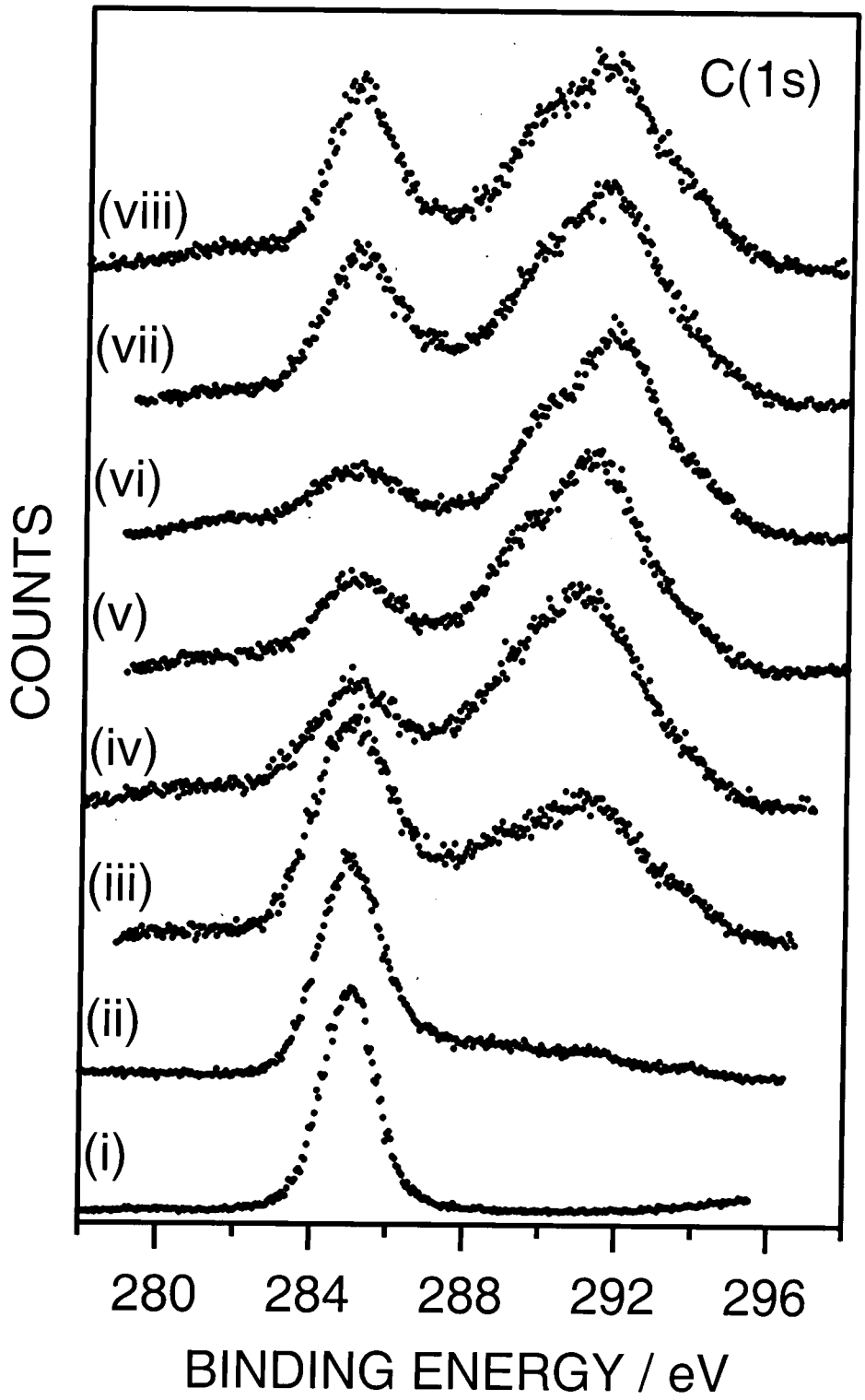

Figure 3: C(1s) XPS spectra of 2.5% PDMS doped polyethylene: (i) ultrasonically washed in 50 / 50 cyclohexane propan-2-ol solvent mixture, followed heating at 80 °C for 30 min; (ii) 20W CF_4 plasma treatment for 1 s; (iii) 20W CF_4 plasma treatment for 5 s; (iv) 20W CF_4 plasma treatment for 15 s; (v) 20W CF_4 plasma treatment for 30 s; (vi) 20W CF_4 plasma treatment for 1 min; (vii) 20W CF_4 plasma treatment for 2 min; and (viii) 20W CF_4 plasma treatment for 5 min.

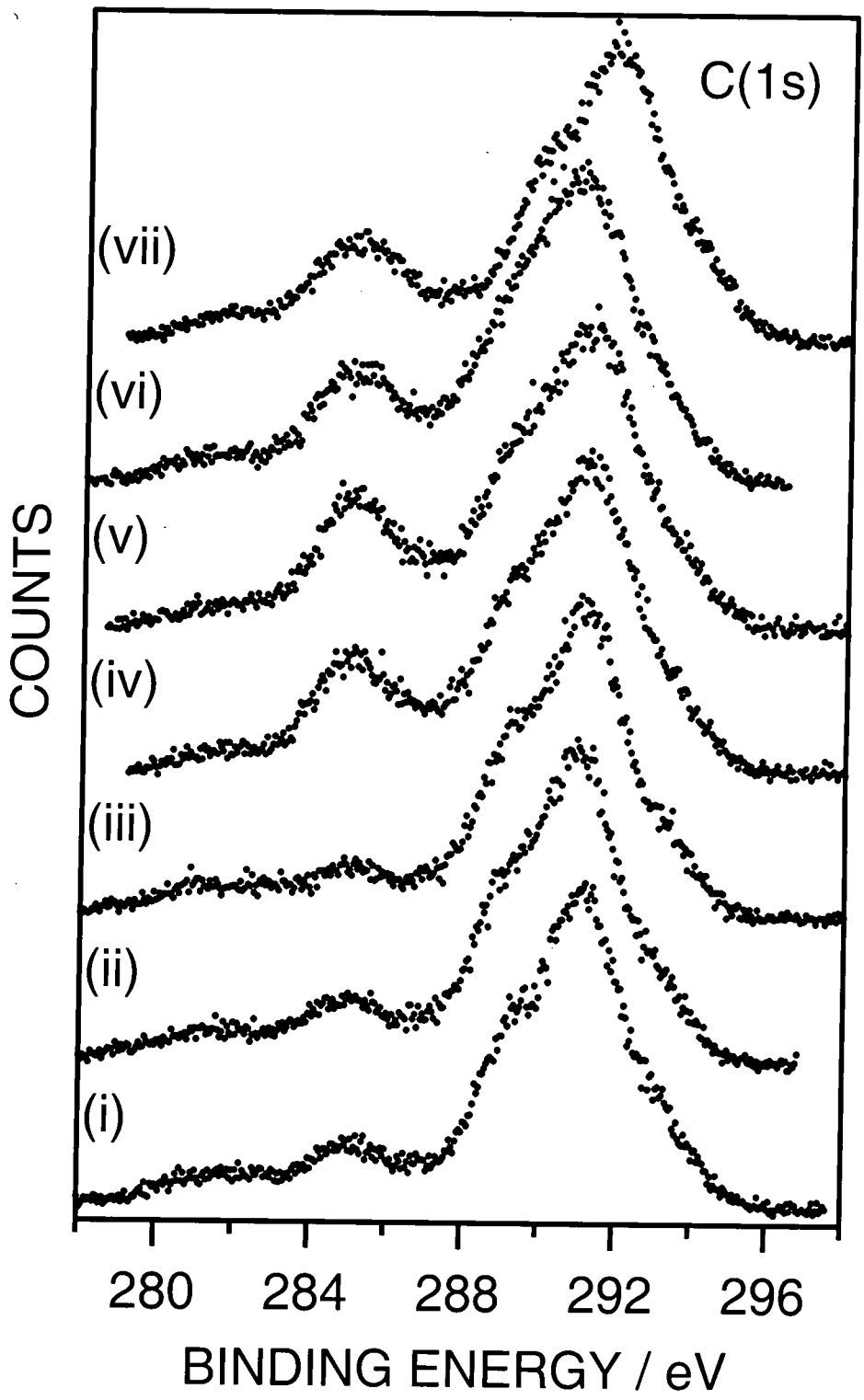

Figure 4: C(1s) XPS spectra of 20 W CF_4 plasma treated for 1 min PDMS doped polyethylene with varying bulk loading: (i) 0 % PDMS; (ii) 0.1 % PDMS; (iii) 0.25 % PDMS; (iv) 0.5 % PDMS; (v) 1 % PDMS; (vi) 2 % PDMS; and (vii) 2.5 % PDMS.

Table 1: Elemental concentrations of the surface of 2.5% PDMS doped polyethylene/polypropylene films following CF_4 plasma treatment at different discharge powers.

	2.5 % PDMS doped PE							2.5 % PDMS doped PP						
	%C ± 1.0	%Si ± 0.0	%O ± 0.8	%F ± 0.6	F/C ± 0.1	%Hydrocarbon Species	%Fluorinated Carbon Species	%C ± 1.0	%Si ± 0.0	%O ± 0.8	%F ± 0.6	F/C ± 0.1	%Hydrocarbon Species	% Fluorinated Carbon Species
W/H	84.5	6.7	8.9	-	-	100	-	91.9	2.8	5.4	-	-	100	-
2W	44.7	0.0	1.0	54.4	1.2	38	62	46.2	0.0	6.2	47.6	1.0	41	60
5W	44.5	0.0	3.2	52.3	1.2	41	61	43.4	0.0	3.3	53.3	1.2	34	66
10W	43.1	0.0	2.9	54.0	1.3	25	73	42.1	0.0	2.1	55.7	1.3	22	77
20W	41.2	0.0	3.2	55.6	1.4	22	78	42.4	0.0	3.2	54.4	1.3	21	79

Table 2: Elemental concentrations of the surface of 2.5% PDMS doped polyethylene films following 20 W CF_4 plasma treatment at different times.

	2.5 % PDMS doped PE						
	%C ± 1.0	%Si ± 0.0	%O ± 0.8	%F ± 0.6	F/C ± 0.1	%Hydrocarbon Species	%Fluorinated Carbon Species
W/H	84.5	6.7	8.9	-	-	100	-
1 s	52.2	2.7	7.5	37.6	0.7	59	45
5 s	45.7	0.4	3.5	50.5	1.1	41	60
15 s	41.0	0.0	2.4	56.6	1.4	27	73
30 s	41.7	0.0	2.9	55.4	1.3	22	76
1 min	41.2	0.0	3.2	55.6	1.4	22	78
2 min	42.0	0.0	6.3	51.6	1.2	30	70
5 min	42.7	0.0	9.8	47.7	1.1	29	71

Table 3: Elemental composition and water contact angles of the surface of pure polyethylene and polypropylene films. Comparison with the results obtained for their doped versions (20 W CF_4 plasma treatment for 1 min).

Treatment	PE							
	%C ± 1.0	%Si ± 0.0	%O ± 0.8	%F ± 0.6	F/C ± 0.1	%Hydrocarbon Species	%Fluorinated Carbon Species	C.A.
Untreated	97.0	1.2	1.9	-	-	100	-	
Plasma treated	38.5	0.0	1.9	59.7	1.6	14	86	130.0±1.0
2.5% PDMS doped plasma treated	41.2	0.0	3.2	55.6	1.4	22	78	129.0±1.5
	PP							
	%C ± 1.0	%Si ± 0.0	%O ± 0.8	%F ± 0.6	F/C ± 0.1	%Hydrocarbon Species	%Fluorinated Carbon Species	C.A.
Untreated	98.7	0.4	0.9	-	-	100	-	
Plasma treated	40.8	0.0	2.2	57.1	1.4	13	87	121.0±2.0
2.5% PDMS doped plasma treated	42.4	0.0	3.2	54.4	1.3	21	79	120.0±1.5

Table 4: Elemental composition and water contact angles of the surface of PDMS doped polyethylene films at various dopant concentrations (20 W CF_4 plasma treatment for 1 min).

% PDMS	% C ± 1.0	% Si ± 0.0	% O ± 0.8	% F ± 0.6	F/C ± 0.1	%Hydrocarbon Species	%Fluorinated Carbon Species	C.A.
0	38.5	0.0	1.9	59.7	1.6	14	86	130.0±1.0
0.1	38.9	0.0	0.4	60.7	1.6	15	85	129.5±0.5
0.25	40.8	0.0	1.4	57.9	1.4	12	88	130.0±1.0
0.5	40.8	0.0	1.3	57.9	1.4	21	79	131.5±1.0
1.0	41.2	0.0	1.8	57.0	1.4	23	77	130.0±1.5
2.0	41.5	0.0	1.3	57.2	1.4	21	79	131.3±1.4
2.5	41.2	0.0	3.2	55.6	1.4	22	78	129.0±1.5

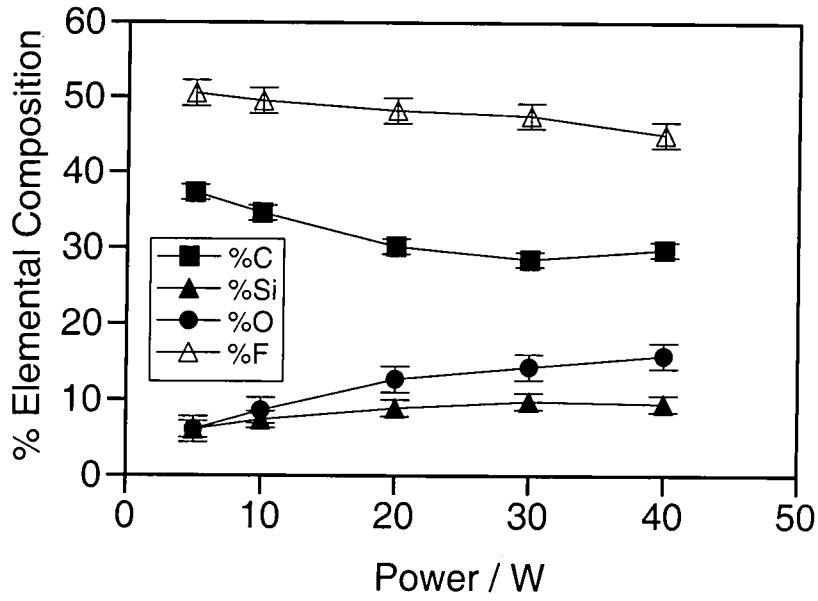

Figure 5: Change in elemental composition at the surface of PDMS as a function of CF_4 glow discharge power level (total duration = 60 s).

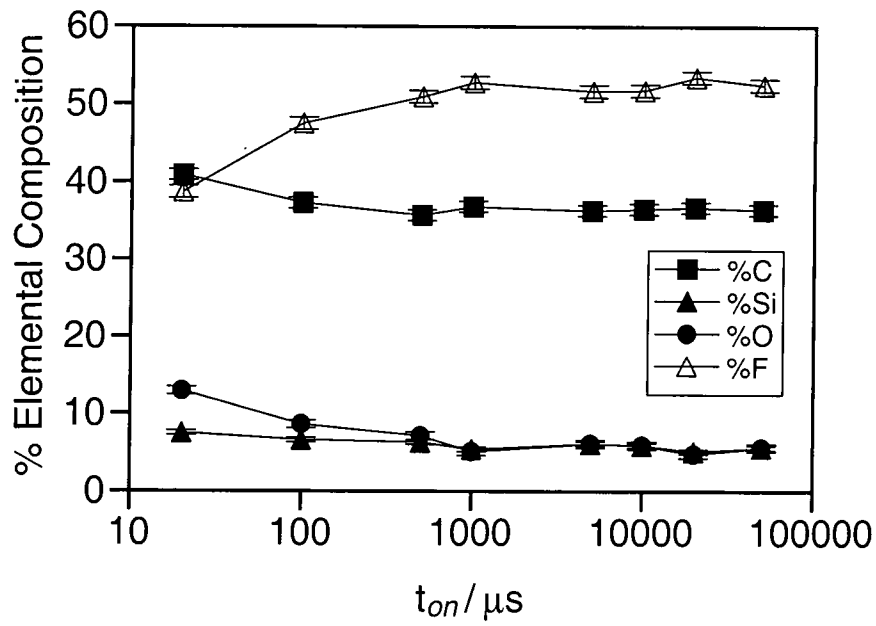

Figure 6: Change in elemental composition at the surface of CF_4 pulsed plasma treated PDMS as a function of t_{on} (P_p = 10 W, t_{off} = 250 μs, total duration = 60 s).

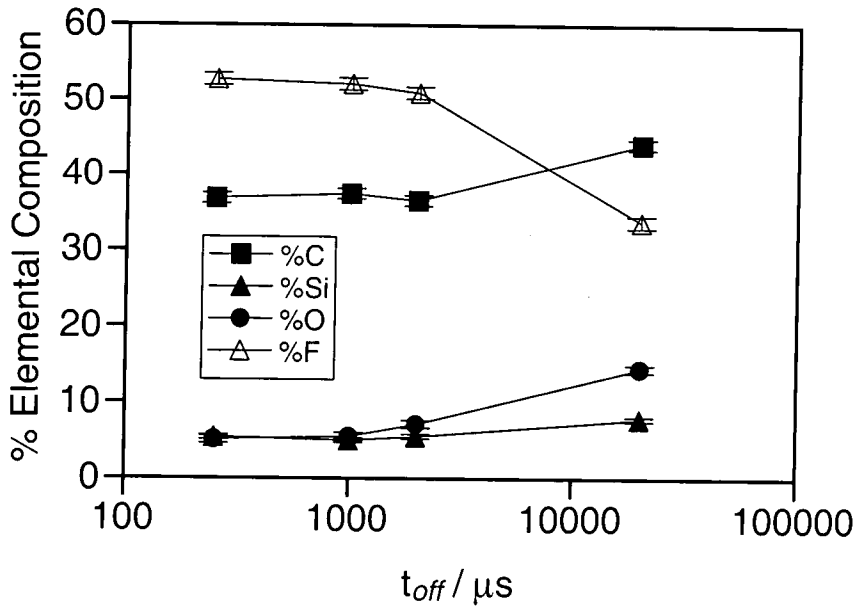

Figure 7: Change in elemental composition at the surface of CF_4 pulsed plasma treated PDMS as a function of t_{off} (P_p = 10 W, t_{on} = 1000 μs, total duration = 60 s).

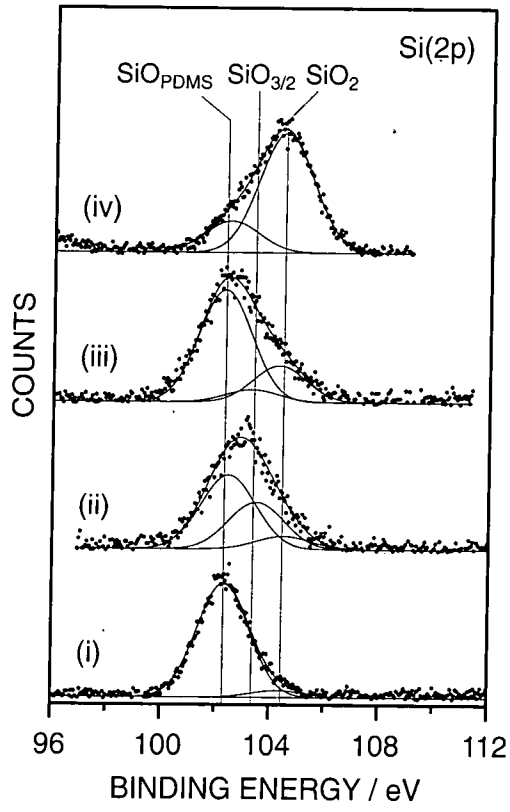

Figure 8: Si(2p) XPS spectra of CF_4 plasma treated PDMS: (i) P_p = 10 W, t_{on} = 20 μs, t_{off} = 250 μs; (ii) P_p = 10 W, t_{on} = 1000 μs, t_{off} = 250 μs; (iii) continuous wave (CW) 5 W; and (iv) continuous wave (CW) 40 W (total duration for all treatments = 60 s).

6.4 DISCUSSION

In the case of the PDMS doped polyethylene/polypropylene blends, CF_4 glow discharge caused the removal of the siloxane-rich topmost layer present at the surface. Subsequent fluorination took place via reaction pathways similar to those reported in the past for polyolefin homopolymers (i.e. hydrogen substitution by fluorine).

The CF_4 plasma treatment of PDMS using different plasma conditions can result in significant differences in the surface produced. At low continuous wave plasma power the elemental composition of the surfaces produced show mainly carbon and fluorine with the proportions of silicon and oxygen reduced from that of the unaltered substrate. The CF_x species present on the surface are predominantly CF_2. These results indicate that two mechanisms may be occurring on the surface. The first is direct fluorination of the substrate by hydrogen abstraction from a methyl group, followed by fluorine attachment. However, if complete direct fluorination of these CH_3 groups on the surface were occurring during plasma treatment, it would be expected that the major CF_x surface component would be CF_3. As this is not the case it is probable that a certain amount of cross-linking between surface carbon groups occurs after abstraction of a hydrogen, before the complete fluorination of the group. This can occur due to the flexibility of the siloxane chains; >Si-CH_2-CH_2-Si< groups have been observed in other work.[7] The second process occurring within the CF_4 plasma is polymerisation of gas phase CF_2 and CF species produced within the plasma, leading to thin film formation on the substrate surface.[8,9]

When progressing to higher continuous wave plasma powers, several trends can be observed. The degree of fluorination of the surface decreases, the silicon and oxygen percentages of the elemental composition rise, and the oxygen to silicon ratio increases. The XPS peak of the silicon within these surfaces is also shifted significantly, Figure 8. These trends indicate that there is an overall increase in oxidised silicon species on the surface, with more silicon-oxygen bonds being created. The possibility that this can be due to etching of SiO_2 from the glass reactor walls followed by redeposition onto the PDMS substrate can be discounted, as the same CF_4 plasma conditions with a PE substrate do not show silicon deposition. Therefore, direct oxidation of the silicon within the PDMS is occurring, accompanied by removal of a (possibly fluorinated) carbon group from the given silicon centre. The oxygen within the

plasma discharge is present due to unavoidable air leaks into the plasma chamber or due to water desorbed from the reactor walls.[10] Alternatively, direct fluorination of silicon atoms followed by post plasma hydrolysis reactions in the presence of moisture under open laboratory conditions could also have been responsible.[11] The fluorine percentages do not reduce to zero under these conditions, nor do silicon and oxygen dominate the composition of the surface. Therefore, while oxidisation of silicon species does occur within the CF_4 plasma treatment, fluorination and cross-linking of remaining methyl groups and thin film deposition of CF_x onto the surface still occurs during these higher power continuous wave plasmas.

Pulsing of a plasma discharge reduces the average power of the plasma. The two figures for the pulsed CF_4 plasmas show that at longer on-times and shorter off-times (which correspond most closely to the low continuous wave powers) the elemental compositions of the resulting surfaces are identical to those produced by low power continuous wave CF_4 plasmas. Therefore the same processes are occurring within these plasmas, i.e. cross-linking and fluorination of methyl groups, and fluorocarbon layer formation. The fluorinated film deposition was proved for pulsed CF_4 plasmas with long on-times as they produced a similar trend in the elemental compositions of the substrate surface when deposited onto clean glass for prolonged times.

At smaller on-times and longer off-times of the pulsed CF_4 plasmas a similar trend to that observed for high continuous wave CF_4 plasmas was observed. I.e. the degree of fluorination of the surface decreases, the silicon and oxygen percentages of the elemental composition rise, and the oxygen to silicon ratio increases. However, in these cases the oxidation is not occurring to the silicon centres, but to carbon centres on the surface resulting in carbon-oxygen bond formation. This is due to competition between fluorine atoms and oxygen atoms within the plasma discharge to react with carbon radical sites formed by hydrogen abstraction. Competition may be occurring due to the lower average powers of these discharges producing fewer fluorine atoms, so allowing oxygen atoms the chance to react with surface radicals. It is also likely that film deposition of CF_x plasma species continues to occur at these low plasma powers.

6.5 CONCLUSIONS

The PDMS doped polyolefin blends, with bulk loading of the PDMS ranging from 0.1% - 2.5% wt, behaved in the same manner towards fluorination by CF_4 plasma, as clean polyethylene/polypropylene homopolymers.

CF_4 plasma treatment of PDMS can result in different types of surface modification. It is likely that thin film formation occurs to varying extents under all plasma conditions, but the direct modification of the PDMS substrate can take different forms depending upon the average energy of the plasma discharge.

6.6 REFERENCES

1 Hopkins, J; Boyd, R. D.; Badyal, J. P. S. *J. Phys. Chem.* **1996**, *100*, 6755.

2 Hopkins, J; Badyal, J. P. S. *Langmuir* **1996**, *12*, 3666.

3 Sigurdsson, S.: Shishoo, R. *J. Appl. Polym. Sci.* **1996**, *100*, 6755.

4 Hopkins, J; Badyal, J. P. S. *J. Phys. Chem.* **1995**, *99*, 4261.

5 Johanson, G.; Hedman, J.; Berndtsson, A.; Klasson, M.; Nilsson, R. *J. Electron Spectr.* **1973**, *2*, 295.

6 Beamson, G.; Briggs, D. In *High Resolution XPS of Organic Polymers: The Scienta ESCA300 Database*; Wiley: New York, 1992.

7 Batten, R. J.; Davidson, R. S.; Ellis, R. J.; Wilkinson, S. A. *Polymer* **1992**, *33*, 3037.

8 d' Agostino, R.; Cramarossa, F.; De Benedictis, S. *Plasma Chem. Plasma Process.* **1982**, *2*, 213.

9 Flamm, D. L. In *Plasma Etching – An Introduction*; Manos, D. M., Flamm, D. L., Eds.; Academic Press: San Diego, 1989.

10 France, R. M.; Short, R. D.; Dawson, R. A.; MacNeil, S. *J. Mater. Chem.* **1998**, *8*, 37.

11 Denes, F.; Sarmadi, M.; Hop, C. E. C. A.; Buncick, M.; Young, R. *J. Appl. Polym. Sci.* **1994**, *52*, 1419.

CHAPTER 7

CONCLUSIONS

7.1 CONCLUSIONS

This thesis has been aimed at the formation of stable silicon dioxide layer at the surface of polyolefin substrates and the investigation of the chemistry involved in the enhancement of the gas barrier properties of aminosilane / acrylate / itaconic coatings onto polypropylene films.

Silicon dioxide surfaces were created by oxygen plasma treatment of PDMS enriched polyolefin surfaces. The highest amount of silica-like material was formed by treating the PDMS triblock copolymer / polyethylene blends by pulsed oxygen plasmas at elevated temperatures. This observation was attributed to thermally activated migration of the PDMS copolymer at the surface during the off-period and to reduced damage caused to the growing SiO_x networks by energetic plasma species. The higher SiO_x yield for the PDMS copolymer samples compared to homopolymer blends was expected due to its more profound PDMS surface segregation.

Coatings of a 4:1:10.4 3-(-2-aminoethylamino) propyltrimethoxy-silane (Z-6020) / pentaerythritol tetracrylate (PETA) / itaconic acid (ITA) mixture onto polypropylene films exhibited good gas barrier properties. This behaviour was found to correlate with the formation of ammonium salt and siloxane-type networks. Heating of the coatings resulted in conversion of the ammonium salt centers to amide linkages with subsequent drop in gas barrier performance. Electron-beam curing provided further reduction in the gas permeability of the coatings. This was due to polymerisation/cross-linking reactions of the carbon-carbon double bonds of the itaconic acid combined with the preservation of ammonium salt species in the coatings.

A novel, single step, solventless deposition method of polymeric salt networks was demonstrated. This involved the pulsed plasma co-polymerisation of unsaturated organic precursors having in their structure carboxylic groups with amine containing monomers and/or ammonia. Good structural retention (i.e. pulsed plasma conditions) was found to be the key factor for producing ammonium salt plasma polymer firms with good gas barrier properties. The reduction in the gas permeability can be attributed to the intermolecular ionic interactions between amine and carboxylic groups in the deposited plasma polymer promoting the formation of a closely packed gas impermeable structure.

CF_4 plasma treatment of the (PDMS/PE) and (PDMS/PP) blends resulted in complete removal of the PDMS-enriched outermost layer. The obtained surface fluorination was found to be similar to that of pure polyethylene, and polypropylene surfaces. In the case of pure PDMS substrates, the extent of fluorination was found to be dependent on plasma conditions.

APPENDIX

COLLOQUIA, SEMINARS, PRESENTATIONS AND LECTURE COURSES

UNIVERSITY OF DURHAM
BOARD OF STUDIES IN CHEMISTRY

COLLOQUIA AND SEMINARS FROM INVITED SPEAKERS

1996

January 17	Professor J. W. Emsley, Southampton University, *Liquid Crystals: More than Meets the Eye.*
January 31	Dr G. Penfold, *Soft Soap and Surfaces.*
February 14	Professor R. Nolte, *Design Strategies for Supramolecular Architectures.*
March 6	Dr R. Whitby, University of Southampton, *New Approaches to Chiral Catalysts.*
March 12	Professor V. Balzani, University of Bologna, *Supramolecular Photochemistry.*
October 22	Professor B. J. Tighe, Aston University, *Polymers for Biomedical Applications.*
October 23	Professor H. Ringsdorf, Johannes Gutenberg-Universitat, *Function Based on Organisation.*
November 6	Dr K. Reid, Nottingham University, *Probing Dynamic Processes with Photoelectrons.*
November 18	Professor G. Olah, *Crossing Conventional Lines in my Chemistry of the Elements.*

November 20 — Professor J. Earnshaw, Belfast University,
Surface Light Scattering: Ripples and Relaxation.

December 4 — Professor K. Muller-Dethlefs, York University,
Very High Resolution ZEKE Spectroscopy.

1997

February 6 — Professor P. Bartlet, Southampton University,
Integrated Chemical Systems.

March 3 — Dr M. Owen and Dr D. Gravier, Dow Corning,
Siloxanes at Surfaces.

March 6 — Professor Toth,
Advances In Scanning Electrochemical Microscopy.

October 15 — Dr R. M. Ormerod, Keele University,
Studying catalysts in action.

October 22 — Professor R. J. Puddephatt, University of Western Ontario,
Organoplatinum chemistry and catalysis.

October 23 — Professor M. R. Bryce, University of Durham,
New Tetrathiafulvalene Derivatives in Molecular, Supramolecular and Macromolecular Chemistry: controlling the electronic properties of organic solids.

November 12 — Dr J. Frey, Department of Chemistry, Southampton University,
Spectroscopy of liquid interfaces: from bio-organic chemistry to atmospheric chemistry.

December 2 — Dr C J. Ludman, University of Durham,
Explosions.

1998

January 14 — Professor D. Andrews, University of East Anglia,
Energy transfer and optical harmonics in molecular systems.

March 11 — Professor M. J. Cook, Dept of Chemistry, UEA,
How to make phthalocyanine films and what to do with them.

October 21 — Professor P. Unwin, Warwick University,
Dynamic Electrochemistry: Small is Beautiful.

October 23 — Professor J. C. Scaiano, Department of Chemistry, University of Ottawa, Canada,
In Search of Hypervalent Free Radicals, RSC Endowed Lecture.

October 28 — Professor J. P. S. Badyal, University of Durham,
Tailoring Solid Surfaces, Inaugural Lecture.

November 3 — Dr C. J Ludman, University of Durham,
Bonfire night Lecture.

November 18 — Dr R. Cameron, Department of Materials Science & Metallurgy, Cambridge University,
Biodegradable Polymers.

1999

January 20 — Dr A. Jones, University of Edinburgh,
Luminescence of Large Molecules: from Conducting Polymers to Coral Reefs.

January 27 — Professor K. Wade, Department of Chemistry, University of Durham,
Foresight or Hindsight? Some Borane Lessons and Loose Ends.

February 10 Dr C. Bain, University of Oxford,
Surfactant Adsorption and Marangoni Flow at Expanding Liquid Surfaces.

February 17 Dr B. Horrocks, Department of Chemistry, Newcastle University,
Microelectrode techniques for the Study of Enzymes and Nucleic Acids at Interfaces.

EXAMINED LECTURE COURSES

Experimental Design and Instrumentation, Prof. J. P. S. Badyal
Spectroscopies, Dr D. P. Halliday
Electron Microscopy, Dr. K. Durose
Nuclear Magnetic Resonance Spectroscopy, Dr A. M. Kenwright